U.S. DEPARTMENT OF COMMERCE
National Technical Information Service

PB-272 096

Significance of Size Reduction in Solid Waste Management

California Univ, Berkeley

Prepared for

Municipal Environmental Research Lab, Cincinnati, Ohio Solid and Hazardous Waste Research Div

Jul 77

PB 272 096

EPA-600/2-77-131
July 1977

Environmental Protection Technology Series

UNITED STATES
ENVIRONMENTAL PROTECTION AGENCY

REPRODUCED BY
NATIONAL TECHNICAL
INFORMATION SERVICE
U. S. DEPARTMENT OF COMMERCE
SPRINGFIELD, VA. 22161

RESEARCH REPORTING SERIES

Research reports of the Office of Research and Development, U.S. Environmental Protection Agency, have been grouped into nine series. These nine broad categories were established to facilitate further development and application of environmental technology. Elimination of traditional grouping was consciously planned to foster technology transfer and a maximum interface in related fields. The nine series are:

1. Environmental Health Effects Research
2. Environmental Protection Technology
3. Ecological Research
4. Environmental Monitoring
5. Socioeconomic Environmental Studies
6. Scientific and Technical Assessment Reports (STAR)
7. Interagency Energy-Environment Research and Development
8. "Special" Reports
9. Miscellaneous Reports

This report has been assigned to the ENVIRONMENTAL PROTECTION TECHNOLOGY series. This series describes research performed to develop and demonstrate instrumentation, equipment, and methodology to repair or prevent environmental degradation from point and non-point sources of pollution. This work provides the new or improved technology required for the control and treatment of pollution sources to meet environmental quality standards.

This document is available to the public through the National Technical Information Service, Springfield, Virginia 22161.

TECHNICAL REPORT DATA

(Please read Instructions on the reverse before completing)

1. REPORT NO. EPA-600/2-77-131	2.	3. RECIPIENT'S ACCESSION NO. PB-272 096
4. TITLE AND SUBTITLE Significance of Size Reduction in Solid Waste Management		5. REPORT DATE July 1977 (Isssuing Date)
		6. PERFORMING ORGANIZATION CODE
7. AUTHOR(S) George J. Trezek		8. PERFORMING ORGANIZATION REPORT NO.
9. PERFORMING ORGANIZATION NAME AND ADDRESS The Regents of the University of California University of California Berkeley, California 94720		10. PROGRAM ELEMENT NO. 1DC618
		11. CONTRACT/GRANT NO. R804034
12. SPONSORING AGENCY NAME AND ADDRESS Municipal Environmental Research Laboratory--Cin.,OH Office of Research and Development U.S. Environmental Protection Agency Cincinnati, Ohio 45268		13. TYPE OF REPORT AND PERIOD COVERED FINAL
		14. SPONSORING AGENCY CODE EPA/600/14

15. SUPPLEMENTARY NOTES

Project Officer - Carlton C. Wiles, Phone 684-7881

16. ABSTRACT

This report provides information from laboratory research conducted to characterize the size reduction of Municipal solid waste (MSW). Results and data are presented on the relationships between refuse size distribution, particle size, grinding speed, moisture content, energy consumption, and feed rate. Also presented are some basic considerations useful for designing solid waste shredders.

17. KEY WORDS AND DOCUMENT ANALYSIS

a. DESCRIPTORS	b. IDENTIFIERS/OPEN ENDED TERMS	c. COSATI Field/Group
Comminution Waste Treatment Refuse	Size Reduction Solid Waste (Theoretical Relationships) Shredder Design	13B

18. DISTRIBUTION STATEMENT Release to Public	19. SECURITY CLASS *(This Report)* UNCLASSIFIED	21. NO. OF PAGES 167
	20. SECURITY CLASS *(This page)* UNCLASSIFIED	22. PRICE PC A08- A01

EPA Form 2220-1 (9-73)

U. S. GOVERNMENT PRINTING OFFICE: 1977-757-056/6475 Region No. 5-11

EPA-600/2-77-131
July 1977

SIGNIFICANCE OF SIZE REDUCTION IN SOLID WASTE MANAGEMENT

by

George J. Trezek
The Regents of the University of California
Berkeley, California 94720

Grant No. R804034

Project Officer

Carlton C. Wiles
Solid and Hazardous Waste Research Division
Municipal Environmental Research Laboratory
Cincinnati, Ohio 45268

MUNICIPAL ENVIRONMENTAL RESEARCH LABORATORY
OFFICE OF RESEARCH AND DEVELOPMENT
U.S. ENVIRONMENTAL PROTECTION AGENCY
CINCINNATI, OHIO 45268

ia

DISCLAIMER

This report has been reviewed by the Municipal Environmental Research laboratory, U.S. Environmental Protection Agency, and approved for publication. Approval does not signify that the contents necessarily reflect the views and policies of the U.S. Environmental Protection Agency, nor does mention of trade names or commercial products constitute endorsement or recommendation for use.

FOREWORD

The Environmental Protection Agency was created because of increasing public and government concern about the dangers of pollution to the health and welfare of the American people. Noxious air, foul water, and spoiled land are tragic testimony to the deterioration of our natural environment. The complexity of that environment and the interplay among its components require a concentrated and integrated attack on the problem.

Research and development is that necessary first step in problem solution, and it involves defining the problem, measuring its impact, and searching for solutions. The Municipal Environmental Research Laboratory develops new and improved technology and systems for the prevention, treatment, and management of wastewater and solid and hazardous waste pollutant discharges from municipal and community sources, for the preservation and treatment of public drinking water supplies, and for minimizing the adverse economic, social, health, and aesthetic effects of pollution. This publication is one of the products of that research and is a most vital communications link between the researcher and the user community.

This report presents information resulting from research conducted on the size reduction of municipal solid waste. Shredding is an important processing step in preparing solid waste for additional processing, including resource recovery. It is hoped that the information provided in this report will help to clarify this important size reduction step and improve overall solid waste processing systems.

Francis T. Mayo
Director
Municipal Environmental
Research Laboratory

PREFACE

The preparation of municipal solid waste (MSW) for the purpose of recovering material and energy resources usually requires primary and often secondary size reduction. Size reduction can be considered a preprocessing step used to prepare the solid waste for many subsequent processing operations ranging from volume reduction before landfilling to fine grinding for pyrolysis to recover oils, gas, char, etc.

As important as MSW shredding has been and continues to be, insufficient data and theory are available to fully understand it. Initially, many assumed that any crusher, grinder, or machine that could size-reduce stone effectively could surely size-reduce MSW. This assumption proved false in most cases. MSW is heterogeneous and contains only about 25% brittle materials. Since the standard stone crusher, grinders, hammermills and similar equipment are designed basically for brittle materials that tend to shatter on impact, their adaptability to a more nonbrittle, heterogeneous material such as MSW proved unsatisfactory. Operating, maintenance, and other costs associated with grinding MSW have therefore been relatively high.

As it became more evident that shredding was to be an important unit operation in solid waste management, the U.S. Environmental Protection Agency (EPA) started some early studies at Johnson City, Tennessee, and New York City to attempt field measurements for evaluating and characterizing the hammermills available at these sites. Most of the currently available data on shredders relate to these projects and others at Madison, Wisconsin, Gainesville, Florida, and St. Louis, Missouri.

In addition to these projects, EPA decided that a more basic approach would be helpful to better define MSW size reduction. The Solid and Hazardous Waste Research Division therefore implemented research aimed at studying and developing data and basic relationships involved in size-reducing MSW. The objectives included accumulation of data for improving the design and operation of MSW size-reduction equipment.

The work was done under controlled laboratory conditions, since field conditions are not conducive to isolation of independent variables. In general, findings have characterized the relationships between refuse size distribution, particle size, grinding speed, moisture content, energy consumption, and feed-rate. Scientific publications arising from this research have made significant contributions to the available knowledge about solid waste size reduction.

The research was conducted by Professor George J. Trezek and his staff at the solid waste laboratory, Richmond Field Station, University of California, Berkeley. This report presents the bulk of the findings to date. The theoretical relationships presented have been developed from actual laboratory measurements. Therefore, though the report provides supporting information of wide interest, it is also valuable to researchers, design engineers, and other personnel involved in the design and operation of selected shredders for MSW processing.

The next logical step in the research and development cycle would be to match the theoretical relationships developed here under controlled laboratory conditions with large-scale equipment in actual operating plants.

Carlton C. Wiles
Project Officer
Solid and Hazardous Waste
Research Division
Municipal Environmental Research
Laboratory

ABSTRACT

This report presents information resulting from investigations conducted on the size reduction of municipal solid waste. The research was conducted by Professor George Trezek under controlled laboratory conditions. The results discussed here characterize relationships between refuse, size distribution, particle size, grinding speed, moisture content, energy consumption and feed rates. Information is presented to provide some basic considerations for refuse shredder design.

This report was submitted in fulfillment of Grant No. R804034 by The Regents of the University of California under sponsorship of the U.S. Environmental Protection Agency. This report covers the period May 15, 1971 to June 29, 1976, and work was completed as of December 1976.

CONTENTS

Foreword iii

Preface iv

Abstract vi

Figures viii

Tables xiii

Metric Conversion Table xiv

1. Introduction 1
2. Size Distribution 34
3. Behavior of the Comminution Parameters 73
4. Wear, Maintenance, and Shredder Selection Aspects of Refuse Comminution 89
5. Analytical Aspects of Comminution 111

References 130

Appendices 137

A. Mill Matrix Circuit Analysis 137

B. Some Size Distribution Relations Prepared by D.M. Obeng 142

FIGURES

Number		Page
1	Stress-strain characteristics of some refuse components.	8
2	Energy required for volume reduction of common containers found in refuse	10
3	Energy requirements for steady compression rate tests	11
4	Compressibility of modified raw solid waste . . .	15
5	Compressibility of solid waste after primary shredding	16
6	Compressibility of solid waste after secondary shredding	17
7	Compressibility of solid waste passed through a rasp.	18
8	Overall view of the V-belt.	23
9	Input conveyor and grinder (size reduction unit).	26
10	Basic dry plant	27
11	Grinder discharge into air classifier and heavies recovery.	28
12	Light fraction processing facility - air classifier, light fraction discharge, and cyclone	29
13	Components of the light fraction processing facility.	30
14	Alternatives for screened lights.	31
15	System flow diagram	32

Number Page

16 Anerobic digestion. 33

17 Cumulative weight (% raw refuse total) of objects with longest dimension greater than given lengths 37

18 Cumulative weight (% raw refuse total) of objects that will pass through a square mesh, plotted vs. mesh size 37

19 Number of objects per ton of raw refuse vs. length (longest dimension of object) for principal categories of refuse. 38

20 Total weight per ton of raw refuse of objects in given length ranges for principal categories of refuse. 39

21 Cumulative distributions of raw waste 40

22 Moisture content analysis. Percent moisture loss vs. drying time. 46

23 Product size distribution for the primary grinding of municipal refuse with 22.0% moisture content. 48

24 Product size distribution for the primary grinding of municipal refuse with 40.4% moisture content. 49

25 Product size distribution for the primary grinding of municipal refuse with 55.3% moisture content. 50

26 Product size distribution for the secondary grinding of municipal refuse with 21.0% moisture content. 51

27 Product size distribution for the secondary grinding of municipal refuse with 19.6% moisture content. 52

28 Product size distribution for the tertiary grinding of municipal refuse with 19.2% moisture content. 53

Number Page

29 Plot of $\ln \frac{1}{1-Y}$ vs. sieve size for primary, secondary, and tertiary grinding of municipal refuse 54

30 Typical particle size distributions for milled refuse from both mills in 1972 56

31 Cumulative distributions of primary waste 58

32 Cumulative distributions of secondary waste 59

33 Cumulative distributions of rasped waste. 60

34 Component size distribution of shredded municipal solid waste - 1,814 kg/hr (2 tons/hr), 1,200 rpm swing hammermill 62

35 Component size distribution of air-classified heavy fraction 64

36 Component size distribution of air-classified light fraction 65

37 Composition of air-classified shredded solid waste - 70%/30% split 67

38 Component size distribution of oversize from 9.5×10^{-3} m (3/8 in.) Trommel screen 69

39 Component size distribution of undersize from 9.5×10^{-3} m (3/8 in.) Trommel screen 70

40 Composition of screen air-classified light fraction 72

41 Size distribution comparison for raw municipal refuse and residential refuse shredded at 1,200, 790, and 555 rpm. Effect of moisture content (MC), and secondary and tertiary grinding 74

42 Effect of moisture content (MC) on particle size distribution 77

43 Effect of grate size on particle size distribution at Madison 77

44 Characteristic particle size vs. grate spacing . . 78

Number Page

45 Effect of hammer wear on particle size distribution - Tollemache Mill. 79

46 Changes in Particle Size Distribution as a result of cumulative hammer wear. 79

47 Specific energy consumption to achieve a given characteristic particle size. 80

48 Specific energy consumption at different grinder rpm (dry weight basis). 82

49 Influence of grinder rotor speed on energy consumption vs. size distribution of residential refuse. 83

50 Effect of moisture content on specific energy consumption for grinder rotor speeds of 1,200 and 790 rpm 84

51 Comparison of Characteristic Particle Size (X_o) and specific energy for commercial and residential solid waste 86

52 Size distribution of refuse from various shredders. 87

53 Characteristic particle size vs. specific energy consumption 88

54 Manganese steel hammer with hard facing weld material applied about the crushing face 90

55 Hammer configuration. 91

56 Non-hard-faced hammers after grinding 70 tons of refuse at 1,200 rpm. 94

57 Summary of worn hammer profiles 95

58 Effect of grinder speed on hammer wear. 96

59 Horsepower required for size reduction of MSW as a function of feedrate and desired product size. 107

60 Grate spacing required to produce a desired product size. 110

Number Page

61 Comparison between computed and experimental product size distributions for primary, secondary, and tertiary grinding using the π-breakage process model. 126

62 Comparison between computed and experimental product size distributions for primary grinding using the π,κ-breakage process model . . .127

63 Comparison between computed and experimental product size distributions for primary grinding using the repeated breakage cycle model 129

A-1 Hammermill analysis. 138

TABLES

Number Page

1 Composition of Municipal Solid Waste, as Discarded, United States, 1973. 4

2 Average Composition for Residential, Commercial, and Industrial Solid Waste for Some San Francisco Bay Area Counties 5

3 Stress vs. Strain Data. 7

4 Municipal-Scale Shredding Operations by State or Country and Date of First Installation. 21

5 Bulk Composition (Weight Percent) of Refuse Samples 35

6 Analysis of Experimental Error: Feedrate (Ton/hr). 44

7 Composition of Madison's Solid Waste (November 1968) 55

8 Summary of Refuse Composition at Gainesville, Florida 57

9 Composition of Air-Classified, Shredded Solid Waste, 70/30 Split. 68

10 Composition of Screened, Air-Classified Light Fraction. 71

11 Hammer Wear 92

12 Grate Bar Wear. 93

13 Average Wear for Hammers and Grate Bars at Different Grinder Operating Speeds. 99

14 Suitability of Hard Facing Coating for Various Base Materials. 102

15 Breakage Function Elements of the First Column b_{i1}. .124

METRIC CONVERSION TABLE

English system	Metric system
Inch	2.54 cm
Foot	30.48 cm
Yard	0.914 m
Square inch	6.452 cm^2
Square foot	0.092 m^2
Square yard	0.836 m^2
Cubic inch	16.387 cm^3
Cubic foot (1,728 in^3)	0.028 m^3
Cubic yard (27 ft^3)	0.7646 m^3
°F	-17°C
Pound	
avdp. (16 dr)	453.592 g
troy (12 oz)	373.24 g
Ton	
long (2,240 lb)	1.016 t
short (2,000 lb)	0.907 t

SECTION 1

INTRODUCTION

The range of applications of size reduction (comminution) in solid waste management is becoming progressively broader. The history of shredding, along with a summary of reasons cited for shredding, has been reviewed recently by Ham (1). In the 1950's, European countries such as England and France initiated the practice of shredding wastes as a preparative step for landfill disposal. Although there was some concern for salvage, (i.e., resource recovery), the predominant early use of shredding in solid waste management was for landfilling. Eventually, shredding procedures began to be used in the United States. One of the earliest uses was as an initial step in composting. Later, in light of the European experience, the possibilities of improving the overall quality of landfills and increasing landfill life through increased compaction and elimination of a daily cover motivated the establishment of the Madison Wisconsin demonstration project by the U.S. Environmental Protection Agency (EPA) (formerly the Public Health Service) in 1966. In general, the Madison experience affirmatively demonstrated that a shredded solid waste landfill could omit a daily cover without causing the rodent, insect, odor, fire, blowing debris, and aesthetic problems that are commonly considered as indicators of the quality of landfilling operations (2).

The physical characteristics of refuse are changed after it undergoes a comminution process. For example, the basic refuse odor may be replaced by a more earthy smell. For the most part, the shredded material becomes unattractive to such scavengers as sea gulls, flies, and rodents. The characteristic particle size is reduced by at least one order of magnitude over that of raw refuse. Size distributions of shredded refuse typically span three to four orders of magnitude. This evidence contradicts the visual claims that state that after refuse is shredded, the size of the product tends to be uniform. Actually, from the resource recovery point of view, it is fortunate that uniformity in size does not occur; as will be discussed, certain materials tend to fall into various size range bands, and as such, they can be separated.

The number of waste processing shredding installations in our country has steadily grown during the past decade. It has been estimated that there are currently some 70 to 100 waste processing shredding installations in operation. The activities conducted at these facilities cover a wide variety of applications dealing with landfilling, reducing bulky wastes, industrial processing, and various material and energy recovery projects. Because of recent energy and certain material shortages, the use of shredding in solid waste management over the last few years has shifted toward recovery operations. It is important to note that although the number of waste processing facilities using shredders has increased, the paucity of data regarding both equipment and facilities design as well as data describing the refuse size reduction process in terms of the quantitative behavior of comminution parameters is only recently being alleviated.

Front end systems, the majority of which employ shredding as the first processing step, are common to most modern material and energy resource recovery processing operations. The modular concept in resource recovery provides for the fact that there is a hierarchy of material values in the waste stream so that the entire stream need not be committed to one type of process. In effect, known technology can be implemented on a scale compatible with existing markets for materials and energy. The spectrum covers options ranging from simple shredding followed by ferrous materials separation, advanced forms of fiber recovery involving shredding and front end processing followed by wet pulping size reduction, and processes for creating refuse-derived fuels that may require secondary shredding.

Ability to control the shredding process is important for the successful operation of subsequent processing stages in resource recovery operations. When the waste stream is to be used for energy, the increased surface area of size-reduced refuse can also serve as an aid in various combustion processes by creating more sites for rapid oxidation. Even though refuse is a heterogeneous mixture, size reduction tends to homogenize the mixture so that a combustion process is presented with a fuel of relatively constant heating value. Various trade-offs between coarse and fine size distributions must be considered in terms of producing a fuel with good combustion characteristics and yet not creating an energy-intensive fuel preparation process such as might be the case if fine grinding were required as a secondary size reduction stage. Densified, pellet-type, refuse-derived fuels usually require primary and secondary size reduction as part of their preparation.

In general, with the exception of explosives and materials yielding potential shock loads, the shredding of industrial, commercial, and residential solid wastes is now accomplished in a relatively reliable and controlled manner. Refuse is a difficult material to size reduce and offers considerable wear and strain on the comminution machinery that still operates under the premise of brute force. Nonetheless, refuse comminution is an emerging technology that will reach higher levels of sophistication as increased operating and design data are generated and advanced predictive methods are developed.

NATURE OF THE WASTE STREAM

The refuse waste stream is a heterogeneous material whose characteristics and properties can have geographical and seasonal variations. Estimates for the rate of municipal refuse generation reported in the literature vary according to the time of their publication; those published before the early 1970's tend to be higher than those made from about 1972 and thereafter (3). The latter are more realistic because they are based to a considerable degree on measured rather than estimated outputs. Estimates based on measured outputs are about 3 lb/capita-day, whereas those geared to estimates are about 5.16 lb/capita-day.

Typical types of materials normally found in municipal solid waste (MSW) are such forms of cellulose or fiber as newsprint, cardboard, mixed paper waste (including high grade stationery), computer printout, tissue, printing rejects, general office wastes, and food packaging containers such as milk cartons, cereal boxes, prepared food containers, etc.; plastics; ferrous, aluminum and other metals; glass, ceramics, stone, etc.; organic components such as putrescible grass and tree cuttings, etc.; and a range of miscellaneous objects encompassing occasional tires, leather and rubber goods, wood wastes, and the like. Different percentages of each category have been reported as being representative of the waste stream. As indicated by the nature of the waste stream, there exists a hierarchy of material values in the total array of objects. When the waste stream is to be processed for material and/or energy recovery, the processing steps will involve some phase of comminution that should be controlled according to the precise waste stream content and processing purpose.

EPA has published a type of national average waste stream composition (4) shown in Table 1.

The waste stream characterization for San Francisco Bay Area Region yields an analysis that differs significantly from the EPA's analysis in certain categories. The average composition for residential, commercial, and industrial solid waste for four large Bay Area counties (Table 2) indicates that the fiber content of the waste stream is on the order of 40% to 50%. In general, these data compare favorably with the composition data presented by National Center for Resource Recovery (NCRR) as a national average for various materials derived from municipal solid wastes (5). Fiber predominates as the major constituent of the waste stream. It is important to note that the local generation of

TABLE 1. COMPOSITION OF MUNICIPAL SOLID WASTE, AS DISCARDED, UNITED STATES, 1973[a,b]

Component	Amount (millions of tons)	% of total
Paper	44.2	33.1
Newspaper	8.0	6.0
Corrugated	11.8	9.0
Office paper	5.4	4.0
Other	19.0	14.1
Glass	13.2	9.9
Ferrous metals	11.0	8.2
Nonferrous metals	1.4	1.0
Food waste	22.4	16.6
Yard waste	25.0	18.5
Other	17.2	12.8
Total	134.4	100.0

[a] Smith, F.A., U.S. Environmental Protection Agency. Unpublished data.

[b] Includes wastes generated in households, commercial and business establishments, and institutions (schools, hospitals, etc.); excluded are industrial process wastes, agricultural and animal wastes, construction and demolition wastes, mining wastes, abandoned automobiles, ashes, street sweepings, and sewage sludge. Wastes now being recycled are also excluded.

fiber in certain areas can far exceed the 40% to 50% value. For example, if a concentration of commercial routes were lumped in some area in the region, the percentage of fiber might be as high as 70% to 85%. Data taken at the Richmond Field Station laboratory support this generalization. Their average fiber content is reported to be about 43%, whereas results obtained from selected areas reach the higher percentages. If processing plants are constructed on the 500 to 1,000 tons/day modular size range, then it is important to adequately sample the waste stream in the particular region and not rely on overall averages. This will undoubtedly have an effect on the combination of processing technology that can be most advantageously implemented to insure optimum materials and energy recovery.

The solid waste generation rate in the Bay Area ranges from 3.5 to 13.7 lb/capita-day. Of interest here is the fact that the national generation rate of 3 to 5 lb/capita-day is often taken

TABLE 2. AVERAGE COMPOSITION FOR RESIDENTIAL, COMMERCIAL, AND INDUSTRIAL SOLID WASTE FOR SOME SAN FRANCISCO BAY AREA COUNTIES

Waste constituent	Alameda	Contra Costa	San Francisco	Santa Clara	MSW Richmond Calif. (6)	Avg. MSW NCRR (5)
Newsprint	9.0	9.0	8.0	8.0	---	---
Corrugated	22.0	6.0	2.0	6.0	---	---
Other paper	12.0	35.0	38.0	31.0	---	---
Total fiber	43.0	50.0	48.0	45.0	43.2	43.0
Ferrous	8.0	7.0	8.0	6.0	7.3	8.0
Aluminum	0.7	1.0	1.0	0.5	0.7	0.7
Other nonferrous	0.3	---	---	---	---	0.3
Total metals	9.0	8.0	9.0	6.5	8.0	9.0
Glass, ceramics, rocks	10.0	10.0	13.0	6.0	10.8	10.0
Plastic, rubber, rags, etc.	5.0	6.0	5.0	6.0	4.5	5.0
Garbage, yard wastes	33.0	20.0	5.0	26.0	23.5	26.0
Other, miscellaneous, unclassified fines	---	6.0	20.0	10.5	10.0	7.0

as valid for regions whose waste is generated by a multitude of various manufacturing, residential, or agricultural activities. Thus one generation rate is taken as valid for all locations but for different reasons.

PHYSICAL CHARACTERISTICS OF REFUSE

The heterogeneous nature of the waste stream gives rise to a material whose components contain a variety of mechanical properties. Measurements have been made of the ultimate strengths and strain and rupture energy for some major refuse components such as magnetic and aluminum cans, kraft paper (from brown paper bags), light cardboard box material (typical of food packaging), and polyvinyl chloride (PVC) and polyethylene (PE) plastics (7). All of the above specimens were actual objects, or parts thereof, found in municipal refuse. The stress-strain data allowed modulus of elasticity values to be computed. A comparison of the stress-strain characteristics of the waste stream components listed in Table 3 is shown in Figure 1.

The steel specimens have the greatest values of ultimate strength (about 82,000 lb/in.^{2}) and the least value of ultimate strain (0.004 in./in.). This value of ultimate strength is in general agreement with those obtained for plane carbon, cold worked steels, which range from 70,000 to 100,000 lb/in.^{2}, depending on the carbon content and degree of cold work of the material. The modulus of elasticity (E) computed from the stress-strain data has a value of 28.5 x 10^6 lb/in.^{2}, which compares favorably with the usual values of E of 29 to 30 x 10^6 lb/in.^{2} for carbon and low alloy steels. Values for the ultimate strength of the aluminum specimens were approximately 30,500 lb/in.^{2}, and they compare with known values, which range between 13,000 and 82,000 lb/in.^{2} depending on the alloy content and heat or cold working treatments. A value of E of 10.0 x 10^6 lb/in.^{2} was computed from the aluminum stress-strain data.

The characteristics of the fiber materials are summarized as follows: Cardboard and paper have ultimate strengths of 6,400 lb/in.^{2} and 4,000 lb/in.^{2}, respectively, and both have an ultimate strain of 0.025 in./in. Modulus of elasticity (E) for cardboard was computed as being 0.5 x 10^6 lb/in.^{2}, and 0.32 x 10^6 lb/in.^{2} for paper. In the paper industry it is common to consider strength in terms of the maximum length (meters) that a strip of paper can hang free before rupture or tearing occurs. If the paper density is known, (p) values of the stress (S) at the top of the strip can be computed; that is, S = w/A = Lp where w is the weight of the strip, L the length, A the cross sectional area, p the weight density, and S the stress. Typical values of strength range from 2,000 to 5,000 meters at maximum stress of 2,100 to 5,200 lb/in.^{2}

The behavior of the plastic samples differs considerably from

TABLE 3. STRESS VS. STRAIN DATA

Material	Type of container	Container shape and specimen locations	Specimen thickness (in.)	Ultimate strength (psi)	Ultimate strain (in./in.)	Rupture energy (ft.-lb/in.^{3})
Steel	12-oz beverage can	Cylinder; specimen cut from side, axially and circumferentially	0.007	82,000	0.005	9.4
Aluminum	12-oz beverage can	Same as above	0.006	31,000	0.012	26.5
Cardboard	Laundry detergent box	Rectangular box; specimen cut from front and back panels	0.025	6,400	0.025	8.3
Paper	Brown paper bag	"Grocery" type bag specimen cut at various locations	0.009	4,000	0.025	5.1
Plastic, polyvinylchloride	Liquid soap bottle	Sculpted molding; specimen cut from front and back panels	0.19 to 0.026	4,000 to 5,000	0.360-$\dot{e}$=0.1[a] 0.130-$\dot{e}$=1.0 0.060-$\dot{e}$=10	111-$\dot{e}$=0.1 44-$\dot{e}$=1.0 19-$\dot{e}$=10
Plastic, polyethylene	Shampoo bottle	Cylinder; specimen cut as in cans above	0.028 to 0.036	1,000	0.80 for $\dot{e}$=0.1 0.84 for $\dot{e}$=1.0 0.90 for $\dot{e}$=10	56-$\dot{e}$=0.1 60-$\dot{e}$=1.0 66-$\dot{e}$=10

[a] Where $\dot{e}$ = elongation rate, all materials were tested at $\dot{e}$ = 0.1, 1.0 and 10 in./min., with the plastics showing the effects of elongation rate as given above. Materials other than the plastics showed no elongation rate effects.

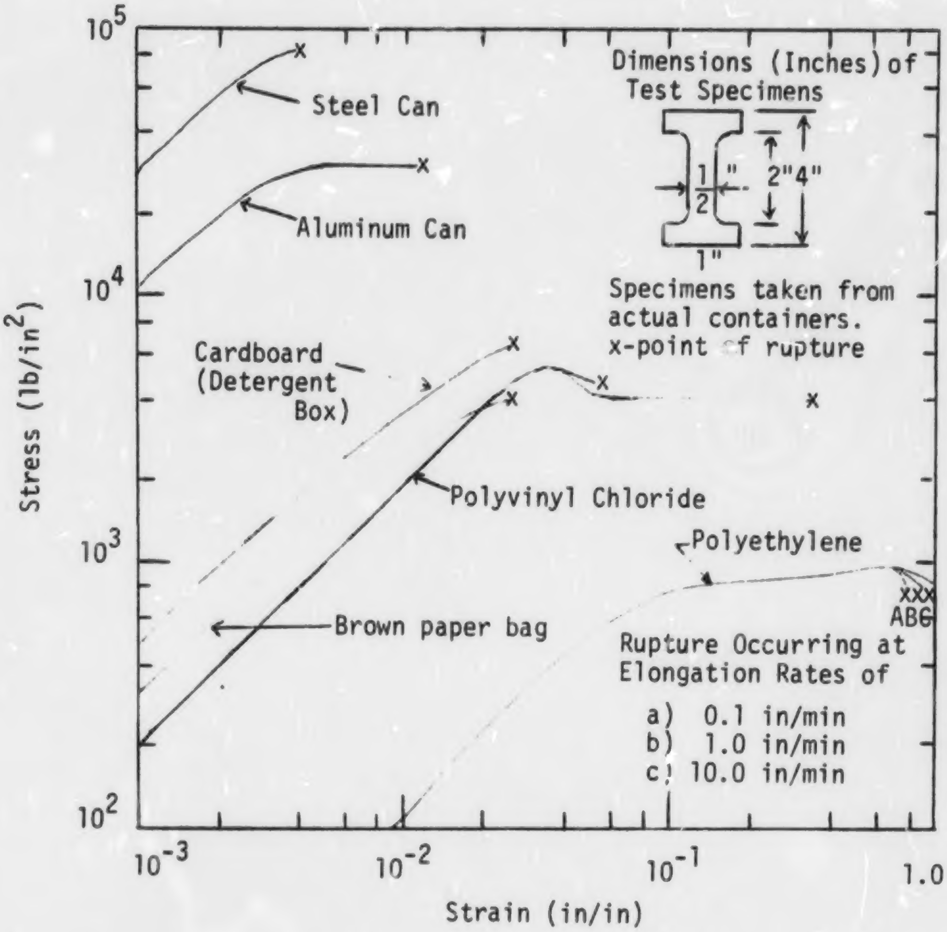

Figure 1 Stress-Strain Characteristics of Some Refuse Components

that of metal and cardboard samples. For PVC the modulus of elasticity was computed as being 0.2×10^6 lb/in.^{2}, and the ranges of ultimate strength and of strain were 4,000 to 5,000 lb/in.^{2} and 0.060 to 0.360 in./in., respectively. The corresponding range of normally accepted values for PVC without plasticizers is a modulus of 0.2×10^6 to 0.6×10^6; and ultimate strength and strain values of 5,000 to 9,000 lb/in.^{2} and 0.02 to 0.40 in./in., respectively. On the other hand, the PE sample has a lower modulus of elasticity (0.014×10^6 lb/in.^{2}), a lower ultimate strength (1,000 lb/in.^{2}), and higher values for ultimate strain (0.8 to 0.9 in./in.). Depending on the polymer density, molecular weight, and manufacturing processes, the corresponding values of modulus, and ultimate strength and strain for PE are within the range of $0 - 01 \times 10^6$ to 0.04×10^6 lb/in.^{2}, 1,000 to 1,400 lb/in.^{2} and

0.5 to 7.0 in./in., respectively.

Energy requirements needed to effect various degress of volume reduction by both pure compression and impact for several types of containers normally found in municipal refuse are available. These data also consider object orientation, because geometrical asymmetries and certain types of supportive elements such as rims on the ends of cans can have an effect on the amount of energy required for a particular amount of volume reduction. Specifically, the orientation of the objects in these tests was as follows: a) The steel and aluminum cans were subjected to separate radial and axial tests; b) cardboard boxes and cartons were tested in the upright and horizontal positions; and c) glass bottles were tested in steady compression until they fractured. In effect, determination of the area under the curve for load vs. volume reduction yields a relation between energy expenditure and volume reduction. The impact tests were performed in a manner in which the energy required to effect a given volume reduction could be obtained directly by impacting an object with a known weight falling through a known distance.

The energy required to effect a certain volume reduction on glass, metal, and cardboard containers normally found in refuse is indicated by the curves in Figure 2. Here the results of both volume reduction techniques are compared, that is, the steady compression method (solid curves) and the impact method (dashed curves). In each case there appear to be two distinct slopes for the energy-volume curves. Except for glass, the first slope occurs at volume reductions up to 60% to 70%. This slope is essentially linear and is representative of the initial buckling and folding of the container wall. In the case of glass, this slope prevailed up to a volume of about 35% and is representative of the initial fracture.

During this linear portion, the forces required to effect a volume reduction are generally constant. It is reasonable to assume that during this phase of volume reduction, the greatest part of the energy or input work is directed toward the elimination of the large interior voids of the containers, and essentially no plastic deformation occurs. As would be expected, after the first phase of volume reduction has occurred, the amount of subsequent work or energy required for continued volume reduction increases rapidly. It is then necessary to begin deformation of the container wall materials and the slope of the force-compression curves approach the elastic moduli of the respective materials. The volume reduction can occur, and this is noted in Figure 2 for the types of specimens considered. The energy data regimes are summarized in Figure 3.

Each of the objects exhibits different behavior. For example, the steel and aluminum specimens, when tested in tension, are not

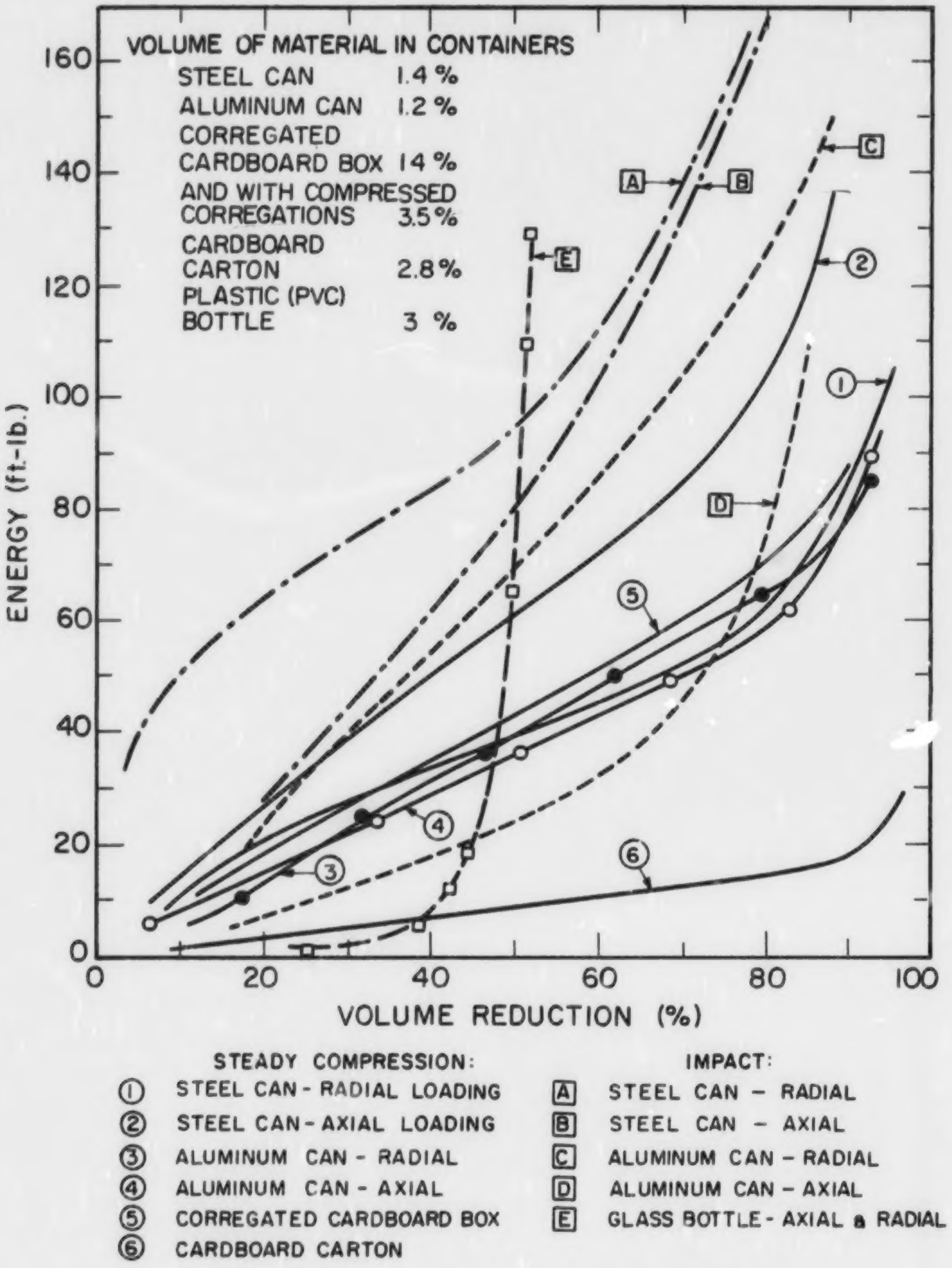

Figure 2 Energy Required for Volume Reduction of Common Containers Found in Refuse

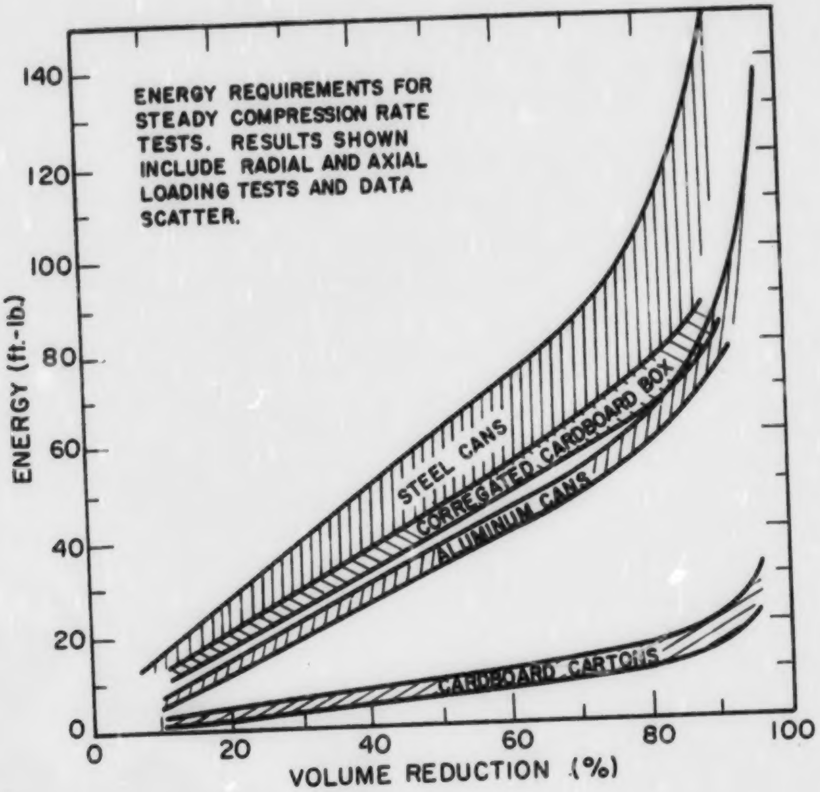

Figure 3 Energy Requirements for Steady Compression Rate Tests

strain-rate-dependent in the range considered and broke abruptly in a manner characteristic of a brittle material. On the other hand, the strain rate had a significant effect on the ultimate strain of the plastic specimens. PVC was more sensitive to this parameter than was PE. Extensive local deformation or "necking" characterized these specimens. In general, the mechanisms involved in straining polymers are complex and not completely understood. Changes in experimental conditions, such as strain rates, are known to affect the probability of fracture under given circumstances. As the strain rate is increased, the typical behavior of such specimens is a localized heating that leads to a decrease in stability and to breaking strains.

During compression, glass bottles have a tendency to break in areas of stress concentration, such as the vicinity of the bottle neck and near the bottom. Bottles with more complex shapes generally fracture at lower levels of stress. As glass pieces become smaller, the stress requirements for further crushing increase. The stress requirements for small glass pieces loaded in pure compression are much greater than for pieces where tensile stresses are also present, such as in bending.

The amount of force required to crush metal cans is affected by the method of load application. The amount depends on both the direction of the application of the force, such as axial or radial compression, and on the shape of the crushing member. With respect to the values reported here, specimens were compressed between large flat plates.

DENSITY AND COMPRESSIBILITY OF REFUSE

Design of various solid waste management schemes requires knowledge of the density and potential compressibility of raw and processed solid waste. This is especially germane to certain aspects of material handling such as conveying and processed material transport in either loose or baled form. Planning for disposal by landfill also requires knowledge of density and compressibility. Ruf (8) has reviewed the available data on the subject, defined terminology in terms of models, and conducted controlled laboratory experiments that produced density and compressibility data for both raw and shredded refuse. In addition, the feasibility of baling refuse has been considered in a report prepared by the Department of Public Works in the City of San Diego, California. Other work dealing with compaction and baling has been prepared by the American Public Works Association (APWA) for the EPA (9, 10).

In his considerations, Ruf defines the particle structure of refuse as being an assemblage of particles interspaced with open air spaces called voids or pores. Unlike soil, the moisture is generally not contained in the voids as free moisture but rather absorbed in the material itself. Certain terminology then follows from the fact that the total volume of material is composed of the volume of the solids plus the volume of the voids or

$$V_m = V_{solid} + V_{void}$$

The void ratio is given as $e = V_v/V_s$ and the porosity is $\eta = V_v/V_m$. The density is the ratio of weight to total volume. A wet weight density is defined as the ratio of total weight, including water, to the volume; the dry density, sometimes referred to as the apparent or bulk density, is given as the ratio of the weight of solids alone to the total volume. The true or absolute density is given as the ratio of the weight of solids to the volume of solids.

In his work, Ruf elaborates on the fact that since solid waste is not rigid, depending on the pressures applied to reduce the void spaces, various values of bulk density can be achieved. Further, the bulk density can vary because of different waste compactions, irrespective of its porosity. Comparison of the density of various materials shows that the components in the waste stream contribute to a wide range of densities. For example, the average density of steel scrap is on the order of 13,000 lb/yd^3, whereas that of highly densified paper bales is only 1,500 lb/yd^3. An average density of refuse computed from the material composition indicates that the theoretically highest density possible for dry refuse compacted in a high density baler is on the order of 1,400 lb/yd^3. According to Ruf, density is not affected by differences in the size of particles, but is instead influenced by the particle arrangement. For wastes high in paper content, the contribution of moisture to the density could be greater than 50%, since in the absence of swelling, the moisture is absorbed, thus contributing to the weight but not the volume. Also, higher densities can be achieved with greater pressure and smaller particle size.

Since refuse contains little free moisture and relatively large particles, the time lag for compression is small compared to a material such as soil, where the water must be squeezed out during compression. Ruf's experiments show that as pressure is applied to solid waste, the volume is reduced and the density increased because of the crushing, deforming, and relocating of individual particles. Such hollow objects as containers begin to collapse at various pressures. For example, cans and bottles begin collapsing at pressures of 10 to 30 psi and 5 to 35 psi, respectively. Thus, some phases of the compaction process are reversible, and others are not. The data obtained by the APWA indicate that the volume reduction of loose residential refuse of similar density was about 9:1 and 13:1 for applied pressures of 900 psi and 3,000 to 3,500 psi, respectively. For different types of refuse subjected to the same pressure, the volume reduction varied between 7:1 and 23:1. The former value was for a high-dirt-content waste. Normal variations were between 8:1 and 18:1. In the APWA experiment, the consolidation theory was observed; namely, larger densities were obtained when the applied pressures were retained.

For the case of shredded refuse, the APWA has concluded that shredding does not aid the compression process or contribute to the stability of the bale as compared to direct baling of unprocessed waste. Data concerning the relationship between applied pressure to the density of shredded refuse has been assembled by the American Baler Company (9).

The effects of springback after the release of pressure and stability in compressed refuse have been considered in several studies. The APWA results show that an approximate 20% expansion occurs a few seconds after pressure release and can continue to 50% to 60% of the original compressed volume after several minutes. In general, this study indicates that the stability of bales improves with increased pressure and application time for proper moisture contents. Pressures in the range of 500 to 1,000 psi produce fragile bales, but 1,000 to 1,500 psi pressures show improved stability. The greatest improvement in stability occurs in the pressure range between 2,000 to 3,500 psi.

The experimental data obtained by Ruf for density (0 pressure) compressibility, and springback are given in Figures 4,5,6, and 7 for raw, primary, secondary, and rasp-shredded wastes, respectively His apparatus consisted of of a 10-ton capacity laboratory model hydraulic press fitted with a compression cylinder test chamber. Approximately 20 3-lb samples of each category (except the rasp samples, which were 9 6-lb samples) were dried for 2 to 4 days at 70 to 75°C and then tested. Ruf found that the compression curves were smoother for the small particle waste. The greatest variation occurred with raw refuse.

SIZE REDUCTION EQUIPMENT

The type of equipment available for the size reduction or comminution of brittle materials along with their subsequent performance characteristics is well documented in the mineral dressing and processing industry (11). Raw material characterization and the type of product specified (e.g., graded, granular, fine, abraded, flake, rounded, sharp, etc.) are the predominant factors considered in the selection of a particular type of mill. Another consideration used in specifying brittle material comminution is the so-called grindability of the material. Basically, this refers to the response of a material to the grinding effort. Materials are generally classed as a) hard, friable, abrasive, b) hard and tough, c) medium hard friable, d) soft, friable, e) soupy, and f) sticky.

Comminution devices generally used for the dry size reduction of brittle materials have been grouped accordingly: 1) Fixed path mills, containing relatively few comminution elements that follow a definite path, and 2) tumbling mills, where the elements are multifarious and not constrained to individual paths. Examples of fixed path mills are attrition mills, impact mills of the hammermill or jet pulverizer type, pan mills, roller mills, and other types and variations of these. Tumbling mills include ball and pebble mills, rod mills, compartment mills, and other modifications of the rotating-drum principle.

Refuse, a heterogeneous material, contains only about 25% brittle materials. As a result. the machine selection criterion used for a purely brittle material is not directly applicable. When the size reduction of refuse is considered, the term "shredding" as opposed to grinding, pulverizing, crushing, etc. has emerged as the terminology depicting refuse comminution. The following types of machines have been designated as shredders by

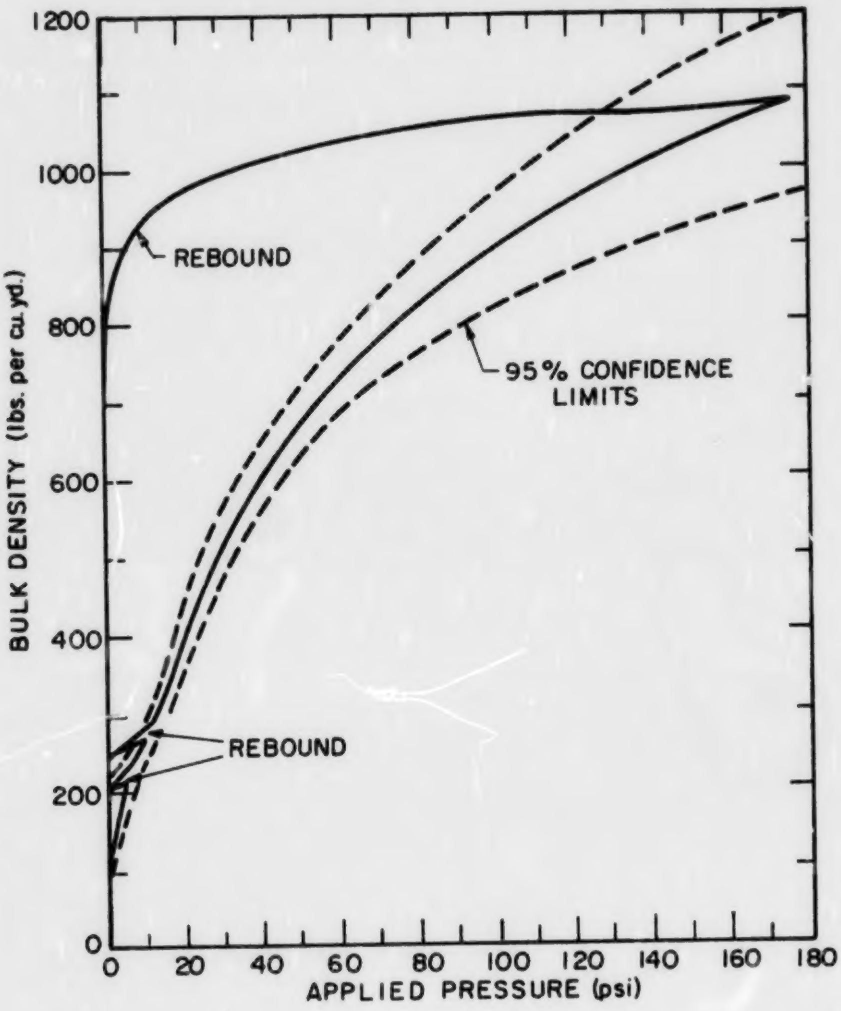

Figure 4 Compressibility of Modified Raw Solid Waste

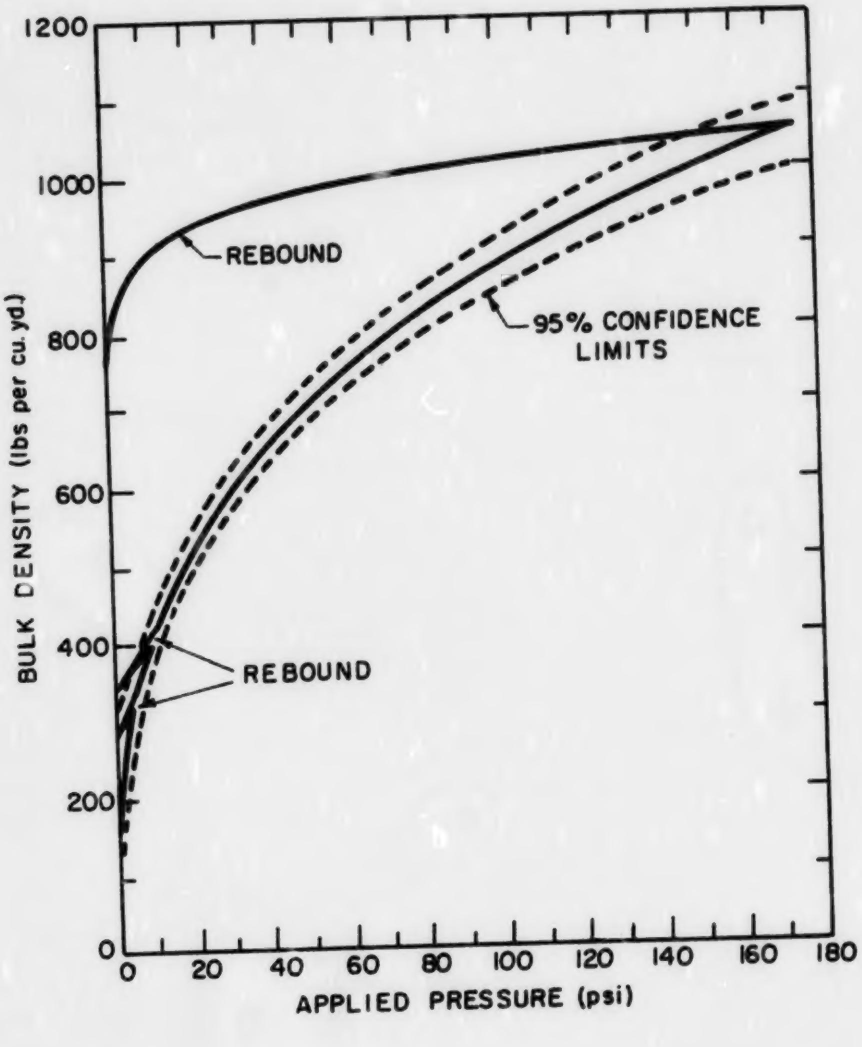

Figure 5 Compressibility of Solid Waste After Primary Shredding

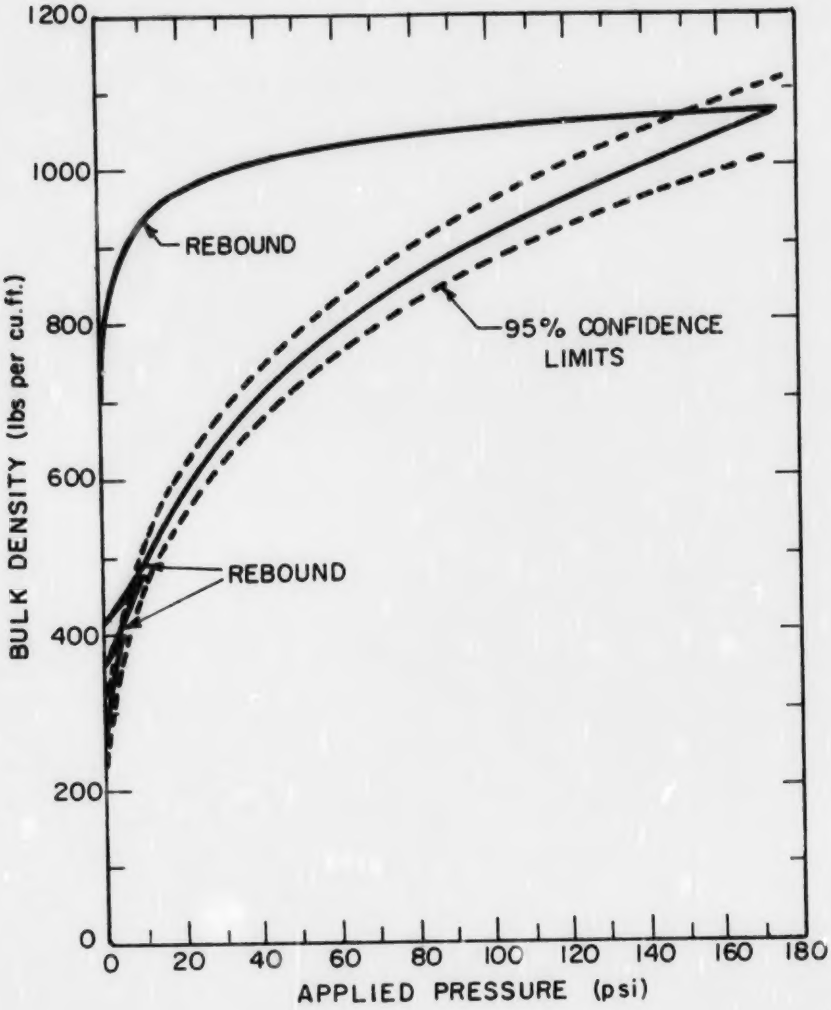

Figure 6 Compressibility of Solid Waste After Secondary Shredding

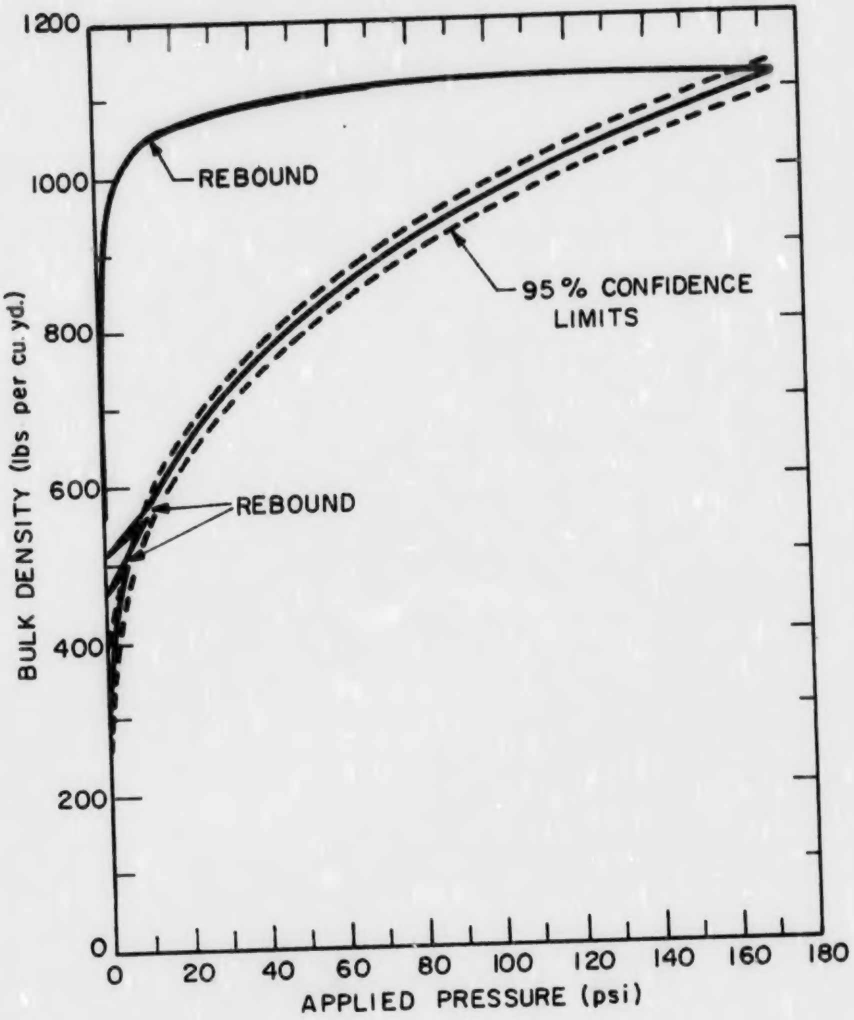

Figure 7 Compressibility of Solid Waste Passed Through a Rasp

the Waste Management Equipment Manufactures Institute: crushers, cage disintegrators, shears, shredders, cutters and clippers, rasp mills, drum pulverizers, disk mills, wet pulpers, hammermills, and grinders.

Hammermills are the most commonly used type of machine in refuse processing. This fact stems from the nature of the waste stream components (particularly the high non-brittle fibrous fraction) and the manner in which the size reduction is effected. As previously mentioned, hammermills are a class of impact crusher in which the load, a combination of tensile, compressive, or shear forces, is applied to the material by striking particles in suspension or by hurling them at high speed against stationary surfaces. This action differs from a typical crushing machine, such as a rock crusher, which takes in a coarse feed and applies pressure gradually to the particles which take the load as simple beams or short columns.

In some sense, the greater part of size reduction of refuse with the hammermill is accomplished by brute force. There are horizontal and vertical shaft machines of either the swing or rigid hammer type. The horizontal swing hammer machine, whose principle parts are the rotor, hammers, grates, frame, and fly wheel, is the type most frequently used. The machine construction is relatively simple. Here the rotor and fly wheel are mounted through the bearings to the frame, the bottom portion of which also holds the grates. The hammers, which can assume a number of configurations, depending on the particular manufacturer, are attached to the rotor by means of the hammer pins. These are long rods, which in effect lace the hammers to the rotor by running them through the holes in the rotor and hammers. Actual hammer configurations vary from simple rectangular blocks having typical dimensions of 12 x 4 x 1 in. to the more elaborate type of chopper, which may have a protruding wearing surface with sharpened edges. When the entire rotor-hammer assembly is rotating (usually at about 1,000 to 1,500 rpm), the hammers fly perpendicularly to the rotor Upon impact with objects being size-reduced, each hammer is free to move in a 180° arc within the plates of the rotor. In a typical commercial installation, the motor is usually attached to the rotor shaft by means of a steel flex coupling. Materials to be size-reduced enter the machine through an infeed chute and interact with the hammers and each other until at least one dimension of the objects has reached a size small enough to fall through the grates in the bottom of the machine.

Experience has shown that refuse is an abrasive material that does not directly conform to the previously mentioned grindability types and is relatively difficult to size reduce. As a result, the comminution processes cause considerable wear to the machine elements, particularly the hammers. The problem of wear is considered in detail in a later section of the report. The residence time of material in the mill and subsequently the size distribution of the product are largely determined by the grate spacing. In addition, other comminution parameters such as feedrate, moisture content, mill speed, etc. influence the product size distribution. The effect of these variables is also considered in detail in another section of the report. There are several safety precautions that must be included in the design of size-reduction installations that involve the use of a hammermill. In this regard, it is important to note that because of the rotating hammers, certain types of large objects (metal objects, for instance), tend to be thrown out or ejected because of impact with the swinging hammers. These airborne objects, which leave through the input opening, are potentially dangerous to the operators of the equipment, especially to the operator loading refuse or to the input conveyor. A chain curtain is often hung over the input opening to deflect the objects that are ejected.

In the vertical shaft machines, the rotor is placed in a vertical position, with the input material moving parallel to the shaft axis, assisted by gravity. Several hammermill-type machines using the vertical principle are being used. A variation of the vertical principle is embodied in a relatively new machine known in the industry by its commercial name - the Eidal grinder or shredder. The principle followed in the design of the machine differs from that of the hammermill in that size-reduction is accomplished by a set of gear-like teeth installed in a rotor (see Figure 4) that fits in a stationary ribbed housing. After the material to be ground is introduced into the upper part of the machine, it passes a set of breaker bars by means of which large objects are torn apart. The material then enters the space between the rotor teeth and the housing ribs. Size reduction occurs in this part of the machine as a result of the induced shear and the mutual self-comminution interaction between the various types of materials. Since the space between the rotor and the housing is tapered, smaller objects are continually worked downward and eventually exit via a peripheral opening at the bottom. The dimension of the opening in this extraction area can be varied. Therefore, it theoretically is possible to adjust the size of the product. Measurements of the size distribution of refuse ground under both the coarse and fine settings show that there is no significant difference in the size distribution of the product leaving this type of grinder. The power requirements of the Eidal grinder are similar to those of the hammermill-type grinder. This machine is relatively slow turning and does not tend to reject objects in the manner of the hammermill.

Additional aspects of size reduction equipment, including installation and material handling, have been previously considered (12, 13).

Utilization and Location of Shredders

An appreciation of the degree to which shredders are being utilized in the solid waste processing industry can be obtained from a recent compilation prepared by Waste Age (14). In 1971, the Waste Age survey revealed 27 municipal-scale waste shredding installations. The number had increased to 87 by 1974 and to 134 by 1975. Table 4 shows the states that have municipal-scale shredding operations and the dates of first installation.

TABLE 4. MUNICIPAL-SCALE SHREDDING OPERATIONS, BY STATE OR COUNTRY AND DATE OF FIRST INSTALLATION[a]

State or country	Date	State or country	Date
Alabama	1965		
California	1969	New Jersey	1974
Colorado	1972	New York	1969
Connecticut	1972	North Carolina	1974
Delaware	1972	North Dakota	1975
Florida	1967	Ohio	1968
Georgia	1963	Oregon	1973
Illinois	1970	Pennsylvania	1966
Indiana	1970	Rhode Island	1972
Iowa	1973	South Carolina	1973
Kentucky	1962	South Dakota	1975
Louisiana	1975	Texas	1965
Maine	1972	Vermont	1968
Massachusetts	1973	Washington	1970
Michigan	1967	West Virginia	1975
Missouri	1969	Wisconsin	1958
Montana	1973	Canada	1970
Nebraska	1974	Jamaica	1962

[a] Data from Waste Age (14).

The Cal Waste Processing Facility

Scientific studies require the ability to systematically modify and control the conditions and parameters germane to a particular investigation. Consistent with this requirement, a size-reduction facility capable of operating on a scale resembling a commercial installation and yet able to produce laboratory quality data was developed for the purposes of conducting the comminution studies sponsored by EPA. The waste processing facility is located at the University of California's (Berkeley) Richmond Field Station. Although the initial emphasis of the laboratory was on size reduction, the facility was later expanded to include complete front end dry processing as well as certain types of back end processing for material and energy recovery. Since the system is modular and differs in many aspects from other waste processing schemes, this processing facility has been called the Cal Recovery System as a means of providing it with an identity. A brief description of the features of this facility follows.

The comminution device is a 10 ton/hr Gruendler Model 48-4 hammermill with 44 free-swinging manganese steel hammers. This machine was formerly at the Johnson City Tennessee Compost Plant and was moved to the Richmond Field Station site after the size reduction in refuse processing research had gotten underway. Power to the hammermill is supplied through a variable speed drive system from a motor rated at 250 hp, 480 V, 3 phase, 310 amps, and 1,200 rpm; the electrical power consists of 480 volts supplied by three 100-kilovoltamps (KVA), 400-amp transformers. A motor starter provides starting, stopping, and overload protection. With the starter, the large current draw (1,600 to 1,800 amps of a 250-hp induction motor) during direct line startup at 480 volts is reduced to a workable draw of 800 to 900 amps by initially providing a reduced voltage (285 volts) to the motor. After a period of about 10 seconds, full voltage is applied. In essence, the overload protection consists of overload relays with heater coils sized to 310 amps and a thermal protection device to guard the autotransformer against overheating. In addition in this installation, an A.C. load current relay and timing relay were included to prevent "blowing" of 12 12,000-volt fuses protecting our 300 KVA transformer bank should a blockage occur in the grinder. The power cable consists of three lines of 500-mcm cable.

The variable speed drive consists of two Gates Super HC Powerbands (four strands each) and five Gates Super HC QD sheaves and bushings (see Figure 8). The speed ratios are 1:1, 1.22:1, 1.52:1, and 2.16:1, and they correspond to 1,200, 985, 790, and 555 rpm at the grinder shaft, respectively. In most commercial installations, the motor is attached directly to the rotor shaft with a Falk steel flex coupling or some type of hydraulic coupling. Here the variable speed drive was required because grinding speed is an important comminution parameter and documenting its effects was part of the study. In certain instances, however, space or equipment layout considerations may make it advantageous to use a belt drive. But the motor, and in some cases the grinder bearings, usually are not sufficiently sturdy to handle the radial load caused by the belt tension (on the order of 4,400 lb in our case). A jackshaft and bearing assembly can be inserted to compensate for this lack. Again, as a design guideline, in this installation 8V-type v-belts were needed to transmit the 250 hp from motor to grinder. An inherent

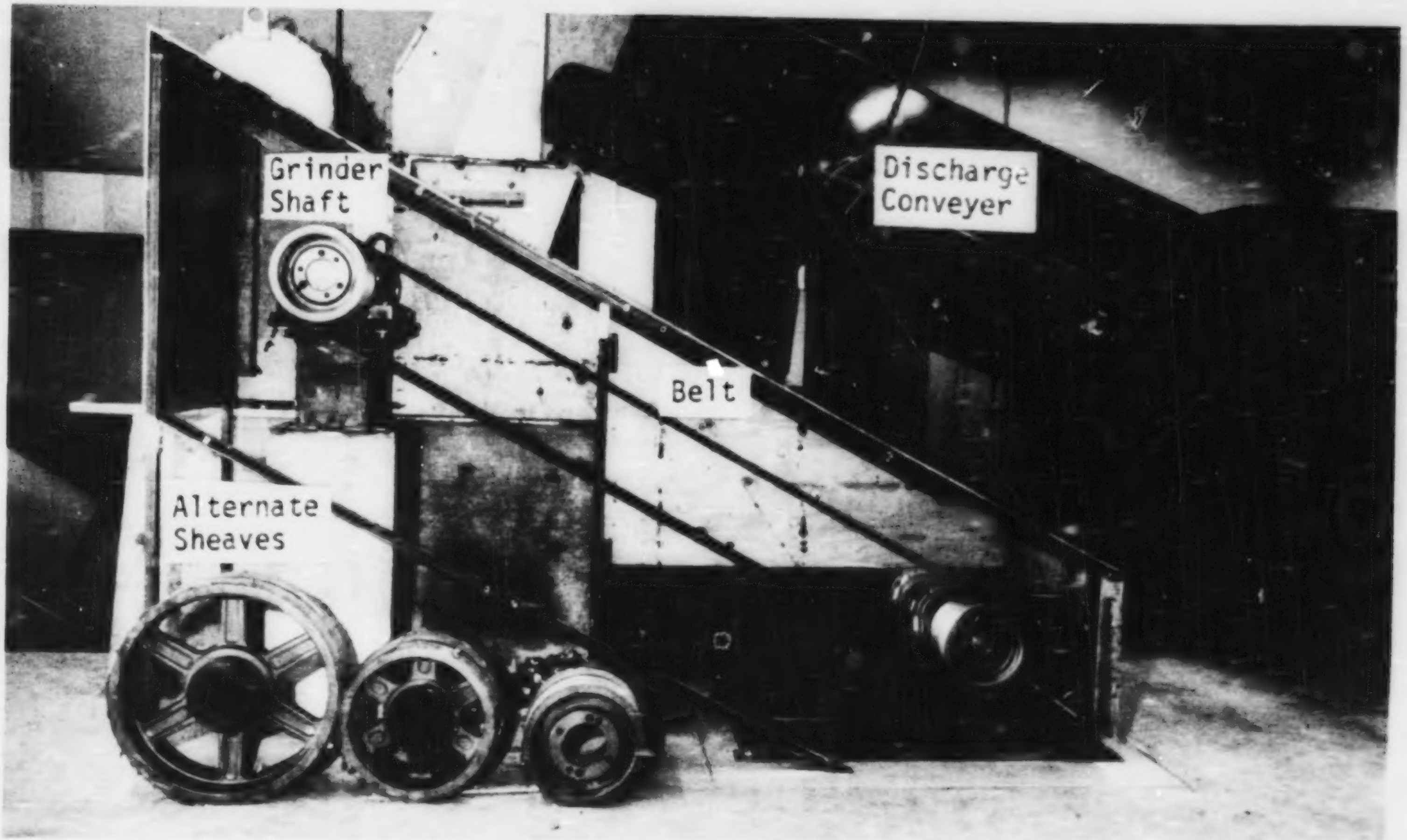
Grinder Shaft
Discharge Conveyer
Belt
Alternate Sheaves

Figure 8 Overall View of the V-belt (Alternate Driven Sheaves are shown in Foreground)

disadvantage of a belt drive system is that it requires a movable motor base so that the position of the motor can be adjusted to apply the necessary belt tension. On the other hand, a chain drive would require a lubrication system.

Mounting the grinder is an important aspect of developing a trouble-free facility. For example, the grinder must be mounted on a foundation structure massive enough to absorb a high degree of vibration and thus result in a smooth-running system. The foundation must be suitably isolated from the enclosing structure so as to avoid transmitting the vibration to the building. In constructing the foundation, sufficient clearance must be allowed between the output of the grinder and the discharge conveyor to prevent the ground material from jamming. A clearance of 4 ft was provided between the grate bars and the discharge conveyor. The base of the foundation is a solid concrete mass extending 6 ft below the floor level. A low water-to-cement ratio concrete (4-in. slump) with 3/4-in. reinforcing iron was used. Although this is a "thick" concrete and somewhat hard to place, it allows a high compressive stress. The full strength of about 3,000 $lb/in.^2$ cannot be reached until the concrete has cured for several weeks. The grinder is secured to the foundation through six 1-in. bolts present in the concrete. Isolation material was placed between the foundation and the existing floor of the building.

Steel belt, piano-hinge-pusher, flight-type conveyors were selected for both the feed and discharge. To accommodate the grinder, the feed conveyor was arranged to have a 22^o angle of incline. Its belt is 4 ft wide. As a design guideline, a belt speed of 7 ft/min would be required to deliver 12 tons/hr with an 18-in. depth of refuse on the belt. Since effects of feedrate were part of the investigation, the input conveyor has a variable belt speed. The variation in belt speed (from 1.8 to 7.0 ft/min), accomplished through the use of a variable-pitch drive sheave and two interchangeable driven sheaves, enables the feedrate to be governed from 1 to 10 tons of packer truck refuse per hour. The controls of the conveyor in this installation are such that the feeding action is synchronized with the power demand of the grinder. The synchronization was such that feeding was stopped when the electrical current demand of the grinder reached a preset level. The discharge conveyor used to remove the ground refuse has a 30^o angle of incline. (The ground material has a particle size such that 80% of it passes through a 2-in sieve.) Since the belt width is 3 ft, a belt speed of about 10 ft/min is required to remove 12 tons/hr of the ground material.

Instrumentation is available for continuous monitoring of power consumption and surges, and also rotational speed of the grinder shaft. A 480-V, 5-amp, 3-phase watt hour meter is used to measure the energy consumed by the grinder motor. To study the power surges, the current from one motor leg is monitored using a strip chart recorder. The rpm of the grinder shaft is measured electronically using an electromagnetic pickup and a Hewlet Packard Counter.

The size reduction portion of the Cal Recovery System is shown in Figure 9. A working relationship established with a local scavenger company (Richmond Sanitary Service) allows a variety of waste streams such as domestic and commercial packer truck refuse to be analyzed and processed. The laboratory has also processed the University waste stream generated on the Berkeley campus. This is a unique stream in that it contains on the order of 90% high-grade paper fraction. This material can subsequently be processed into a high-grade mixed paper waste. The additional features of the system, which were developed after the size reduction studies matured, are described as follows.

The next stage of processing involves air classification, where the stream is separated into light and heavy fractions - the so called lights and heavies. A schematic representation of the basic dry process is given in Figure 10. Air classification and heavies processing equipment is shown in Figure 11. Here the air classifier is fed directly from the grinder discharge conveyer. With typical packer truck refuse, the split of the incoming material stream after air classification is about 70% lights and 30% heavies. The heavy fraction, essentially devoid of fiber, is further processed into its components, which consist of ferrous and nonferrous metals, glass, and organic and miscellaneous compounds. Referring to Figure 10, this processing can be delineated as follows: The heavies, conveyed from the bottom of the classifier, first pass under a ferrous magnet whose belt travels perpendicularly to the discharge conveyor causing the ferrous scrap to be ejected into an adjacent bin. The stream then proceeds into a trommel screen, where the minus fraction is conveyed to a device that results in the separation of this stream into a glass-rich fraction and an organic fraction. The plus fraction component of the trommel screen contains aluminum, organics, and other miscellaneous materials (Figure 11).

The air-classified light fraction ("lights") exits the top of the classifier and is de-entrained from the air stream by means of a cyclone separator. As seen in Figure 12, the lights are pneumatically conveyed to the top of the cyclone, where the material and air are separated. The duct leading to the fan as well as the fan discharge can also be seen. Basically, the air-classified light stream is predominantly fiber, but it is contaminated with plastics and fines composed of myriad substances, principally fine glass, dirt, some fine organic components, etc. The contaminating material is removed by screening (see Figure 13). Here the light fraction is removed from the cyclone by means of a rotary air lock feeder and then conveyed to a trommel screen for removal of the fine contaminants. A number of options are

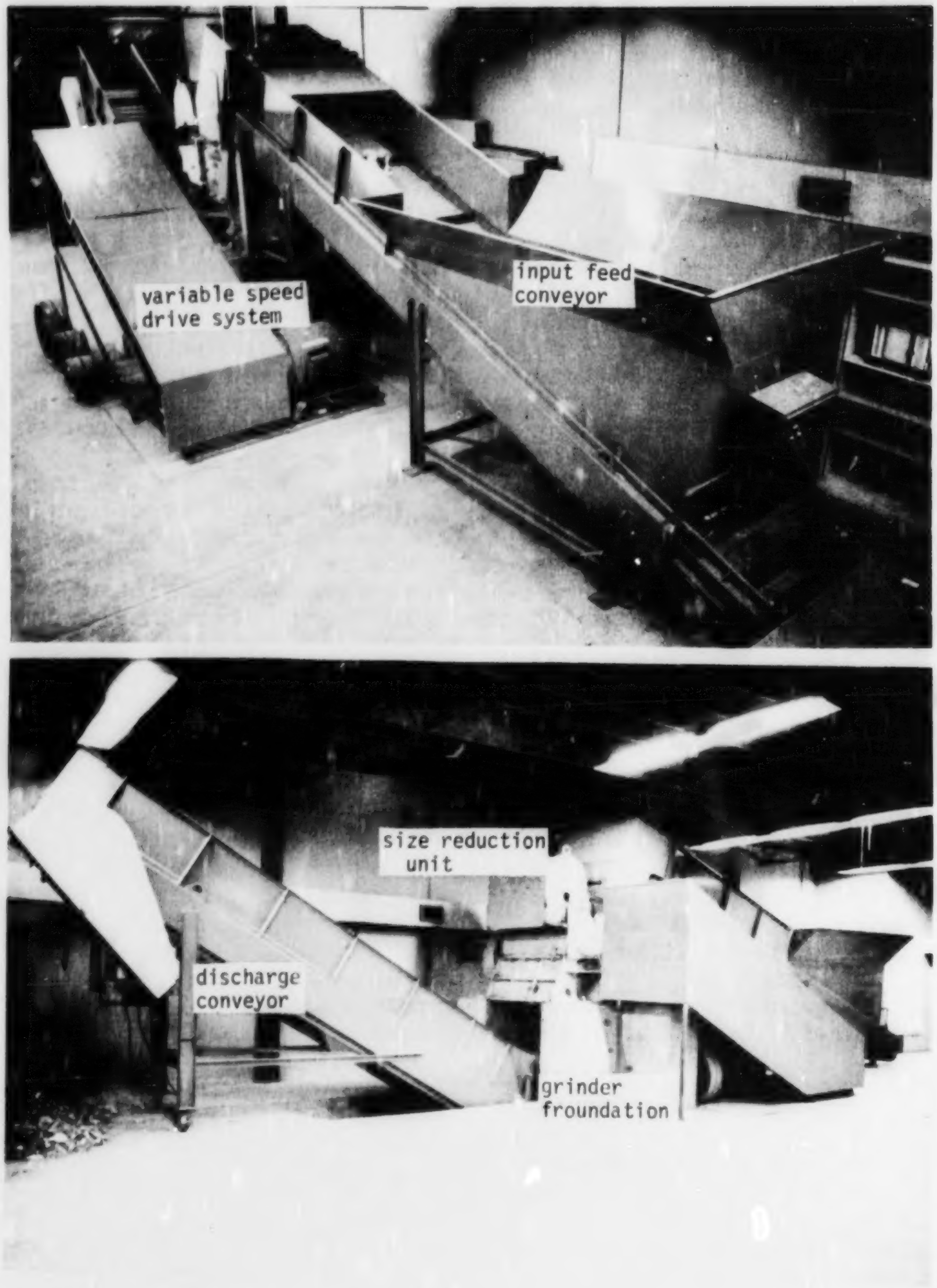
variable speed drive system
input feed conveyor
size reduction unit
discharge conveyor
grinder froundation

Figure 9 Input Conveyor and Grinder (Size Reduction Unit)

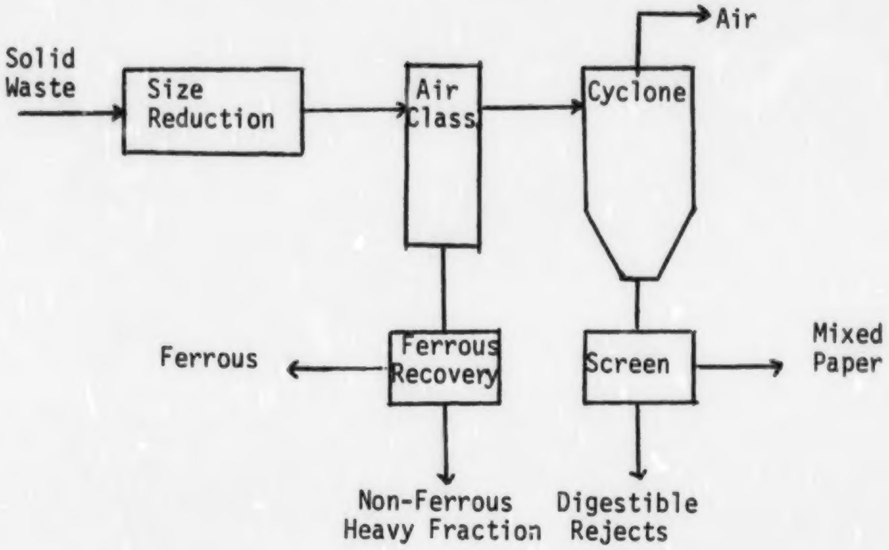

Figure 10 Basic Dry Plant

available for processing the cleaned light fraction (Figure 14). They are essentially as follows: 1) The material can be baled and sent away to be used as a fuel supplement, or it can be shipped to a paper mill equipped for handling secondary fiber contaminated with plastic, hot melt, etc. Since almost all of the organic substances have been removed, the baled material will not deteriorate when stored - that is, it has a long "shelf-life." 2) The material can be subjected to further size reduction and used as a fuel for certain types of combustion applications. This option is attractive in view of the present demand for energy sources - as contrasted with the existing uncertain secondary fiber market. 3) The material can be further processed by way of a wet processing step. At this point, it should be noted from the preceding description that the system has followed a basic principle of subjecting as little as possible of the incoming waste stream to the wet phase of the process, which is the subject of the following paragraph. It is important to note that when the material is used as energy (item 2), the subsequent fuel has a heating value on the order of 7,300 BTU/lb, an ash content of 5% to 10%, low sulfur content, and combustion compatibility with coal, gas, or oil. The further densification of this material into pellets enhances its transportation, storage, and in some cases its feeding characteristics.

The wet phase of the system, shown schematically in Figure 15, is designed so that contaminants remaining after the dry processing of the lights are efficiently removed. The wet phase is begun by pulping the cleaned light fraction from the dry

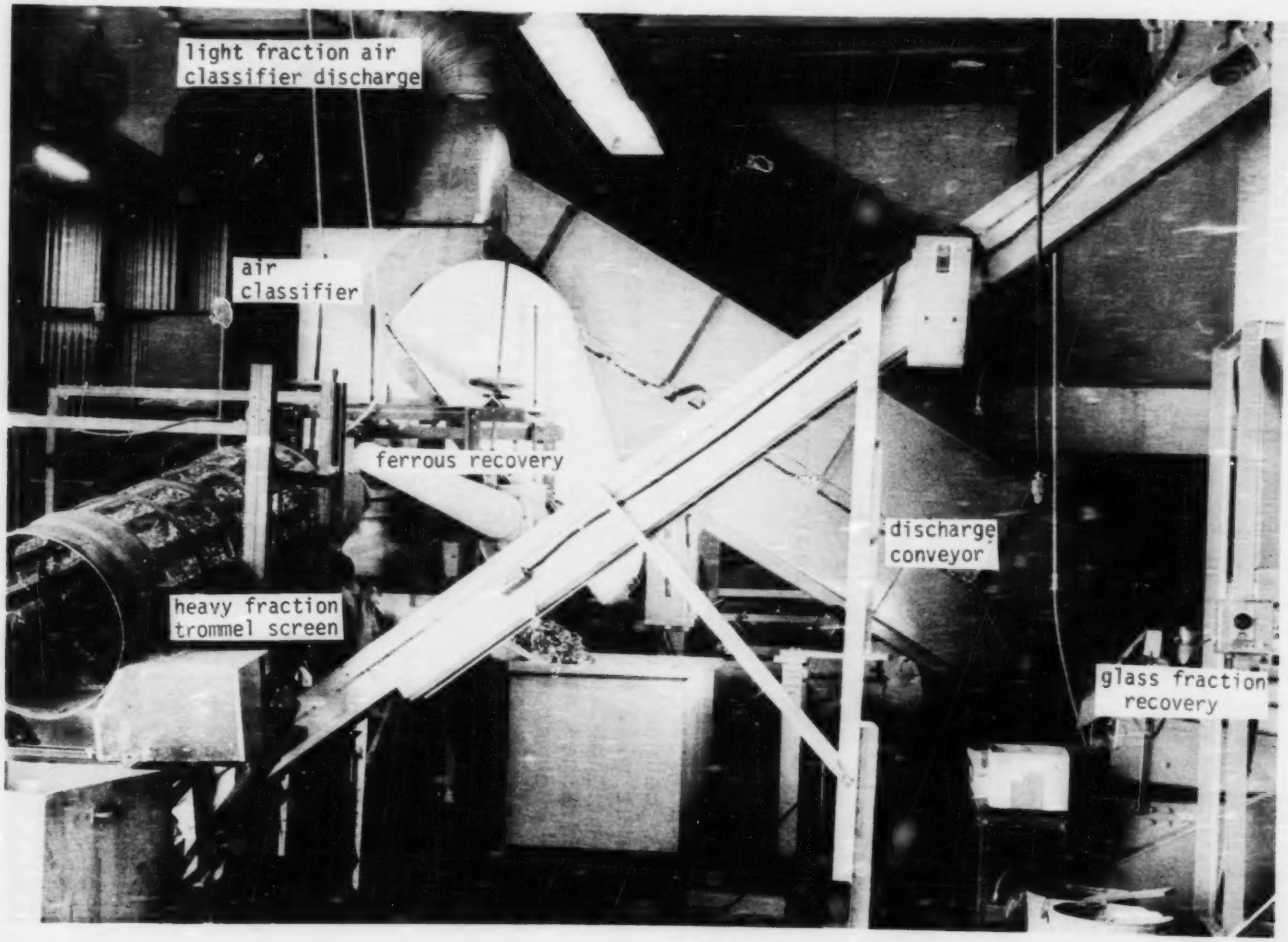
light fraction air classifier discharge
air classifier
ferrous recovery
heavy fraction trommel screen
discharge conveyor
glass fraction recovery

Figure 11 Grinder Discharge into Air Classifier and Heavies Recovery

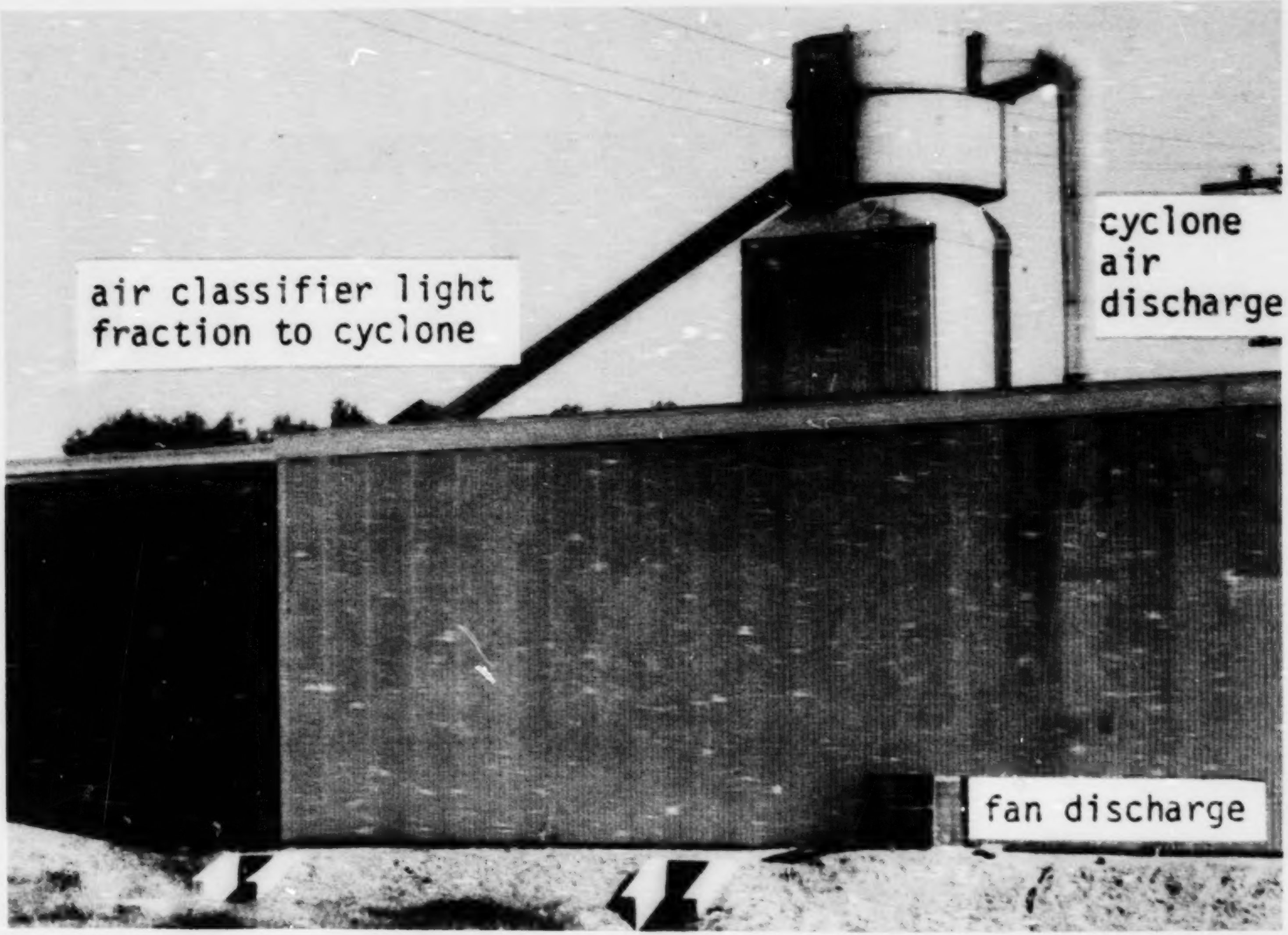
air classifier light fraction to cyclone
cyclone air discharge
fan discharge

Figure 12 Light Fraction Processing Facility - Air Classifier Light Fraction Discharge, and Cyclone

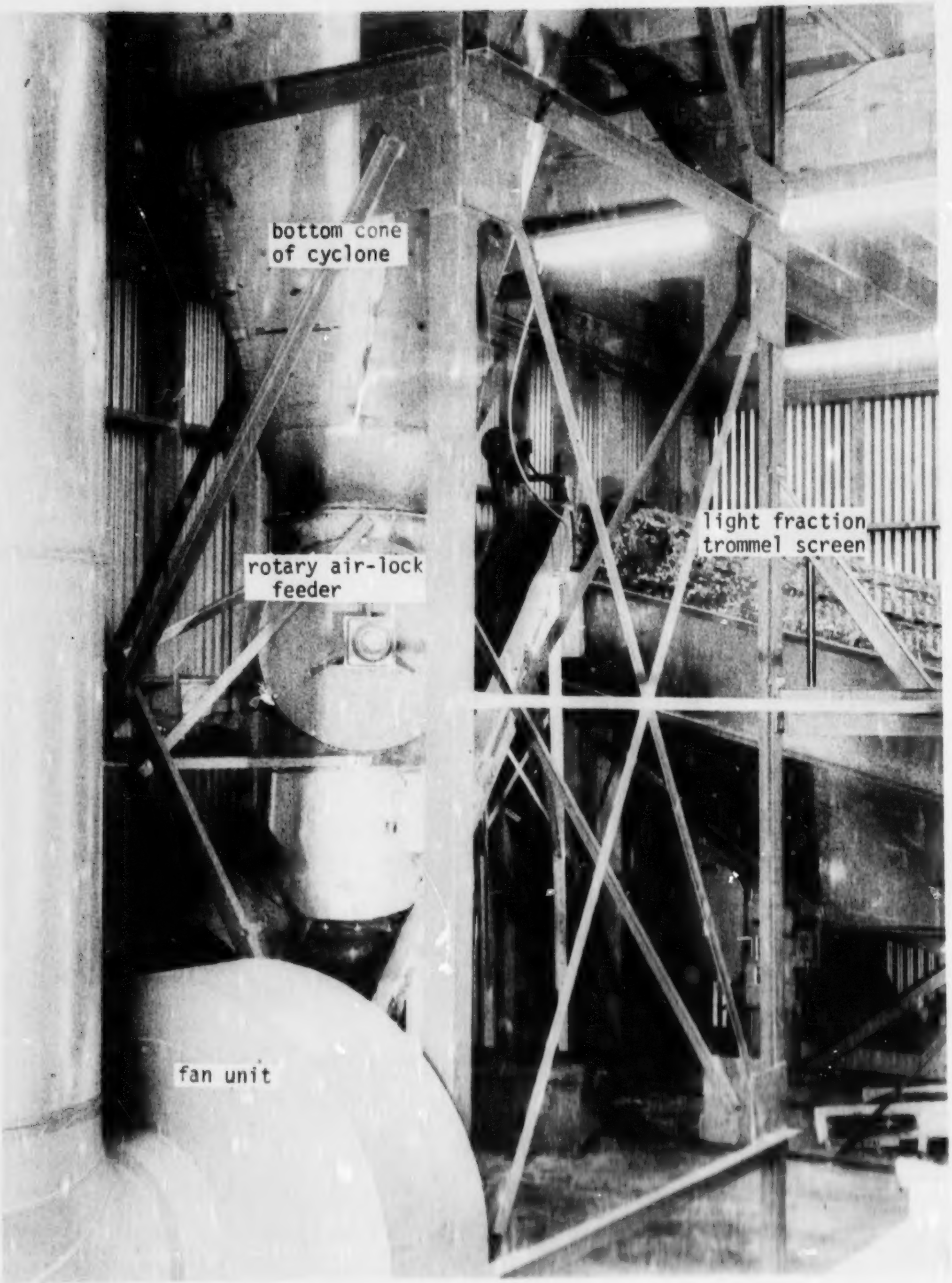
bottom cone
of cyclone
light fraction
trommel screen
rotary air-lock
feeder
fan unit

Figure 13 Components of the Light Fraction Processing Facility

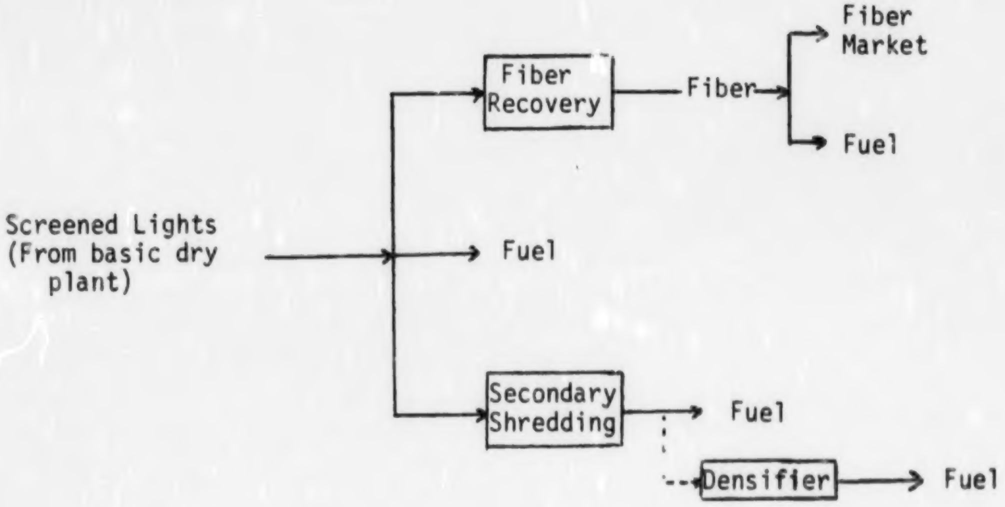

Figure 14 Alternatives for Screened Lights

process at a consistency of about 3% in a manner that allows the fibers to be slurried while the plastic component retains its large particle size. A conventional ragger can be incorporated into the pulping operation. Plastic removal follows pulping. The pulper discharges into the head tanks, which feed the plastic removal screen. This operation is designed to dilute the fiber slurry to a consistency of about 0.5% at the time the plastic is being removed. A 0.5% concentration is compatible with centrifugal cleaning. The fiber slurry after plastic removal is pumped to the first holding tank. Each tank communicates with the first and second stage of centrifugal cleaning where "triclean-type" cleaners are used. In the first step, very fine glass, grit, and dirt contaminants as well as fiber bundles and some usable fibers are removed. These materials exit through the bottom of the cyclone with which centrifugal cleaning is accomplished, while hot melt, wax, and some remaining fine plastics are discharged through the center probe of the cleaner. Since the reject stream contains usable fibers, a separate step is used to clean it. The accepts from the reject cleaner are combined with the first stage cleaner accepts. The rejects from the reject cleaner are discharged from the system and constitute a fiber loss of about 5% of the total fiber entering the system. A similar procedure is followed in the second cleaning step. However, because the center probe and bottom rejects are considerably less contaminated than those from the first step, the stream is returned to the beginning of the first stage and reprocessed. In some cases, it may be desirable to include a large holding tank or

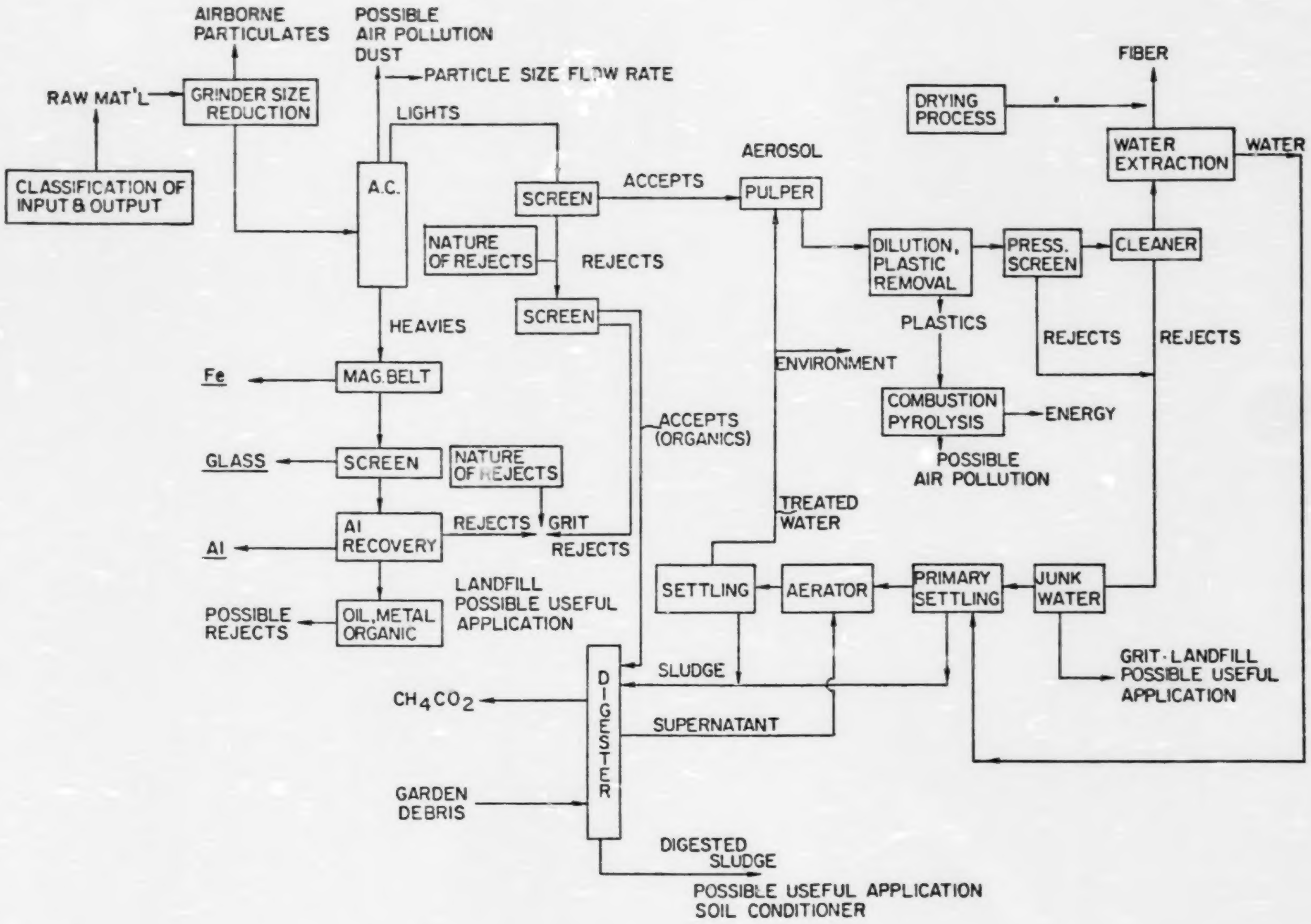
AIRBORNE PARTICULATES
POSSIBLE AIR POLLUTION DUST
PARTICLE SIZE FLOW RATE
RAW MAT'L
GRINDER SIZE REDUCTION
LIGHTS
FIBER
DRYING PROCESS
WATER EXTRACTION
WATER
AEROSOL
CLASSIFICATION OF INPUT & OUTPUT
A.C.
SCREEN
ACCEPTS
PULPER
NATURE OF REJECTS
REJECTS
DILUTION, PLASTIC REMOVAL
PRESS. SCREEN
CLEANER
SCREEN
HEAVIES
PLASTICS
REJECTS
REJECTS
ENVIRONMENT
Fe
MAG.BELT
COMBUSTION PYROLYSIS
ENERGY
ACCEPTS (ORGANICS)
GLASS
SCREEN
NATURE OF REJECTS
POSSIBLE AIR POLLUTION
TREATED WATER
Al
Al RECOVERY
REJECTS
GRIT
REJECTS
SETTLING
AERATOR
PRIMARY SETTLING
JUNK WATER
LANDFILL POSSIBLE USEFUL APPLICATION
POSSIBLE REJECTS
OIL, METAL ORGANIC
GRIT · LANDFILL POSSIBLE USEFUL APPLICATION
SLUDGE
CH_4CO_2
DIGESTER
SUPERNATANT
GARDEN DEBRIS
DIGESTED SLUDGE
POSSIBLE USEFUL APPLICATION SOIL CONDITIONER

Figure 15 System Flow Diagram

pond between the first and second cleaning steps. This would allow dirt loosened in the centrifugal cleaner and carried with the accepts to be floated off and thereby removed from the system. A noticeable brightening of the fiber takes place after the first stage of the cleaning process.

After the two cleaning steps, only an occasional small contaminant is present. The fiber produced in the two steps is suitable as a secondary stream for media and liner board manufacture. The addition of yet another cleaning step would lead to the production of a fiber slurry having only occasional speck contaminants. The final step in the fiber processing involves the use of conventional dewatering, and possibly of drying and baling for shipment. All of the process water is recirculated within the system. After each pass, 25% of the water is subjected to a conventional primary and secondary activated sludge wastewater treatment process. Makeup water is introduced at the pulping stage. Samples of the fiber recovered by way of the system have been subjected to rigorous analyses and found to be satisfactory by potential users in the paper-making industry.

Another module of the Cal Recovery System involves the anaerobic digestion of the light fraction rejects and the heavy organic fractions, shown schematically in Figure 16. After removal of the inerts, these two fractions are combined and mixed with sewage sludge and are introduced into an anaerobic digester in which a gas mixture composed primarily of methane (55% to 65%) and carbon dioxide (35% to 45%) is produced. The gaseous product can be used directly by way of injection into existing natural gas pipelines, or it can be scrubbed to remove the CO_2 and other impurities and used directly as a substitute for natural gas. Digestion results in a significant volume reduction of the heavy and light organic fractions and the production of a relatively stable sludge. The sludge can be used as a soil conditioner or as a burner fuel. It has a heating value of approximately 4,800 BTU/lb.

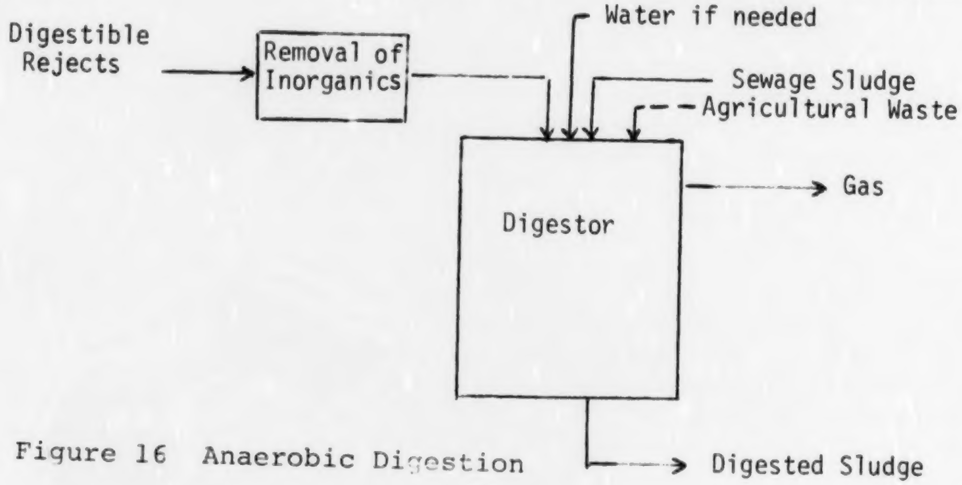

Figure 16 Anaerobic Digestion

SECTION 2

SIZE DISTRIBUTION

The waste stream contains a multitude of different-sized objects. Collectively, they give rise to a material, the size of whose components usually spans an order of magnitude. Thus, the material is said to have a certain size distribution. Several modern solid waste management practices dealing with materials and energy recovery take advantage of the existence of the material size distribution. Certain types of materials in both the raw and processed waste stream tend to occur within various size-range bands within the overall size distribution spectrum. Distributions for various states of the waste stream are given. These include the raw unprocessed packer truck refuse, the waste stream after being subjected to various shredding or size-reduction operations, and the waste stream components after recovery with a dry, front-end processing system.

RAW REFUSE

Characterization of the raw waste stream's size distribution is important for several reasons, which include the ability to successfully use analytical predictive methods for determining processed product size distributions, the successful operation of certain types of recovery schemes that involve the raw waste stream, etc. Detailed studies of the composition and size of the raw waste stream on an item-by-item basis have been performed by Winkler and Wilson (15). They examined form samples totaling 1,152 lb from high-, middle-, and low-income neighborhoods. These samples were collected in January in such a manner that a 600-lb sample came from one source, and 175-lb samples came from other sources. No statistically significant differences were found. In this area there is also a separate municipal collection for food waste (garbage) that would tend to affect relative amounts in each waste category. This group also examined 915 lb of waste from Middlebury, Vermont, which was collected from mid March to June. This sample contained a large fraction of commercial refuse. This, along with the fact that an alternate site for disposing yard and garden wastes was available, had a tendency of diluting the domestic waste contribution. Waste stream objects were categorized by weight, dimension (length, width and height), and material composition. In this study, objects were defined as items that would be expected to remain intact after a reasonable amount of mechanical handling. Plastic bags were allowed to rip open after they were grasped at two points and shaken; in effect, this was considered mechanically breakable. Size analysis went down to 1 in., with the remainder being considered as miscellaneous. Since their findings indicated that many objects in the waste steram are composite materials, secondary and tertiary material composition classifications were performed. Although some 50 categories were established, the bulk composition of their material was reported in terms of 9 principal categories (see Table 5).

TABLE 5. BULK COMPOSITION (WEIGHT PERCENT) OF REFUSE SAMPLES (Percent by weight, wet basis)

Constituent	Cambridge, Mass.	Middlebury, Vt.
Paper	35.8	48.9
Newsprint	7.8	3.0
Metals	9.2	9.1
Ferrous	8.3	8.8
Nonferrous	0.9	0.3
Glass	18.6	16.6
Plastics	4.1	2.4
Cloth, rubber, leather	5.2	2.5
Wood	1.1	0.4
Food	5.9	4.7
Yard and garden	0.5	0.3
Misc. and uncategorized	19.6	15.1
	100.0	100.0

The sample size and the manner in which it is obtained are important aspects of properly categorizing the waste stream. Wilson (15) found and reported that perhaps the most satisfactory method of obtaining a typical sample of manageable volume is to take material from the lengthwise side of the pile dumped by a packer truck instead of choosing a sample from one end. In this manner, Wilson claims a sample of the entire load may be obtained. Other investigators have obtained samples by randomly grabbing them from conveyor belts or by using such procedures as the quartering technique, in which a sample of only several pounds is eventually obtained from a large sample of several thousand pounds. Both the American Society for Testing and Materials (ASTM) and American Public Works Association (APWA) have put forth procedures dealing with the use and application of the quartering technique. In general, adaptation of this procedure does not favor materials with large particles. Further, most of these procedures have been applied in the analysis of homogeneous, usually brittle materials where the sample size is considered to be related to the characteristics of the material, the available form, and the requirements of the analysis and subsequent sample processing. Our experience with categorizing raw refuse is consistent with that of Wilson, and the sample used to obtain the size distribution of our raw waste was obtained in a similar fashion.

Some of the results of the Winkler and Wilson study (15) are given in Figures 17 and 18. Size distribution information is given in Figure 19, where the cumulative weight is given versus the longest dimension and also mesh size. The latter was calculated from the fact that an object must have at least two dimensions smaller than a given mesh size to pass through it. This, in effect, corresponds to a 100% screening efficiency. Histograms given in Figure 20 show the relation of objects and weights per ton versus size. Some of the interesting results of this work indicate that 70% of the objects have a length greater than 5 in. Also, half of the total weight of metallics, mostly cans, occurred in the 3- to 5-in. range and accounted for 40% of the refuse in this range. Approximately 94% of the bottles remained intact, caused a peak in the 5- to 10-in. range, and made up 38% of the refuse in this range. Further, paper objects predominated in the size range greater than 12 in. This material was estimated to have a high recycle value.

Both the composite and component size distributions of raw refuse have been reported by Ruf (8). His samples averaged from 4.7 to 16.5 lb and were obtained from the Gainesville, Florida, compost plant. This work used the random collection and a quartering procedure. In his thesis, Ruf presents an extensive review of sample selection and screening procedures. The results of his work for raw refuse size distributions are given in Figure 21.

The raw refuse size distribution can be compared to that obtained by Wilson and at the Richmond Field Station laboratory (Figure 41 p.74). Those given by Wilson fall in a larger size range than the Richmond and Gainesville data. Also, the Wilson data are approximately linear on a log-log plot of percent passing versus screen size, whereas, the other data tend to be more sigmoidal in character. These differences may have arisen because the Richmond and Gainesville data may be more representative of domestic packer truck refuse or the geographic variation of the waste stream.

SHREDDED REFUSE

After the raw waste stream has been processed through a comminution device such as a hammermill, its size distribution will be reduced by several orders of magnitude. At this point, expedient characterization must be by mechanical means rather than hard measurement. As mentioned previously, sample size

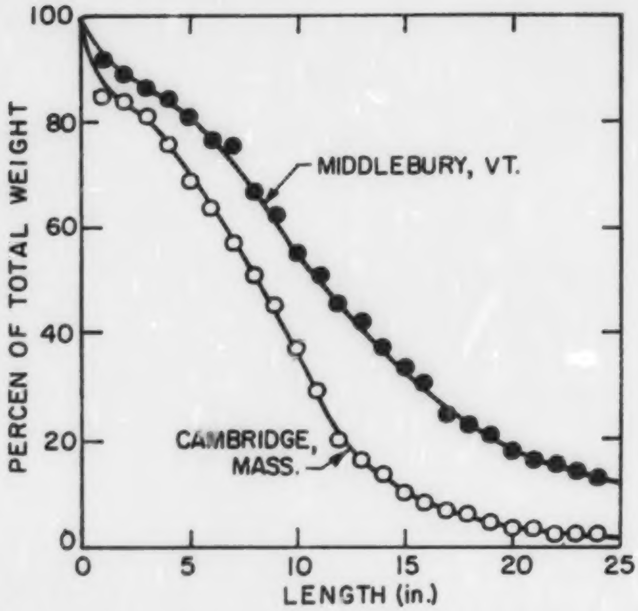

Figure 17 Cumulative Weight (% Raw Refuse Total) of Objects With Longest Dimension Greater than Given Lengths

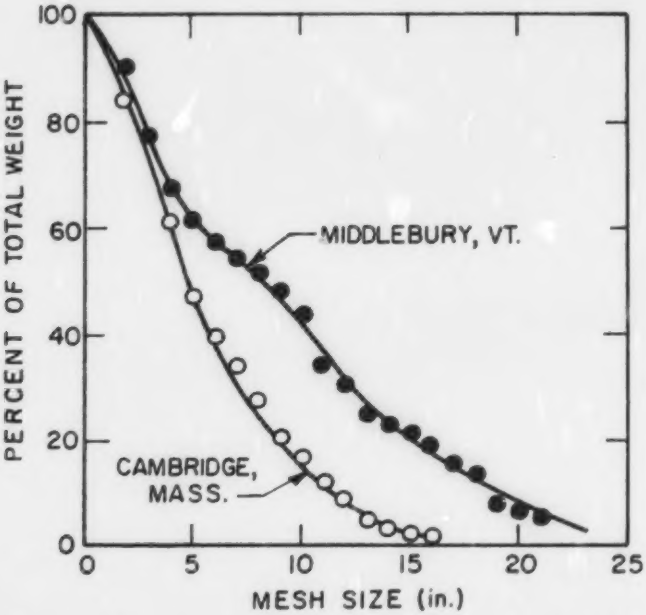

Figure 18 Cumulative Weight (% Raw Refuse Total) of Objects that Will Pass Through a Square Mesh, Plotted vs. Mesh Size

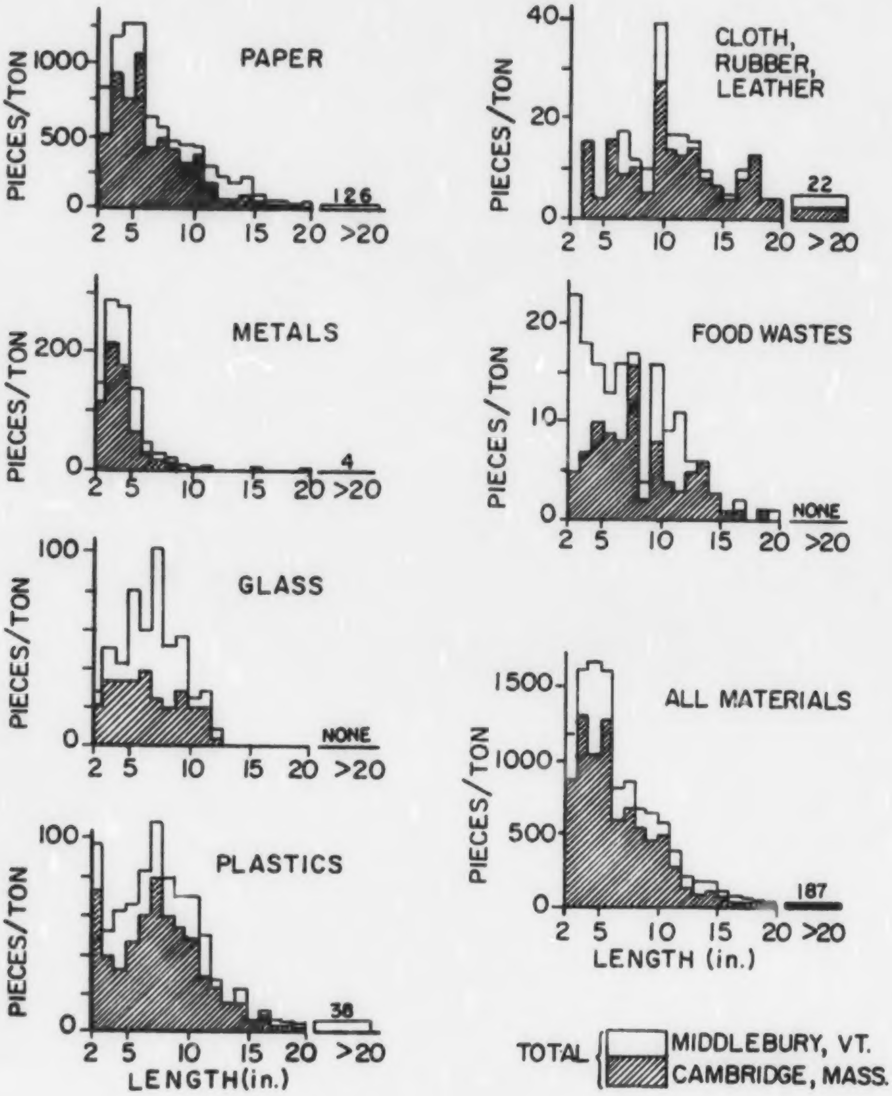

Figure 19 Number of Objects per Ton of Raw Refuse vs. Length (Longest Dimension of Object) for Principal Categories of Refuse. Total Height of Each Bar Gives Weighted Average of Cambridge and Middlebury data, with Relative Contributions Indicated by Shading. Note Different Vertical Scales.

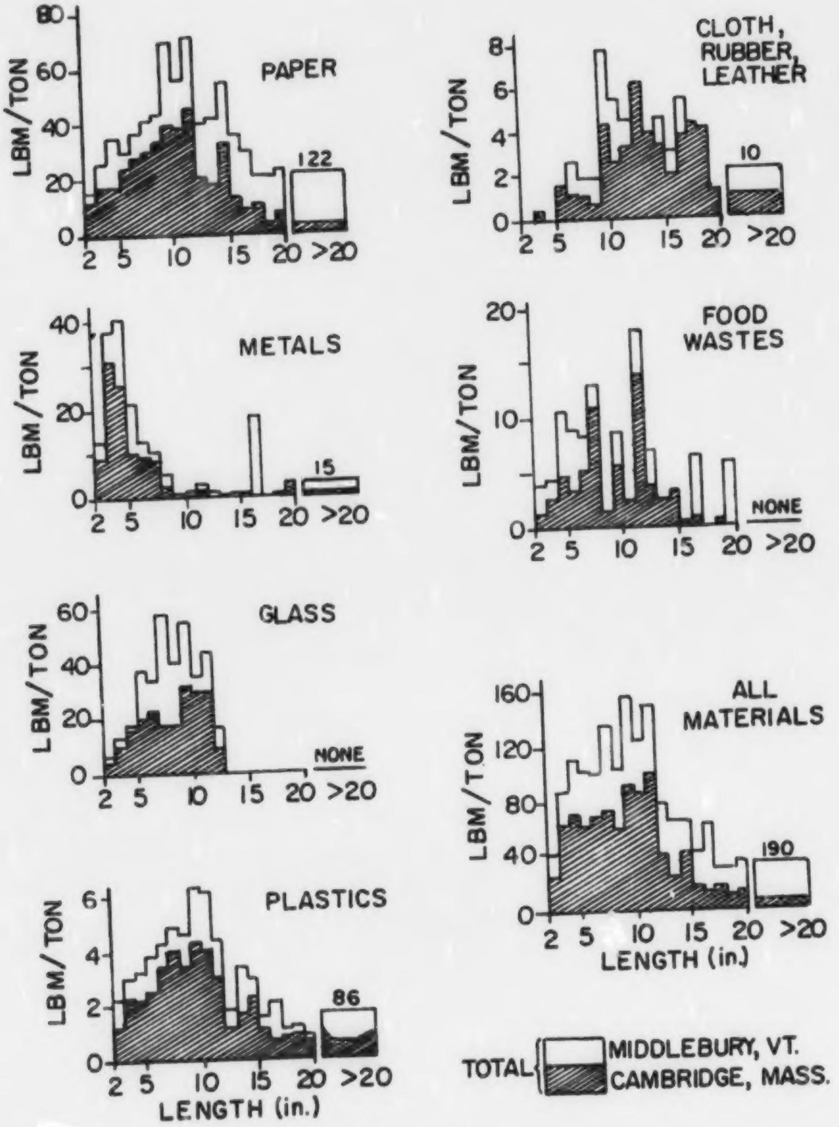

Figure 20 Total Weight per Ton of Raw Refuse of Objects in Given Length Ranges for Principal Categories of Refuse. Note Different Vertical Scales.

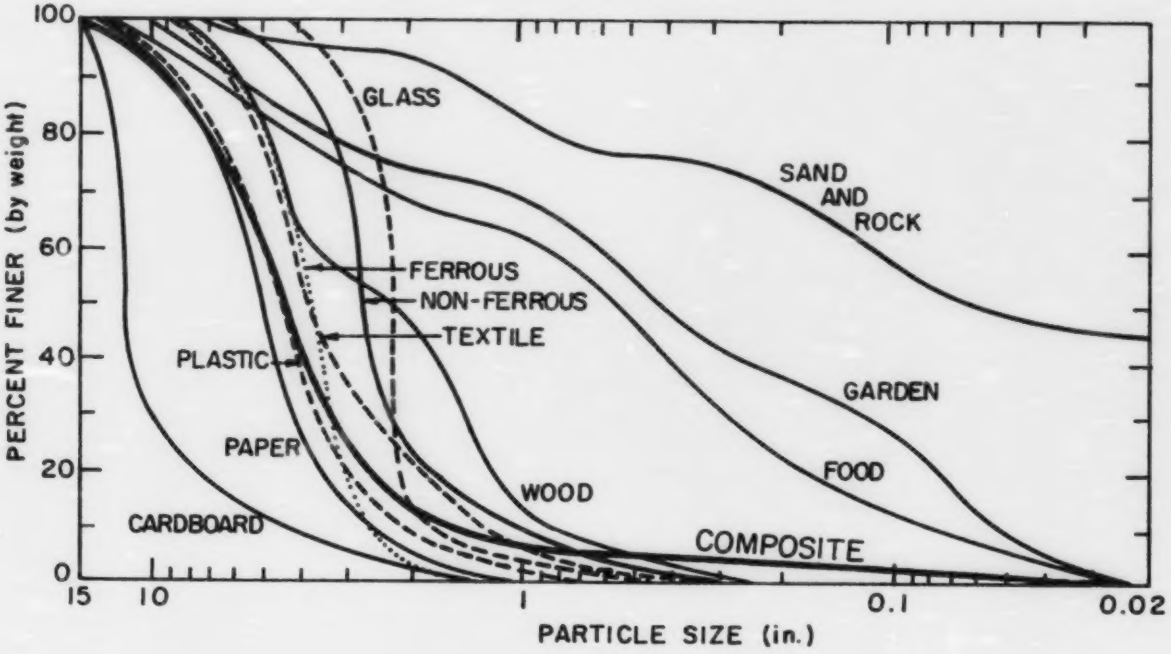

Figure 21 Cumulative Distributions of Raw Waste

determination and screening procedures have been established for characterizing homogeneous brittle materials such as ores, coal, etc. Shredded refuse, having only 25% brittle materials, poses certain additional problems in performing a size distribution analysis. The general area of screening materials has been reviewed in the thesis of Ruf (8). Details of sample size, sample preparation, screening times, peculiarities of various screens, etc. are given. In addition, Ruf elaborates on the fact that sieves classify particles according to geometric similarity regardless of the density and that both the shape of the particles and the shape of the openings affect the size of the particle that can pass through a given opening. The probability that a particle will present itself at an aperture depends on a number of factors, including the particle size distribution of the material, the number of particles on the sieve, the physical properties of the particles, the method of shaking the sieve, the dimension and shape of the particles, the geometry of the sieving surface (open area/total area), etc. In addition, the distribution given by the sieving operation also depends on the duration of sieving, the variation of sieve aperture, wear, errors of observation and experiment, errors of sampling, effects of different equipment and operations, etc. These factors suggest that there may be doubt in comparing the size distribution results obtained in various laboratories that follow widely differing procedures.

DISTRIBUTIONS OBTAINED AT THE CAL WASTE PROCESSING FACILITY

Extensive size distribution measurements of shredded refuse were made as a part of the comminution studies conducted at the University of California, Richmond Field Station laboratory. The details of the shredding and screening procedure are summarized as follows: Refuse was loaded onto the feed conveyor with a tractor loader. After some experimentation, a feeding procedure was established that produced a relatively constant feedrate. It is important to note that since feedrate is one of the comminution parameters, it must be known and controlled when the effects of other parameters are being determined. Thus size distributions must be reported for a feedrate as well as in terms of the other comminution parameters if they are to be completely meaningful. In our experiments, feedrate control was achieved by having the loader-operator concentrate on picking up the same volume of material each time, dumping the bucketfuls side by side on the belt, and using a mirror and levelling board on the conveyor. A value for feedrate is determined by weighing a size-reduced sample from a 3-ft section of the discharge conveyor. This was chosen as a matter of convenience, since the discharge conveyor has 4-in. cleats at 36-in. spacings on the belt. Knowing the sample weight, section length, and belt speed, the feedrate (m) can be computed as follows:

$$\dot{m} = \frac{\text{sample weight}}{\text{section length}} \times \text{belt speed}$$

Preliminary analyses of size distributions were performed as a means of determining what constitutes an appropriate sample size and what effects the various sieving parameters have on the size distribution. Initially, measurements of size distribution were performed by shaking a sample in a series of Tyler standard screens using a Ro-Tap testing sieve shaker. The sample size for a given run is a function of the material and the volume that can fit into the screens. In general, for ground refuse materials, the sample sizes were on the order of 100 to 200 g. Later, a Sweco 18-in. rotary screen was used to perform the size distribution analysis. The side parts on each deck of the screen were blocked so that all materials were required to remain on their appropriate screen in the screen deck assembly. In general, the sample sizes were larger (on the order of 5 lb) than those used with the Tyler screens. Typical screening times were 20 min with the Tyler screens and 5 min with the Sweco screens.

A moisture loss generally occurs during sieving, which has an effect on the percent passing a given sieve size. In other words, it is possible to define the percent passing as either (a) percent passing equal to the ratio of weight passing over sample weight before sieving (which reflects the initial moisture content of the material) or (b) percent passing equal to the ratio of weight passing over sample weight after sieving (which reflects the water loss during sieving). Again a correlation of experimental data requires that the basis on which percentages are calculated be given. Both methods of analysis have been presented here for comparison, and a distinction is made between them where appropriate.

A detailed description of the experimental procedure used in the field station studies is given below:

1. The hammermill was run at prescribed speeds, and the freewheeling power was measured by timing a number of revolutions of the meter disc.

2. The output conveyor belt was run at its fixed speed of 10 ft/min, and the input conveyor belt was run at a speed commensurate with the required feedrate. The raw material was then loaded onto the input conveyor belt for grinding.

3. The energy measurements were again carried out after steady state grinding process had been achieved (usually from 15 to 30 min) and generally were recorded over a period of 1/2 hr. The actual power for grinding the material was obtained by subtracting

the freewheeling power from the new power measurement. During this time, the feedrates were being monitored from the discharge end of the grinder.

A steady state is established when approximately equal and consistent values are obtained over a period of 1/2 hr for the recorder readings, power measurements, and weights of product samples taken from 3-ft sections between the cleats of the discharge conveyor; the values of power and feedrates must line within the limits given in Table 6.

4. Two samples of the product were taken at different times from the output conveyor belt. Each sample was divided into two parts - one part for wet sieve analysis and the other for dry sieve analysis and moisture content determination. The part for the wet sieve analysis was screened immediately and that for dry sieve analysis was predried before sieving.

   The term "wet sieve analysis" used here is different from the usual meaning in the terminology of the sieving process where the material is sprayed with water in damp screening. In this thesis it is used to denote the case in which the product to be screened is not predried but retains its own moisture from the grinding process.

5. The sieving was done in two stages. The very coarse and relatively large materials were removed from the sample by shaking the sample over 4-, 2-, 1-, and 3/8-in. wire mesh. Weights of the materials retained on these screens were recorded and included in the overall size distribution analysis.

6. The undersize from the 3/8-in. sieve was screened in batches of approximately 200 g on a Ro-Tap sifter for 20 min using a standard Tyler series (geometric ratio of 1/2) of sieves from 9,423 microns to 147 microns (100 mesh).

7. Weighings were made on a two-place Mettler balance. The weight of each fraction was determined by the difference between sample plus sieve weight and the weight of the empty sieve. This procedure was adopted to prevent errors introduced by transferring each fraction from the sieve to the balance before weighing.

8. To ensure the proper drying period of the sample

TABLE 6. ANALYSIS OF EXPERIMENTAL ERROR: FEEDRATE (TON/HR)[a]

Sample mean $\bar{x}$	Standard deviation σ_x	Coefficient of variation[b] C.V. = $\sigma_x/\bar{x}$
1.20	0.1414	0.1179
1.95	0.2828	0.1451
2.70	0.4243	0.1571
4.20	0.4243	0.1010
5.08	0.3889	0.0766
9.05	0.9899	0.1094

[a] Approximate 95% confidence interval for a single observation.

$$\text{Feedrate} = (\text{Feedrate})_{\text{observed}} (1.0 \pm t_{0.025}\ \text{C.V.}_{\text{average}})$$

$$= (\text{Feedrate})_{\text{observed}} (1.0 \pm 0.303)$$

[b] $\text{C.V.}_{\text{average}} = 0.1178$

for the dry sieve analysis, this sample was dried under the same conditions as the sample for moisture content determination in a thermostatically controlled, heated room at an average temperature of 80°F.

9. The moisture content was determined from weighing the wet sample initially and then subsequently over a period of time (24 to 36 hr) until no change in the weight of the sample was noticed in consecutive measurements. The percent moisture content given in this study was computed as percent moisture = [(wet weight)-(final dried weight)]/wet weight.

   Figure 22 shows a typical graph that was drawn to monitor the moisture content. A sample for moisture content analysis is split into two parts; the moisture contents for these parts are determined independently and the average value of these results is accepted as a representation of the condition of the experiment if these individual results lie within prescribed confidence intervals. Differences in the results of 1A and 1B arise from incomplete mixing of the product and also from differences in the proportions of the various material components in each part.

10. To study the effect of variations of moisture content on the grinding of refuse, the feed was sprayed with water at the inlet of the hammermill. Different moisture contents for different runs were obtained by varying the rate of water supply to the spray (2, 4, and 8 gal/min were found to be adequate to attain different conditions).

11. The whole procedure from 1 to 10 was repeated when the product from a primary grinding process was used as the feed for a secondary grind, and also when the product from a secondary grinding was the feed for a tertiary grinding process.

12. The precision of sieving was determined by splitting the primary product from preliminary grinding of raw packer truck refuse into 10 portions and sieving these as described above. The sample means and standard deviations and coefficients of variation were determined for

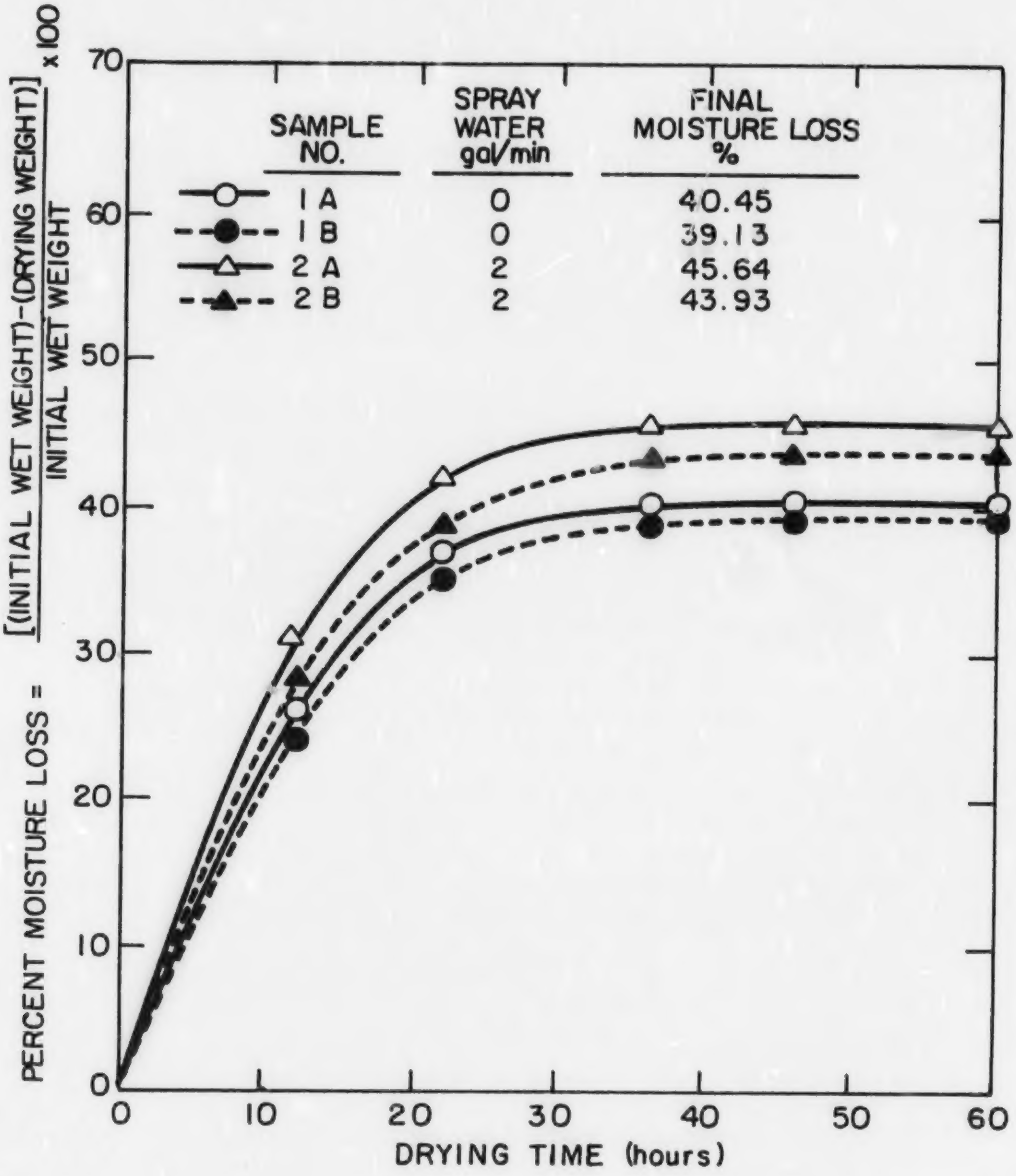

Figure 22 Moisture Content Analysis. Percent Moisture Loss vs. Drying Time

> the nine size fractions - 2-in., 1-in., and 1 x 2, 3 x 4, 6 x 8, 10 x 14, 20 x 28, 35 x 48, and 65 x 100 mesh.
>
> The overall precision of experiments was preliminarily estimated by conducting six independent experiments under the same conditions. The data for these experiments were pooled to obtain estimates of overall sample means and variances. For example, we notice that the coefficient of variation does not depend strongly on the mean moisture content with which it is associated; that is, they are all of the same order of magnitude. Thus it is reasonable to approximate the coefficient of variation for all moisture contents by the mean value of the seven moisture contents examined, C.V. average. Similar averages can be used for particle size, feedrate, and power consumption.

Some typical size distribution results are presented for representative grinding conditions in Figures 23-28. These curves show a downward concavity for primary, secondary, and tertiary grinding products. In addition, plots of ln(1/1-Y) vs. sieve size for the dry analysis indicate that these size distributions conform to the Rosin-Rammler distribution equation (Figure 29). The average value of the index n of the Rosin-Rammler equation for the size distributions of the primary grinding was found to be 0.99 (with a standard deviation, σ = 0.13), and 0.87 (with σ = 0.07) for secondary grinding, and 0.75 for tertiary grinding. The corresponding average values of the characteristic particle size, x_o (size at 63.2% cumulative passing) for the primary, secondary, and tertiary grindings were 0.61, 0.33, and 0.23 in., respectively.

The graphs for the wet sieve analysis show a similar shape to those of the dry sieve but have greater slopes in the smaller size range. The differences between the curves for the two analyses can be explained by the fact that, in the wet analysis, some of the smaller particles agglomerate with the bigger ones. This gives a higher percentage of retained weight on the bigger sieves and smaller values for sieves with small openings. Moisture losses during sieving of the wet samples also contribute to the differences between the results of the two analyses.

DISTRIBUTIONS OBTAINED AT MADISON

A project demonstrating the use of shredded refuse in landfilling was initiated by the EPA at Madison, Wisconsin, in 1966 (2). The shredding facility contains both a horizontal and a vertical hammermill. The former is a Gondard mill with free

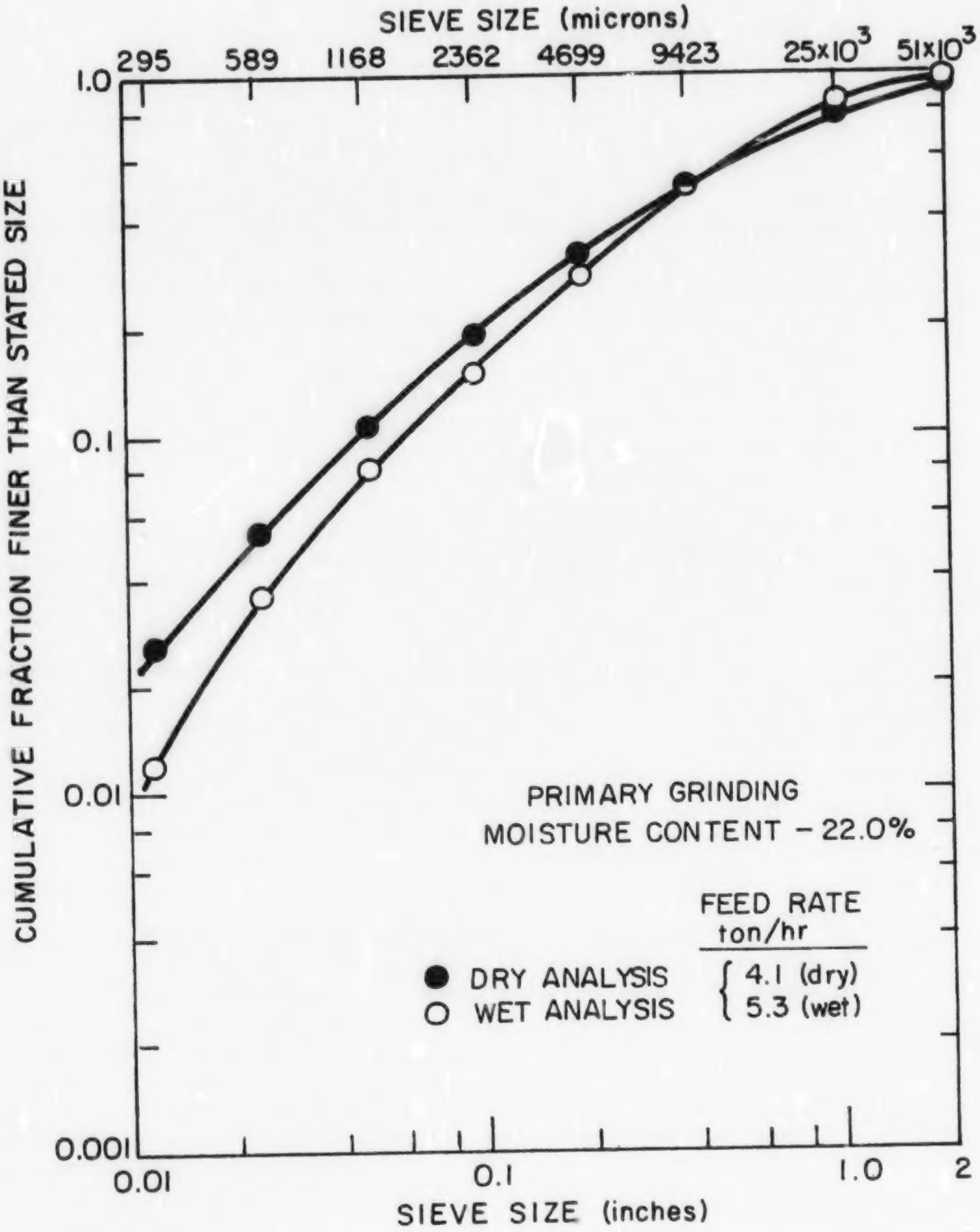

Figure 23 Product Size Distribution for the Primary Grinding of Municipal Refuse with 22.0% Moisture Content

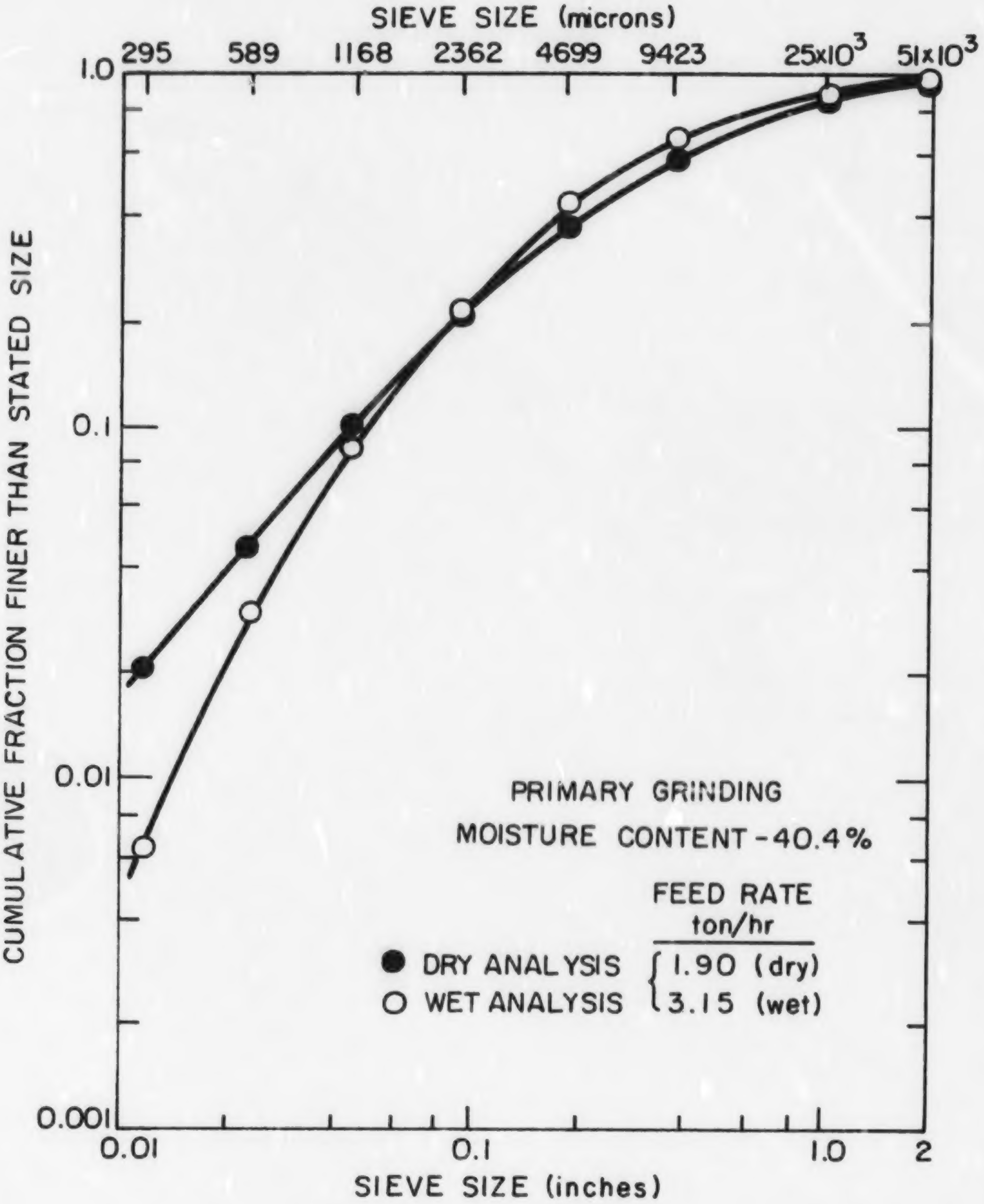

Figure 24 Product Size Distribution for the Primary Grinding of Municipal Refuse with 40.4% Moisture Content

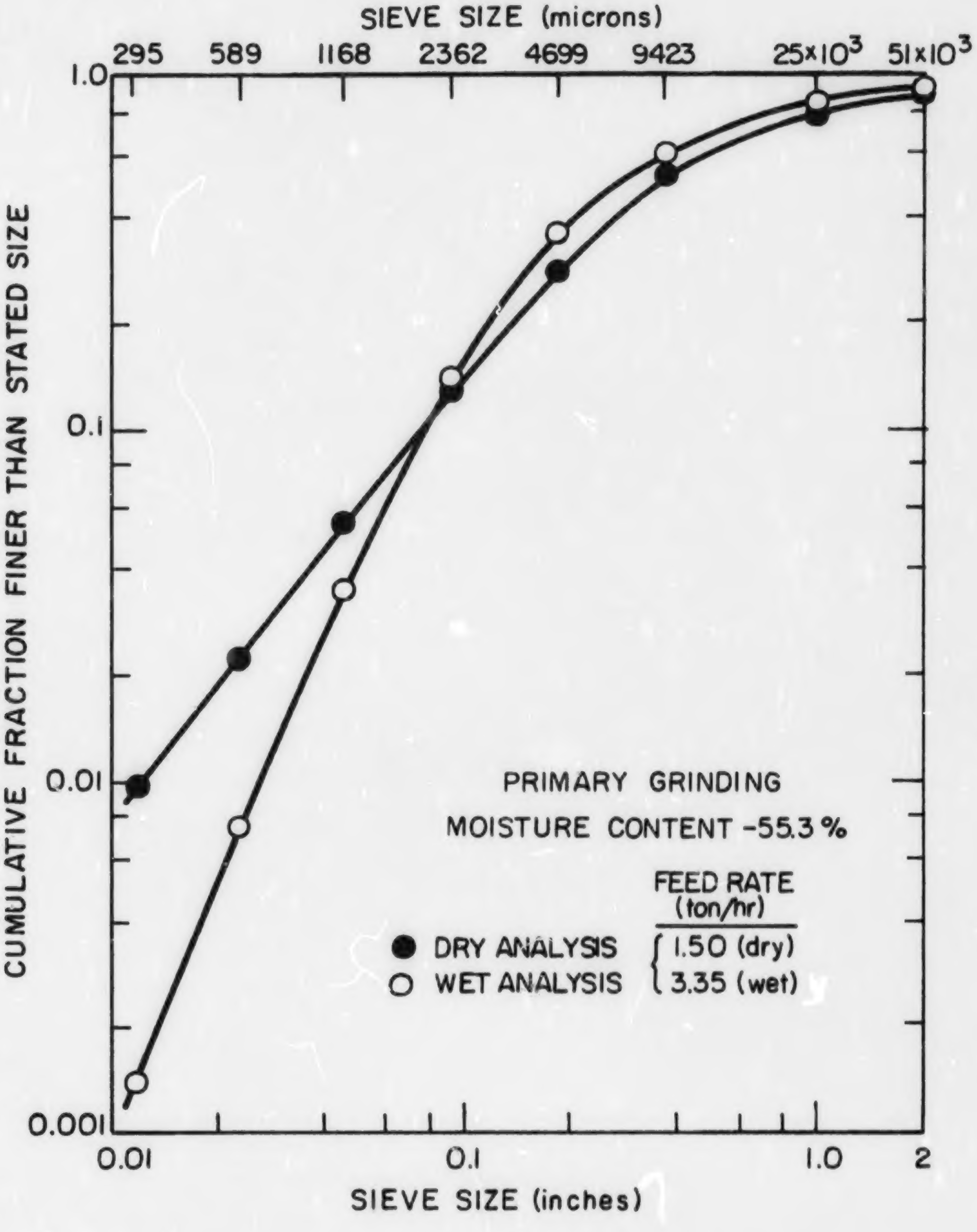

Figure 25 Product Size Distribution for the Primary Grinding of Municipal Refuse with 55.3% Moisture Content

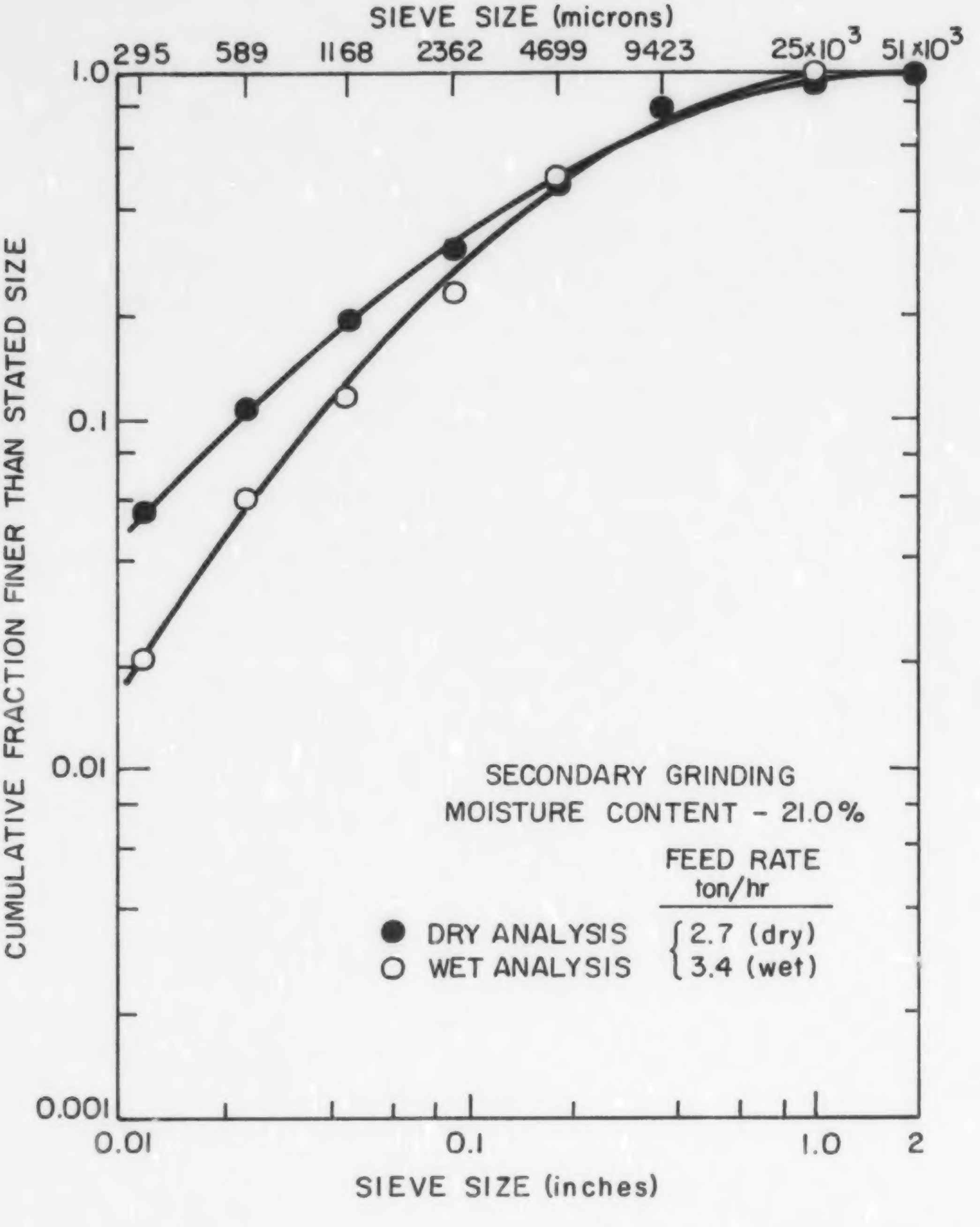

Figure 26 Product Size Distribution for the Secondary Grinding of Municipal Refuse with 21.0% Moisture Content

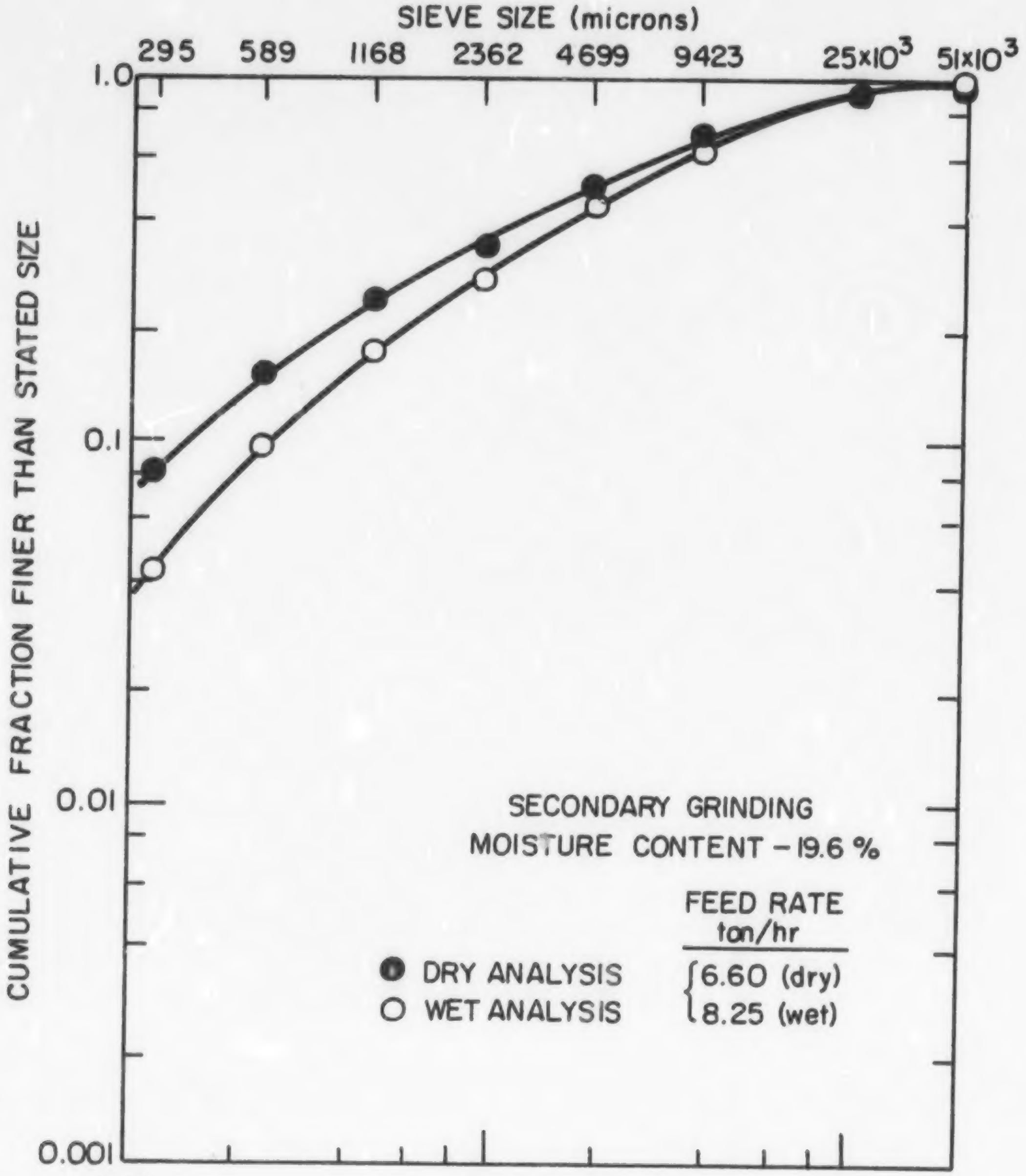

Figure 27 Product Size Distribution for the Secondary Grinding of Municipal Refuse with 19.6% Moisture Content

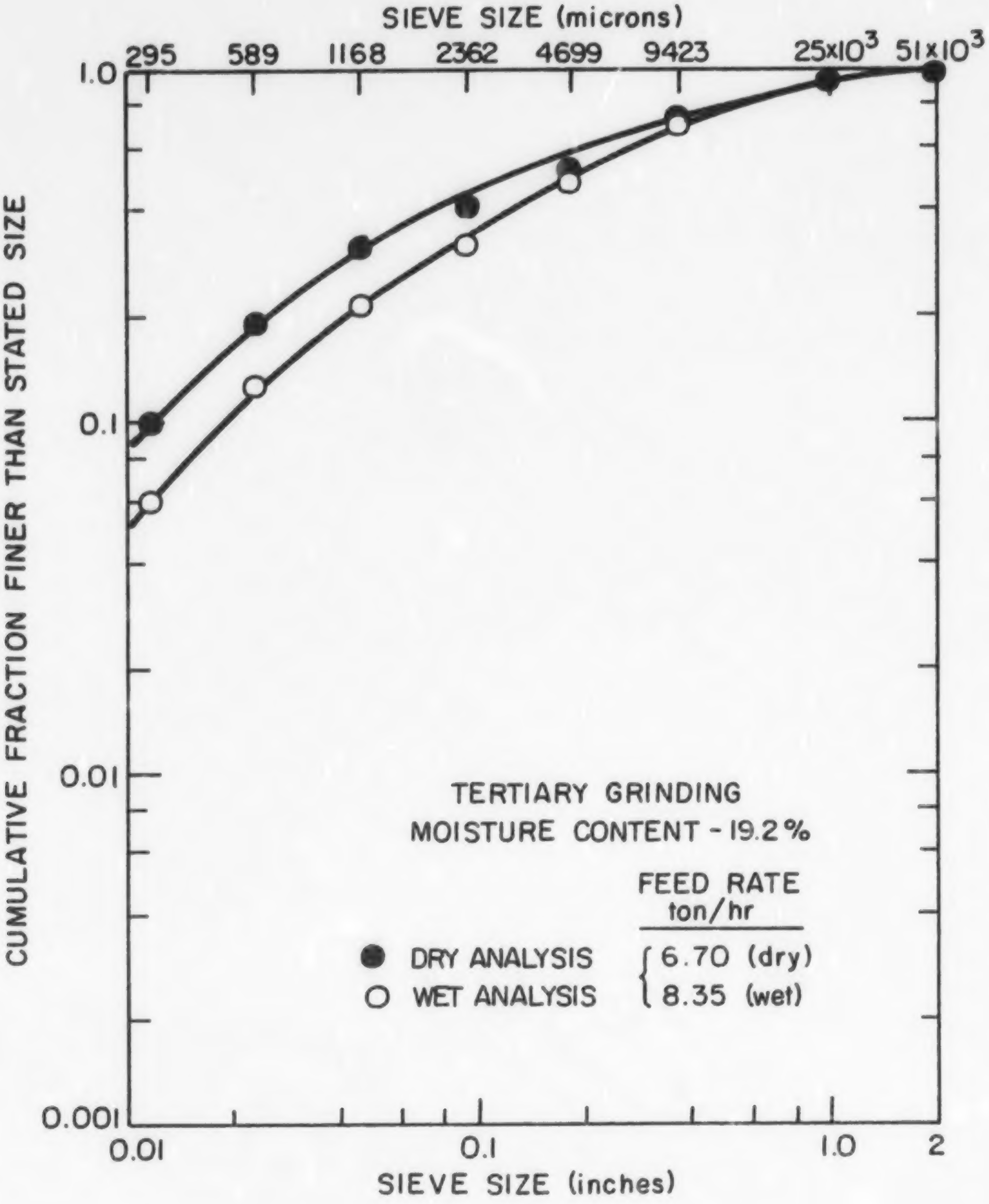

Figure 28 Product Size Distribution for the Tertiary Grinding of Municipal Refuse with 19.2% Moisture Content

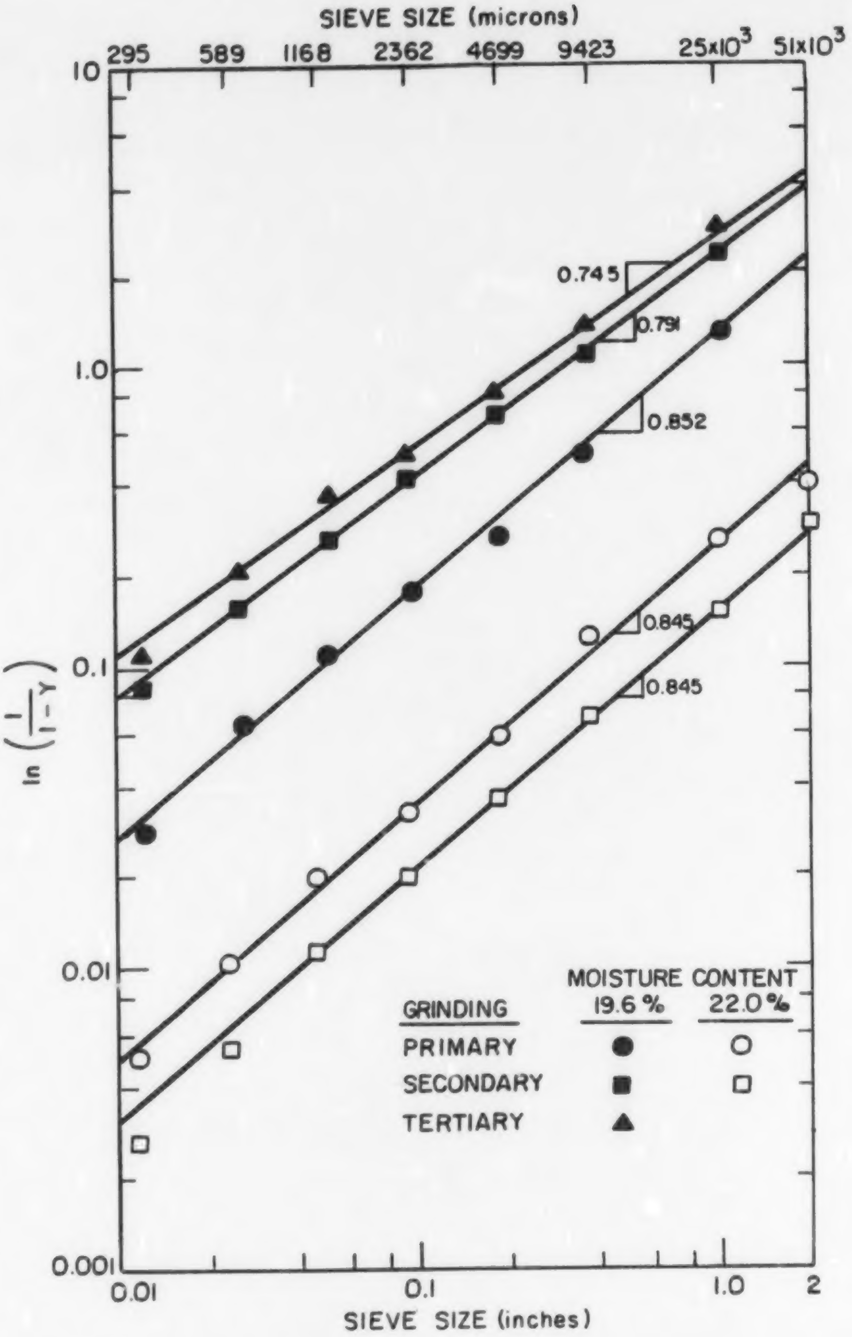

Figure 29 Plot of ln$\left(\frac{1}{1-Y}\right)$ vs. Sieze Size for Primary, Secondary, and Tertiary Grinding of Municipal Refuse

swinging hammers and a bottom grate. It operates at 8 tons/hr, 150 hp, 1,200 rpm, and at 12 Kwh/ton milled. The vertical machine is a Tollemache with no retaining grate to control particle size and has the following operating data: 15 tons/hr, 200 hp, 1,300 rpm, and 7 Kwh/ton milled. The composition of the raw waste stream at Madison is given in Table 7.

The results of the size distribution of shredded refuse processed at the Madison facility have been reported by Gawalpanchi, Berthouex and Ham (16). In their work, a standard U.S. sieve series was used to analyze dried, shredded refuse. This sieving procedure involved the use of 7-lb samples dried in 200-g lots to a constant weight for 18 to 24 hr at 104°C, and sieved in a 13-sieve column in 60- to 100-g batches. They tested the accuracy of sieving with hand ruler measurements and found that discrepancies can occur in the size range of particles larger than 1/2 in. The shaking time was on the order of 100 to 125 shakes, or about 2 min. Comparative tests performed on the method of shaking the sieves showed that the shaking motion was unimportant. In general, they found sieving reproducibility to within the estimated variance because of experimental error of 3.82%, and accuracy of the estimated mean percentage of material passing a sieve to within approximately 2%. Their conclusion is that the simple sieving method is sufficiently accurate to serve as a tool to evaluate operational factors. Typical size distribution data from the Madison site are given in Figure 30.

DISTRIBUTION OBTAINED AT GAINESVILLE

Results of the size distribution of refuse shredded at the Gainesville, Florida, composting plant are reported in the thesis of Ruf (8). This plant was constructed in 1967 and began processing municipal refuse the following year. The facility has

TABLE 7. COMPOSITION OF MADISON'S SOLID WASTE,[a] NOVEMBER 1968 (% wet weight basis)

Category	Minimum	Maximum	Average
Food wastes	4.4	28.9	15.3
Garden wastes	0.0	31.1	13.8
Paper products	35.1	53.2	42.4
Plastics, rubber, leather	0.3	3.7	1.8
Textiles	0.1	7.8	1.6
Wood	0.0	2.6	1.1
Metals	5.0	14.5	6.7
Glass, ceramics	4.4	17.6	10.1
Rock, ash, etc.	0.6	17.6	7.2

[a] Determined by Federal solid waste management personnel.

primary and secondary Williams swing hammer hammermills rated at 30 and 20 tons/hr, respectively. Each machine has a 400-hp motor directly coupled to the rotor shaft with a flexible coupling. The grate openings in the primary shredder were 4 1/2 x 8 in. for the grate box near the breaker plate and 12 x 8 in. at the opposite end. In the secondary shredder, the grate spacing was 3 1/2 x 10 in. throughout, and each grate box had six openings. The breaker plates in these machines were periodically adjusted to the point of nearly touching the hammers. The typical waste stream composition is given in Table 8. About 10% of the incoming waste was manually removed as bulky materials before shredding. This included such items as mattresses, sofas, tires, large pieces of wood, heavy metal and appliances, etc.

As part of his thesis, Ruf (8) surveyed the various types of screens and considered their suitability for analyzing shredded refuse. He selected the Gilson mechanical testing screens (Model No. CL-325) from Soil Test, Inc. This machine holds six screen trays and the dust pan simultaneously. The screens are stacked vertically, 4 in. apart, with a clear space of 1 3/8 in. between them for observation. The screens operate with a vertical agitation and a 7/16-in., 10-cycle/sec oscillation. The test samples ranged from 2 to 8 lb, and screening time was about 5 min. In addition, some particles in the 2- to 4-in. range were tested by hand to see if they would fit through the openings. The detailed procedures used by Ruf are given in his thesis. He considers the effect on the size distribution of a host of screen-

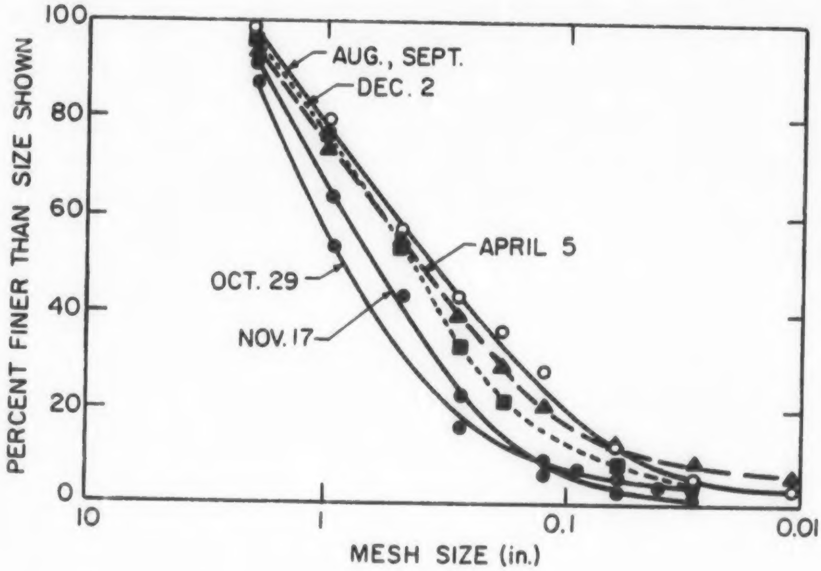

Figure 30 Typical Particle Size Distributions for Milled Refuse from both Mills in 1972

TABLE 8. SUMMARY OF REFUSE COMPOSITION AT GAINESVILLE, FLORIDA

Refuse category	Range, % (wet wt. basis)	Weekly average % (wet wt. basis)
Food waste	0.31 - 21.96	5.23
Garden waste	0 - 55.19	12.71
Paper products	22.69 - 91.55	49.65
Salvageable[a]	1.43 - 63.18	23.64
Cardboard	0 - 57.45	14.95
Other	0 - 26.13	8.69
Nonsalvageable	8.94 - 48.90	26.01
Plastic, leather, rubber	0.26 - 21.94	4.61
Textiles	0 - 7.31	1.61
Wood, limbs, sawdust	0 - 29.11	6.20
Miscellaneous combustibles	0 - 5.39	0.30
Metal	0.33 - 20.51	8.04
Ferrous	0.26 - 20.26	7.44
Nonferrous	0 - 2.42	0.60
Glass and ceramic	0 - 19.12	7.06
Ash, earth, rock, etc.	0 - 27.60	4.59
Total	---	100.00

[a] As used here, the term "salvageable paper" refers to those pieces of paper that appear to be large enough, dry enough, and clean enough to be separated at the sorting platform for subsequent sale.

ing variables, which include screening time, overloading the screens, screening efficiency, etc. He further undertook component classification studies in which the screened fractions were classified into 13 different categories. The size distribution results of this work are given in Figures 31 and 32 for primary and secondary shredded waste, respectively. Ruf also analyzed primary shredded waste from the Don-Oliver Rasp located at the Johnson City, Tennessee, compost plant. This machine has a rasp that revolves at 8.3 rpm, is designed for 10 tons/hr, is driven by two 40-hp motors, and passes material through a perforated plate grate with 1 1/4-in. openings. The size distribution results for the rasped waste are given in Figure 33.

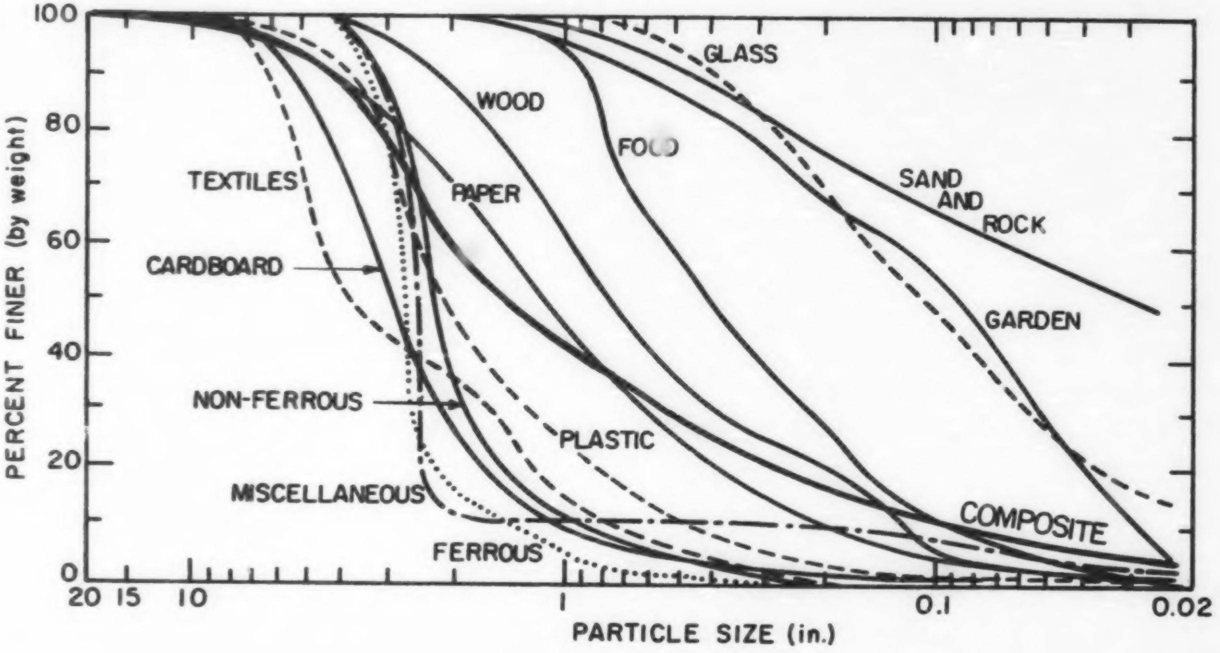

Figure 31 Cumulative Distributions of Primary Waste

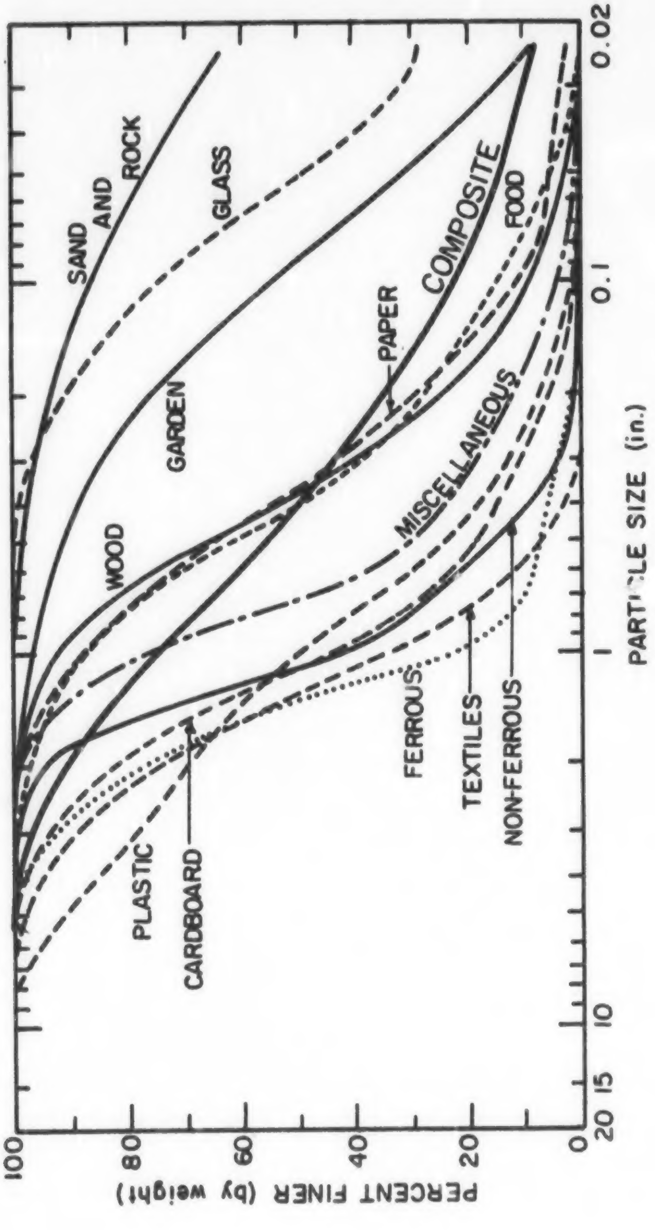

Figure 32 Cumulative Distributions of Secondary Waste

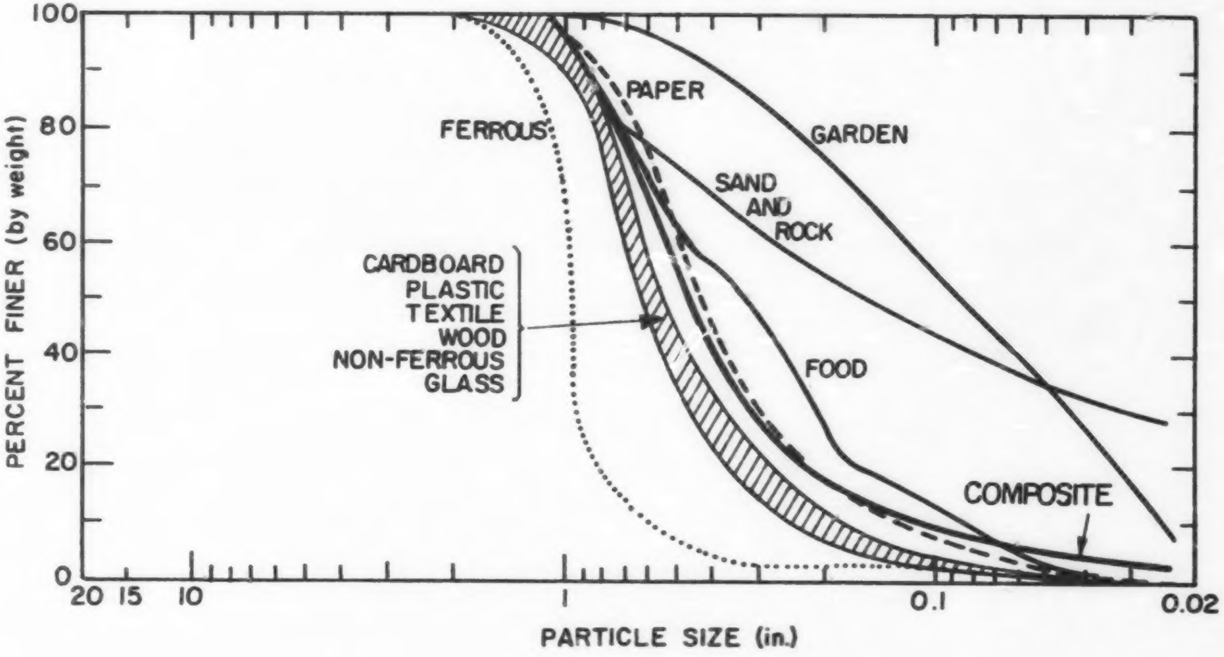

Figure 33 Cumulative Distributions of Rasped Waste

RECOVERY SYSTEM COMPONENT SIZE DISTRIBUTIONS

Although data have been presented that deal with the shredded waste stream component size distribution, this may not be entirely useful to predicting the material flow characteristics of a resource recovery operation. As a means of aiding the clarification of this problem, the component size distributions, after each stage of processing in a typical front-end recovery system, were studied in the Cal Recovery System. The light fraction recovered in this process is suitable for use in a fiber recovery process or for use as a refuse-derived fuel. The description of the system has been given previously. Briefly, the resource recovery system consists of a horizontal swing hammermill, air classifier, and rotary cylindrical (trommel) screen for screening the air-classified light fraction and is capable of handling a throughput of up to 2,722 kg/hr (3 tons/hr) on a continuous basis. The shredded refuse is fed by conveyor into a vertical air classifier. The heavy fraction falls to the bottom of the air classifier chamber and is removed by a conveyor. The light fraction is carried by fan suction through the top of the air classifier and removed from the air stream by a cyclone separator. A rotary air lock valve discharges the light fraction from the cyclone onto a conveyor, which subsequently feeds the trommel screen. The recovery system has been optimized for recovery of magnetic metal and glass from the air-classified heavy fraction and paper fiber from the air-classified light fraction.

Samples of refuse from various stations of the recovery system have been analyzed for size distributions and composition. The size distribution analyses were carried out using a Sweco 0.457-m (18-in.) rotary screen. Samples having a weight of 2.3 kg (~5 lbm) were screened for 15 min and were subsequently hand picked to determine sample compositions. Because of the difficulty of differentiating components at small sizes, no attempt was made to determine compositions below 14-mesh, 1.3-mm (0.051-in.) screen opening.

SHREDDED COMPONENT SIZE DISTRIBUTIONS

A comparison of raw and shredded refuse size distributions (Figure 34) shows that size reduction has the deleterious effect of increasing the number of particles and the homogeneity of the product. With an arbitrary cumulative percent-passing range of 1% to 95%, it can be seen from Figure 34 that the overall size distribution of the shredded refuse spans three orders of magnitude - 0.076 mm (0.003 in.) to 76 mm (3 in.). On the other hand, the size distribution of municipal solid waste as dumped from a packer truck occupies roughly two orders of magnitude - 2.54 mm (0.1 in.) to 0.254 m (10 in.). This order of magnitude increases in the nonuniformity of particle sizes and the added degree of mixing enhances the randomness of the system of particles and

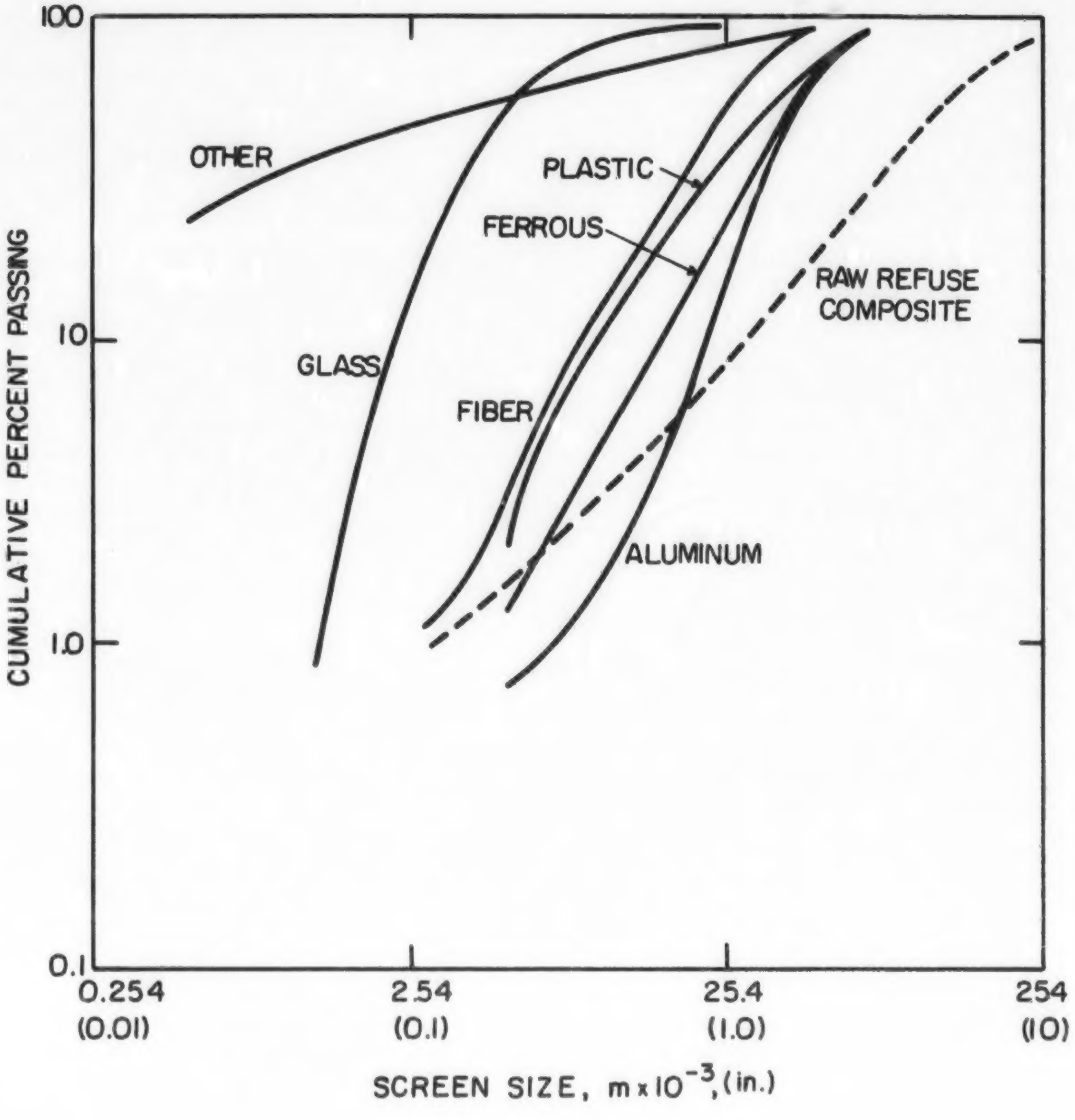

Figure 34 Component Size Distribution of Shredded Municipal Solid Waste - 1,814 kg/hr (2 tons/hr), 1,200 rpm Swing Hammermill

therefore makes separation more difficult. This consequence suggests that shredding should be as coarse as possible to maintain maximum efficiency in the down-stream separation processes. Of course, the size distribution must be consistent with the type of equipment being used in the processing line.

Size reduction of raw municipal solid waste shredded at 1,200 rpm through 63.5-mm x 152-mm (2.5-in. x 6-in.) grate openings yields the component size distribution shown in Figure 34 as a log-log cumulative percent passing versus screen size plot. The major constituents worth recovering, either because of quantity or economic value (aluminum, magnetic metals, glass, plastic, and paper fiber), and a miscellaneous fraction called "other" are shown to occupy distinctive regions of the size spectrum. In the coarser sizes, the "other" fraction contains leather goods, rubber, wood, rags, nonferrous/nonaluminum metals, and organic matter. As seen from the curve, the "other" fraction also contains most of the finer material (< 14 mesh) - namely, dirt, lint, and other material unidentifiable to the naked eye because of its small size. The glass size distribution essentially exists in the range of 1.3 mm (0.05 in.) to 25 mm (1.0 in.). In the larger sizes (> 9.5 mm, or 3/8 in.), the glass particles are flat and perhaps 3 mm (1/8 in.) in thickness. Particles roughly cubic in shape characterize the pieces less than 4 mesh. The fiber and plastic fractions tend to be much larger than the glass. The size distributions of fiber and plastics tend to be similar, with the latter being slightly coarser. The size distribution of the fiber fraction is between 2.5 mm (0.1 in.) and 50 mm (2 in.); for plastics it is between 6.4 mm (1/4 in.) and 76 mm (3.0 in.). The coarsest products are the ferrous and aluminum fractions. The aluminum fraction, 6.4 mm to 76 mm, undergoes the least amount of size reduction, presumably because aluminum is so malleable. The smaller particles of aluminum are generally flat and irregularly shaped. The larger particles are mostly the twisted remains of aluminum cans. The ferrous materials exist in the range of 5 mm to 76 mm. As with the aluminum, the finer ferrous particles are irregularly shaped flat pieces, and the coarser particles are the larger remains of bar stock, wire, and tin cans.

AIR-CLASSIFIED FRACTIONS SIZE DISTRIBUTIONS

Direct processing of the shredded refuse (whose size distribution is shown in Figure 34) through a vertical air classifier produces a "heavy" fraction and a "light" fraction (Figures 35 and 36, respectively). Under optimum conditions for recovery of paper fiber or a lights fuel fraction, a flow split of 70% lights and from 30% heavies is typical for raw solid waste moisture contents in the range of 20% to 30%. Higher moisture contents reduce the ratio to 60%/40%. Conversely, lower moisture contents increase the ratio to 85%/15%. Thus, in general, higher moisture contents tend to produce a higher percentage of heavy fraction,

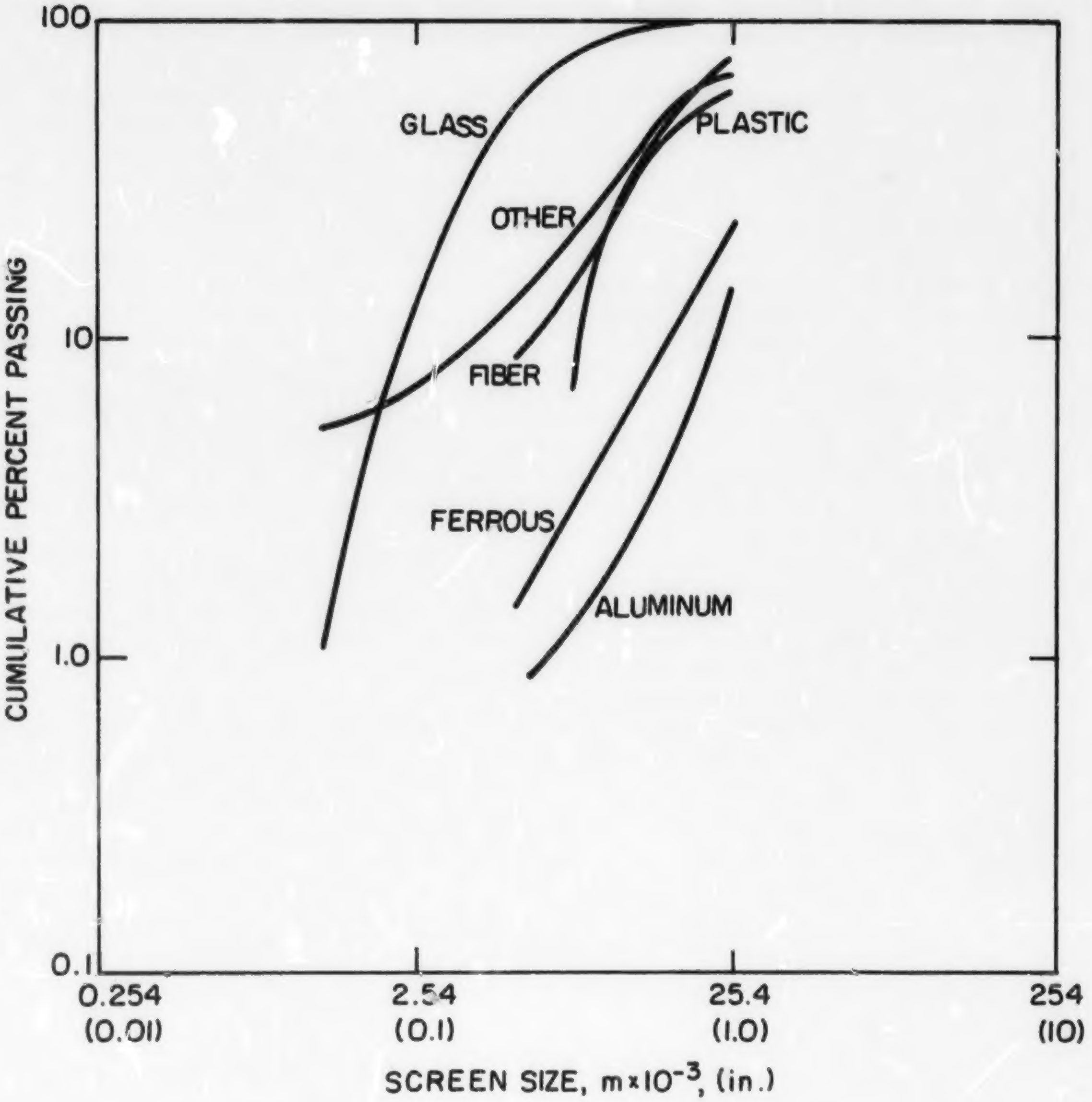

Figure 35 Component Size Distribution of Air-Classified Heavy Fraction

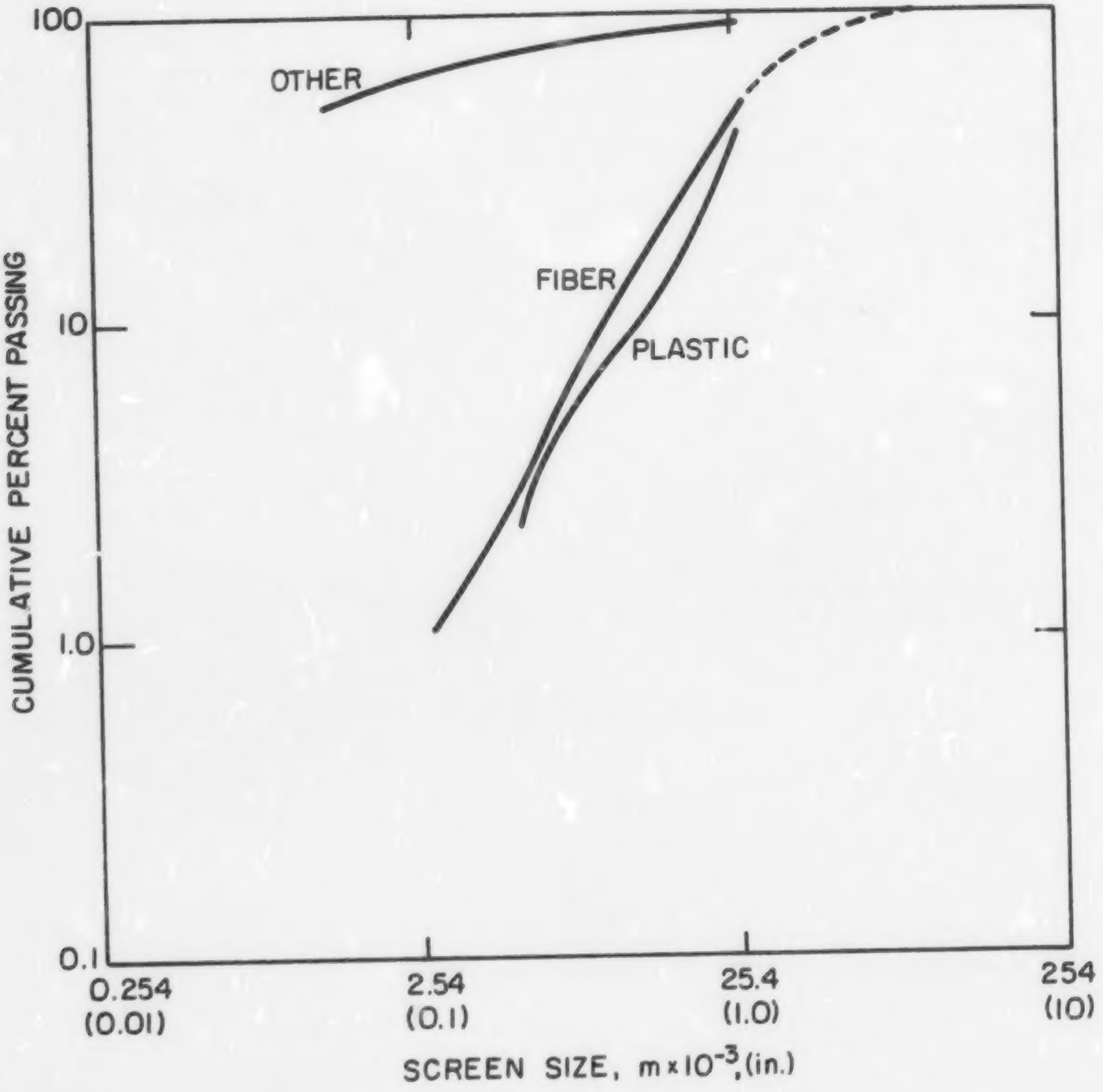

Figure 36 Component Size Distribution of Air-Classified Light Fraction

and lower moisture contents tend to result in a lower heavy fraction. Ideally the heavies fraction would contain the densest components of refuse such as ferrous, aluminum, other metals, ceramics, stones, and glass. Practically, however, the heavies consist of those components just mentioned plus paper, plastics (other than film), and other materials such as wood splinters, garbage matter, leather, rubber, and rags. The degree of contamination of the heavies depends on the air flowrate through the air classifier, the moisture content of the refuse, and the size distributions of the various refuse components.

With a 70%/30% split, the density of the heavy fraction is typically 400 kg/m^3 (25 lb/ft^3), and that of the light fraction is 80 kg/m^3 (5 lb/ft^3). The size distributions for various components of refuse after air classification at a 70%/30% split are shown in Figures 35 and 36. Comparing the size distributions of the feed (Figure 34) to that of the air-classified heavies (Figure 35), several conclusions can be drawn. First, the ferrous, aluminum, and glass (> ~ 10 mesh) size distributions remain the same after air classification because essentially all these components report to the heavies fraction. Second, the paper and plastic particles present in the heavies tend to be the finer pieces. The coarser particles of paper and plastic tend to be in the light fraction (Figure 36). Comparison of the "other" fraction after air classification shows that the coarser particles fall out with the heavies (Figure 35) and the finer particles are carried away in the air stream (Figure 36).

The relative amounts of various components of air-classified solid waste as a function of screen size are given in Figure 37. The dark bands represent that portion of a particular component that falls out with the heavy fraction. The remaining (or light bands) material reports with the light fraction. The potentially recoverable materials - ferrous, aluminum, and glass - account for 62.6% of the heavy fraction. Paper fiber represents 60.2% of the light fraction, with plastic and other material accounting for the remaining 39.8%. Table 9 presents a detailed breakdown of the heavy and light fractions of air-classified shredded solid waste.

SCREENED LIGHT FRACTION SIZE DISTRIBUTION

Further treatment of the air-classified light fraction employing a rotary cylindrical (trommel) screen results in a screened light fraction usable in a fiber recovery system or as refuse-derived fuel. Size distributions of oversized and undersized material obtainable using a 9.5-mm (3/8-in.) wire mesh trommel screen are shown in Figures 38 and 39, respectively. As shown in Table 10, the +9.5-mm material essentially contains paper fiber (78.8%), plastics (7.8%), and other material such as hair, string, wood, etc. (13.4% by weight). The -9.5-mm fraction is composed of 78.7% other material (dirt and glass fines, string, lint,

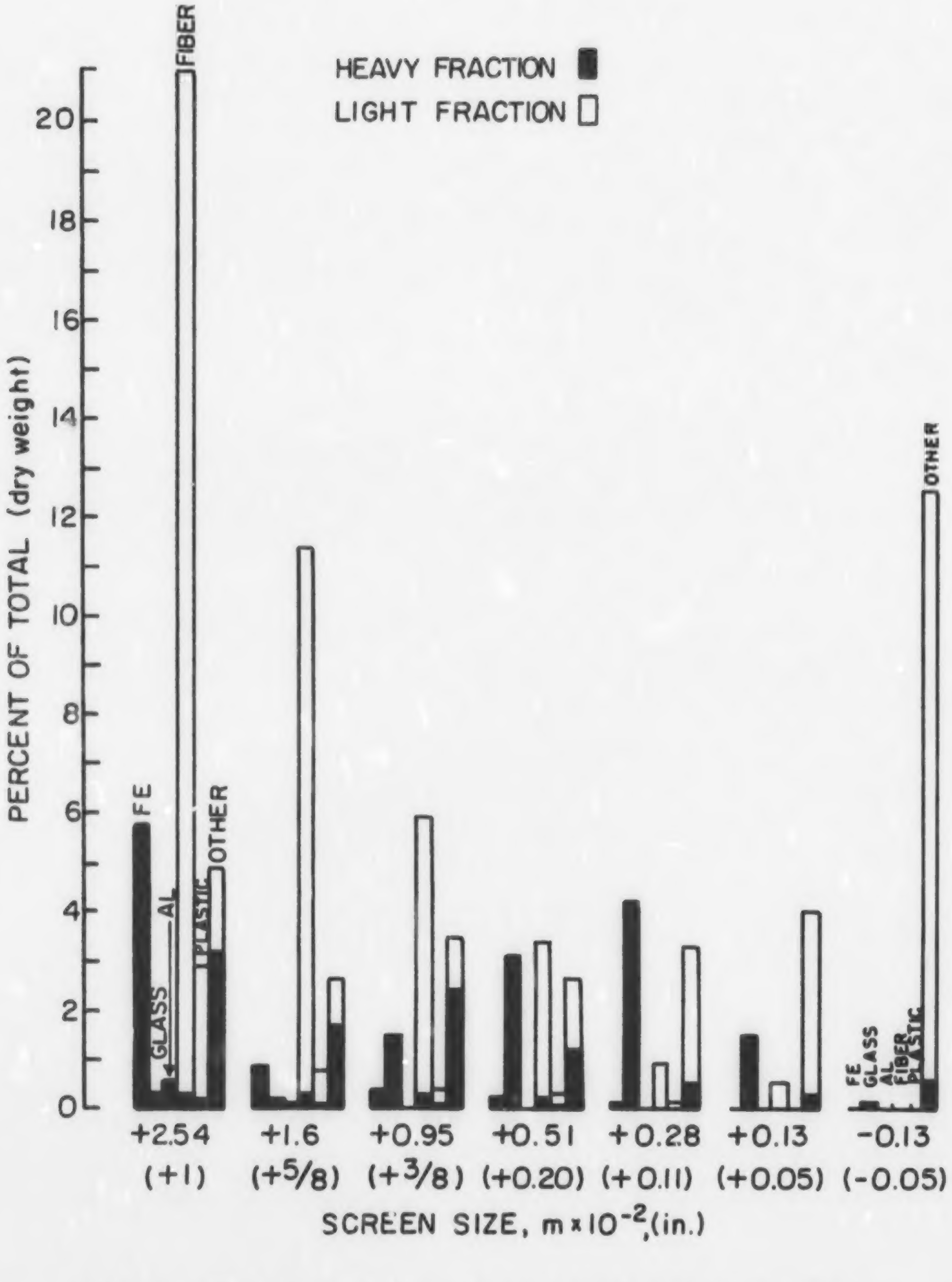

Figure 37 Composition of Air-Classified Shredded Solid Waste - 70%/30% Split

TABLE 9. COMPOSITION OF AIR-CLASSIFIED SHREDDED SOLID WASTE, 70/30 SPLIT

Component	Weight %
Heavy fraction:	
Magnetic metals	24.2
Glass	36.1
Aluminum	2.3
Paper fiber	3.6
Plastic	1.7
Other	32.1
Total	100.0
Light fraction:	
Paper fiber	60.2
Plastic	5.7
Other	34.1
Total	100.0

organic matter, etc.), 19.9% paper fiber, and 1.4% plastics, percent by weight. The composition of the +9.5-mm and -9.5-mm material is shown in Figure 40. Paper fiber dominates each screen size from +25 mm down to +9.5 mm. Below 5 mm (0.2 in.), dirt, glass fines, and stringy materials, which compose the "other" category, dominate the composition of the -9.5-mm fraction. Elimination of this material enhances fiber or fuel recovery. If such fine materials were allowed to remain in the light fraction, serious cleaning and water treatment problems would occur in any subsequent fiber recovery process. Similarly, these fines would also lead to scaling, furnace contamination problems, and dilution of the heating value if the light fraction were used as a refuse-derived fuel.

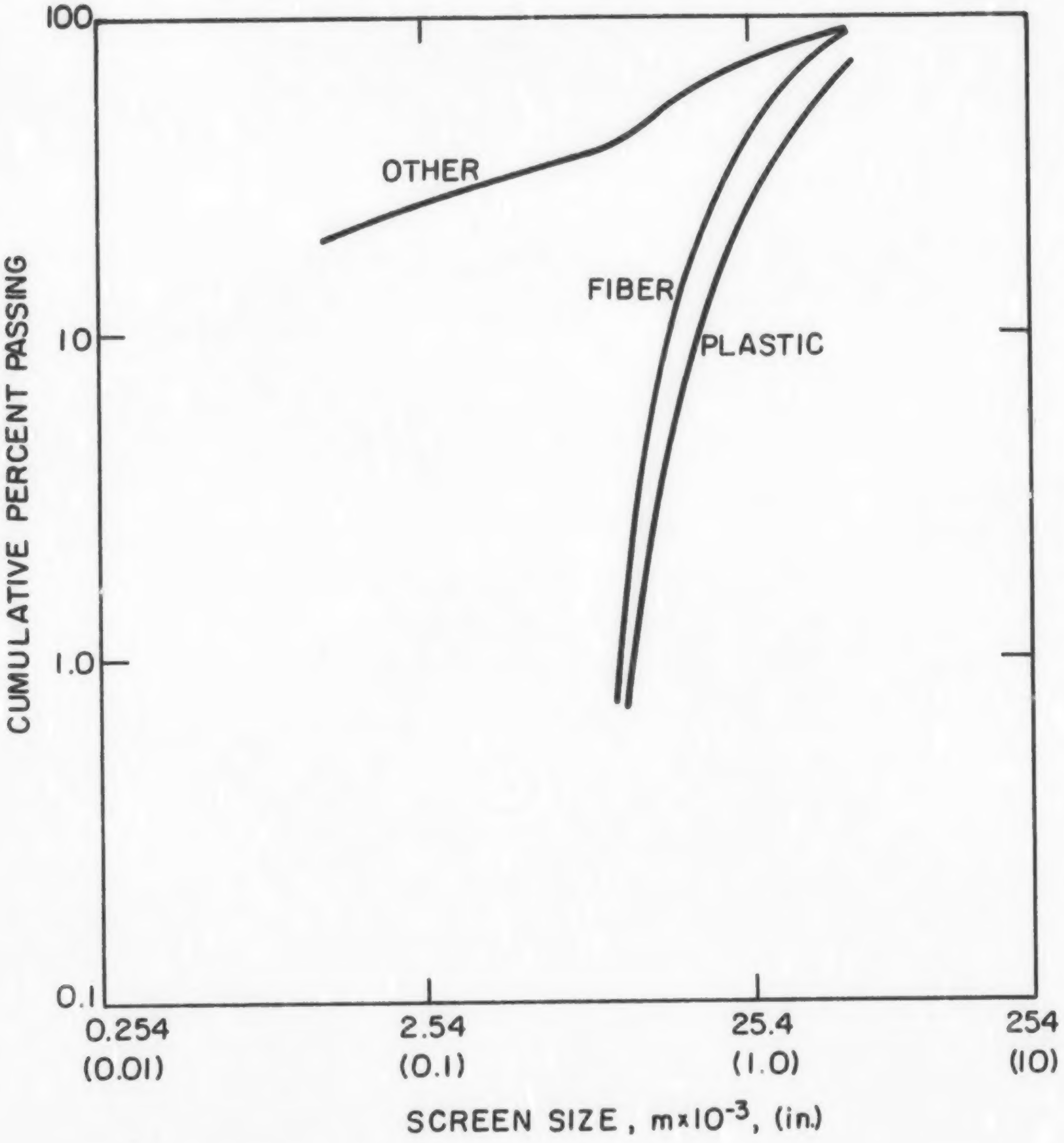

Figure 38 Component Size Distribution of Oversize from 9.5×10^{-3}m (3/8 in.) Trommel Screen

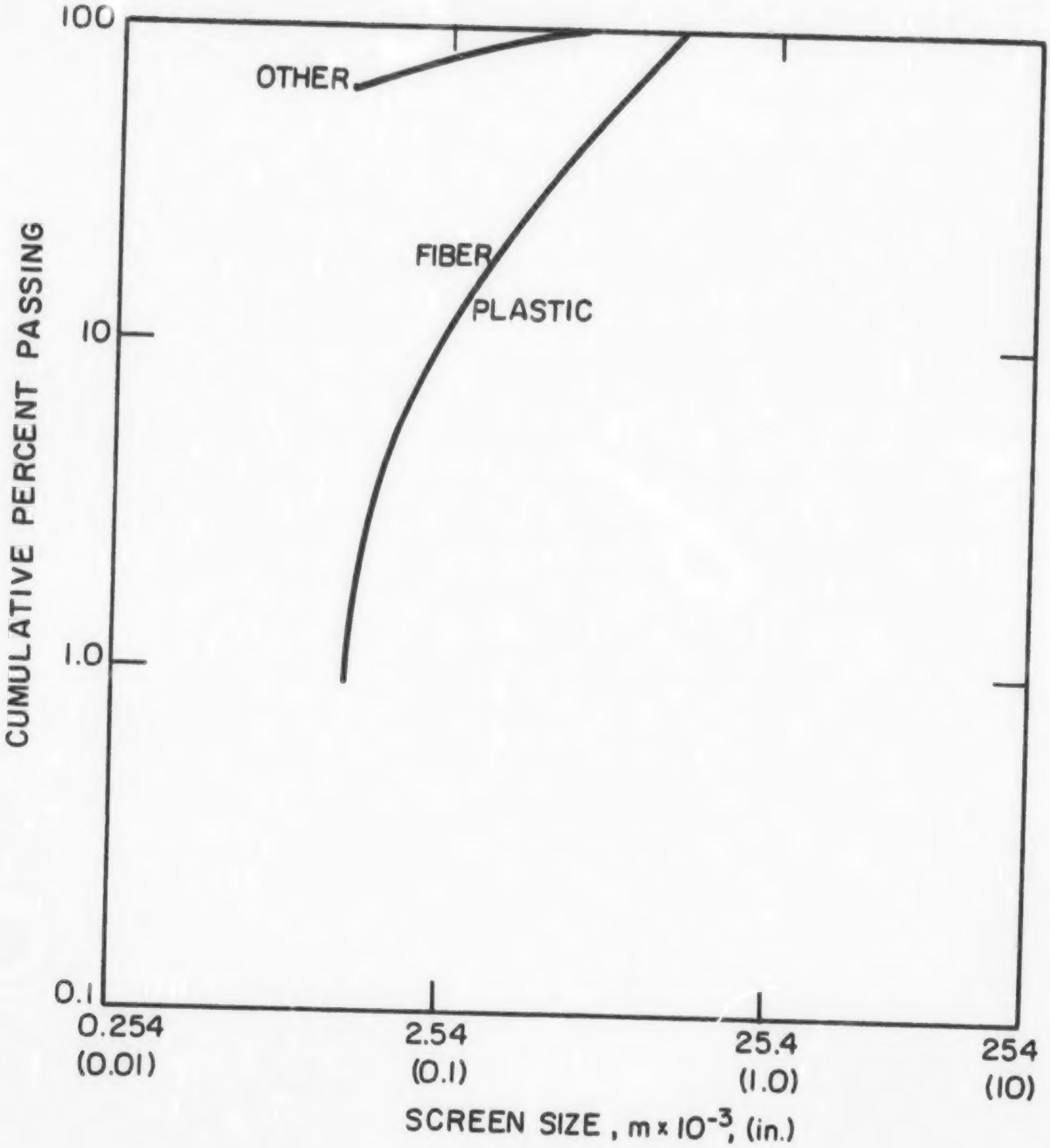

Figure 39 Component Size Distribution of Undersize from 9.5 x 10^{-3}m (3/8 in.) Trommel Screen

TABLE 10. COMPOSITION OF SCREENED, AIR-CLASSIFIED LIGHT FRACTION

Component	Weight %
+9.5-mm material:	
Paper fiber	78.8
Plastic	7.8
Other	13.4
Total	100.0
-9.5-mm material:	
Paper fiber	19.9
Plastic	1.4
Other	78.7
Total	100.0

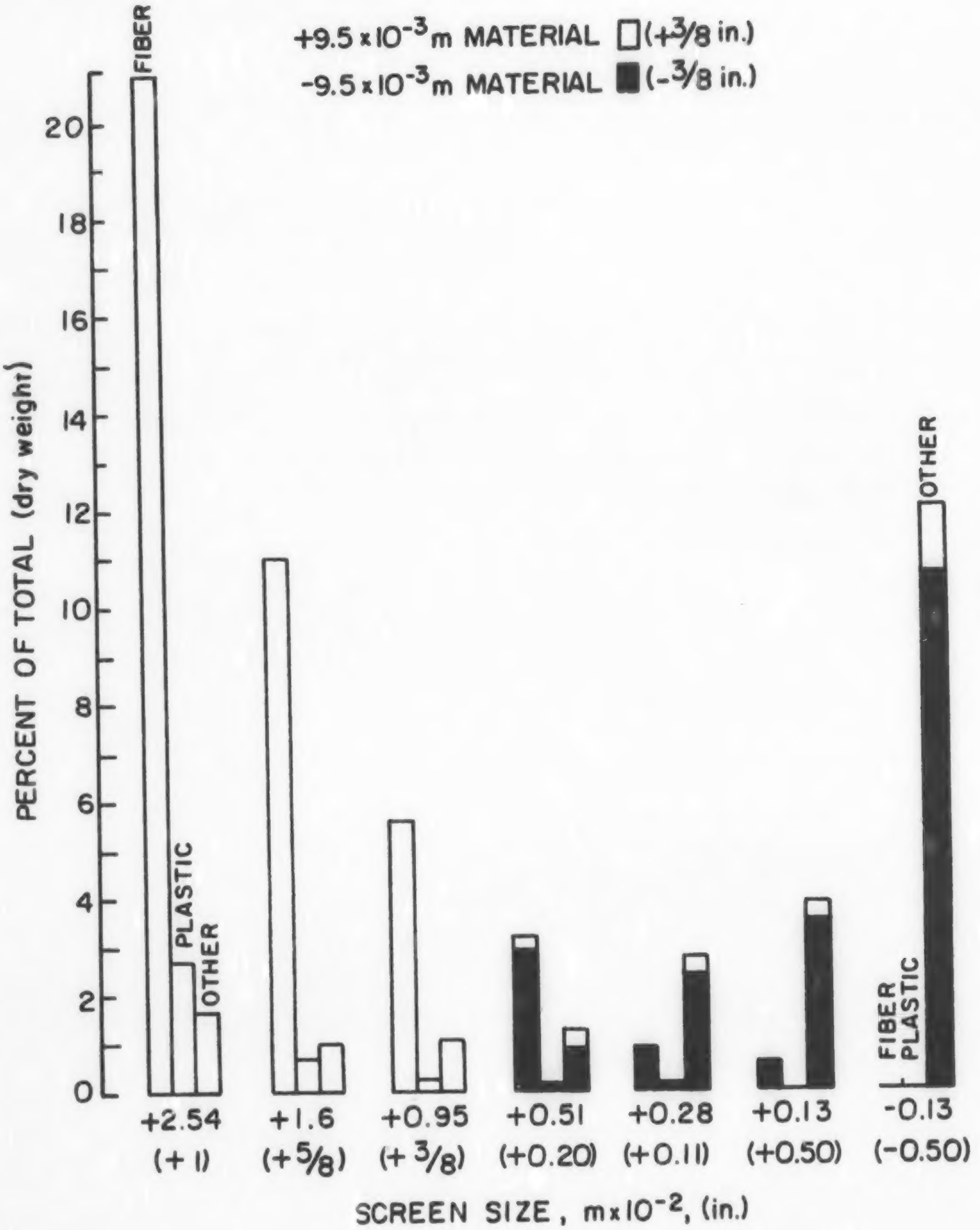

Figure 40 Composition of Screen Air-Classified Light Fraction

SECTION 3

BEHAVIOR OF THE COMMINUTION PARAMETERS

Shredder performance can be characterized through the parameters that effect the comminution process. In addition, the capability for control and predictability of the size distribution of the ground product is vital to the successful performance of the subsequent stages of processing and can only be achieved through understanding of the behavior of the comminution variables.

The three quantities that taken collectively characterize the ability of a particular comminution device to size reduce refuse are the specific energy consumption (Kwh/ton), the product size distribution, and the machine wear. In effect, these quantities are manifestations of the physics of the comminution mechanisms. The important operating parameters that influence these three dependent variables are the set of five independent variables - the feed size distribution, the flow of material through the device, the moisture content of the materials, the grate or extraction spacing, and the relative velocities of the size reduction apparatus in the machine, such as the rpm or tip speed of the hammermill hammers. The interrelationship between these variables and their influence on quantities characterizing a comminution process will be discussed first in terms of their effect on the product size distribution and then their effect on the energy consumption.

FACTORS AFFECTING SIZE DISTRIBUTION

The measurement of raw and shredded refuse size distributions has been considered in a previous section. Since they characterize the feed and product respectively, both are important. Even though the size distribution of the incoming raw refuse feed is a significant variable in the comminution process, it is perhaps the most poorly measured and least controllable parameter. It can span a two- to three-order-of-magnitude size range and vary between successive packer trucks. From the previously discussed comparison of raw refuse size distributions (Figure 41), a range of 90% cumulative passing between 12 and 25 in. can be expected. Furthermore, there is a significant difference between residential and commercial solid wastes; the latter tend to be bulkier and have a generally coarser size distribution because of the large amounts of packaging and cardboard present (approximately twice as much).

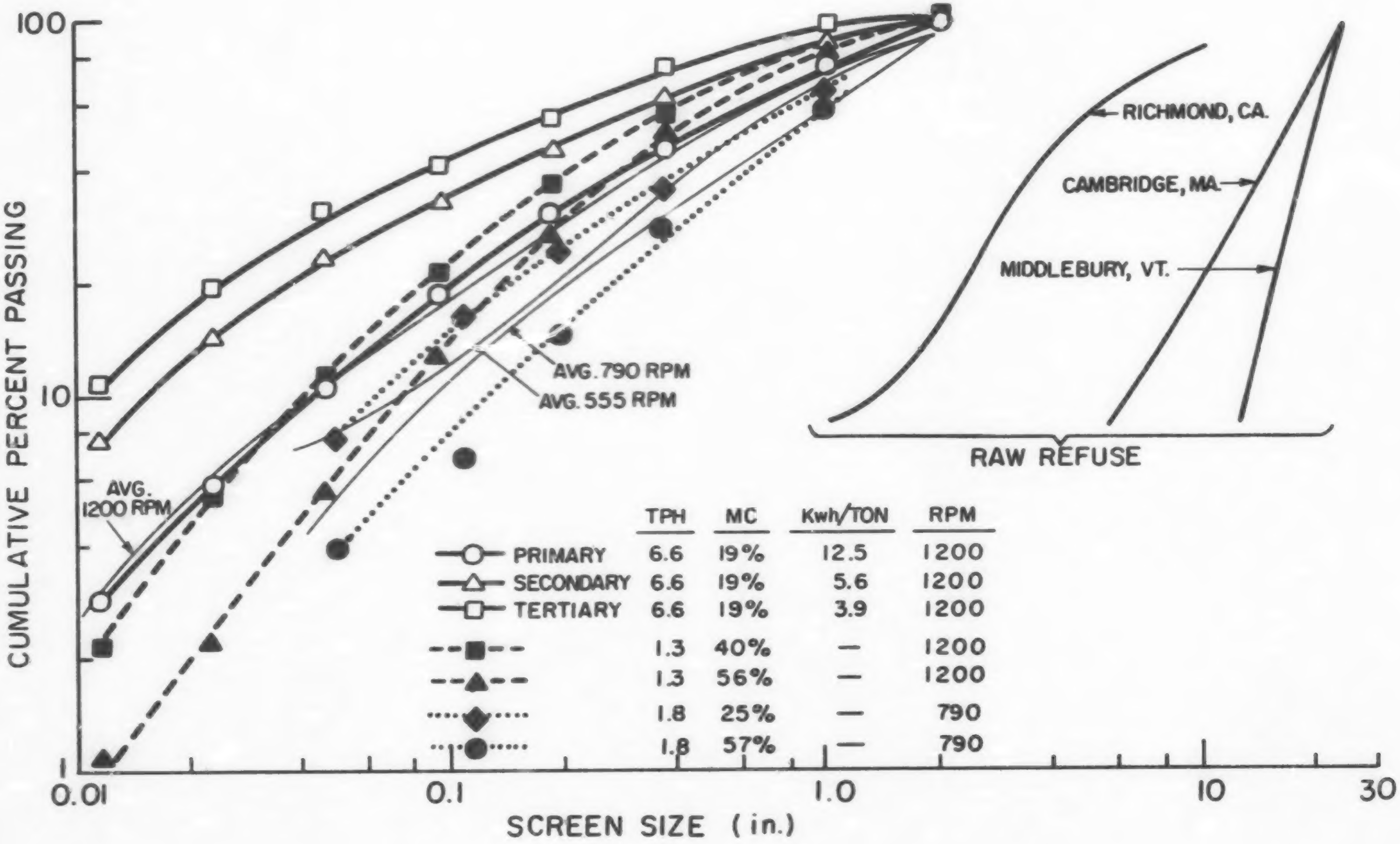

Figure 41 Size Distribution Comparison for Raw Municipal Refuse and Residential Refuse Shredded at 1,200, 790, and 555 rpm. Effect of Moisture Content (MC) and Secondary and Tertiary Grinding

Because the product size distribution can be represented analytically, a semi-empirical predictive theory has been developed in terms of breakage and selection functions to allow prediction of the product size distribution for any input feed. Although this theory can be further used to study the interrelation and effects of the comminution variables, examination of the size distribution itself provides useful insights into the behavior of these variables. Our experience, as well as that obtained at other shredding installations, indicates that product size distributions can be represented by a Rosin-Rammler relation of the type

$$y(x) = 1 - \exp\left[-(x/xo)^n\right] \tag{1}$$

where y(x) is the cumulative percent passing screen size x. The exponent n (sometimes referred to as the n index) is essentially the slope of the line $\ln[1/(1-y)]$ versus x on log-log coordinates. Also, the value of x_o is the size corresponding to 63.2% cumulative passing or, alternatively, the value of x where $\ln[1/(1-y)] = 1.0$. It is interesting to note that the individual values of n obtained for all grinding conditions lie between the limits ($0.5 \leq n \leq 1.3$) of the values for the grinding of brittle materials in hammermills. Lower values of n are usually associated with a more scattered distribution over a wider size range, while higher values of n are associated with uniform particle structure over a narrow size range. Also, the Rosin-Rammler distribution physically indicates that for a particular value of x_o, as the value of n increases, the cumulative percent passing a size x (i.e., [y(x)]) decreases, a result that can be interpreted as larger size particles or a coarser product. Operating at 1,200 rpm, values of the characteristic size (x_o) in the range of 0.6 to 1.0 in. were obtained for primary grinding. Values previously given for x_o and n for primary, secondary, and tertiary grinding of the product (x_o = 0.6 to 1.0, 0.33, and 0.23, respectively; and n = 0.99, 0.87, and 0.75, respectively) indicate that when the number of grinding cycles increases, the product size distribution shifts toward the finer sizes and a higher percentage passes at lower sizes. In short, a finer product is obtained with successive cycles of grinding, as would be expected (Figure 41).

A study of the effect of comminution speed on the product was conducted by operating the shredder installed with a belt-pulley drive system at 1,200 (rated speed), 790, and 555 rpm. For the case of primary grinding, the resulting product size distributions for these three speeds (Figure 41) yield values of the n index of 0.81, 0.97, and 0.91, respectively. The respective corresponding average values of the characteristic particle size (x_o) are 0.78, 1.08, and 0.88 in. In general, the decreased speed produces a coarser product, or, conversely, the higher speeds should yield a finer product because of a greater number of impacts per unit time. A definitive differentiation of the product size distribution at the two lower speeds was not possible, suggesting that when a minimum speed is attained, the speed variable does not participate in a dominant manner in the overall description of the comminution process.

It was found that the increase of moisture in the range of 37% to 63% had the effect of producing a coarser size distribution as shown in Figure 41 for both the 1,200 and 790 rpm speeds. At a feedrate of 1.8 tons/hr (790 rpm) and a moisture content of 25%, the n index has a value of 0.82 in. The effect of doubling (57%) the moisture content is to increase the values of n and x_o to 1.06 and 1.1 in., respectively. On the other hand, data obtained from the Madison facility for a moisture content of 46% to 92% indicated the opposite trend (Figure 42). The Madison group (16) indicates that for a given refuse composition, an increase in moisture content tends to yield a smaller average particle size and a more uniform size distribution. Two hypotheses regarding the moisture content effect are advanced by the Madison group. They claim that certain refuse components, principally the fibrous ones, become weaker when wet and are more readily torn apart; moisture also increases frictional resistance of the refuse and thus allows greater shearing forces to develop. It is important to note that the ability to accurately measure the size distribution at high moisture contents (around 60%) is diminished because of coagulation, clumping, and balling of the shredded material. In the high moisture state, the shredded refuse product will have a certain size distribution, but after drying, the size distribution may be considerably different because of clumping - most noticeably, the shredded paper components. For these reasons, results of experiments that interpret size distribution at moisture contents over 60% are not reported here.

In general, it has been found that smaller grate spacings will produce a finer product size distribution. This has been demonstrated on the Gondard mill at Madison, which operated with grate spacings ranging from 3 1/2 to 6 1/4 in. (Figure 43). The effect of grate spacings on particle size can also be considered in terms of the characteristic particle size (Figure 44). Here a trend is established by comparing the data obtained for various model shredders. Data for St. Louis (17) are not predicted by this trend, either because of a difference in raw refuse composition or, more significantly, by the fact that the St. Louis machine has 3-in.^{2} grate openings, whereas the others (with the exception of the Eidel, which does not have grates but an extraction opening at the bottom) have rectangular grates, with the smallest dimension occurring perpendicular to the axis of the rotor.

The effect of hammer wear has been studied at the Madison site (Figure 45). Their experience indicates that a coarser size distribution results as hammer wear increases. The change is greatest immediately after installation of new hammers because the

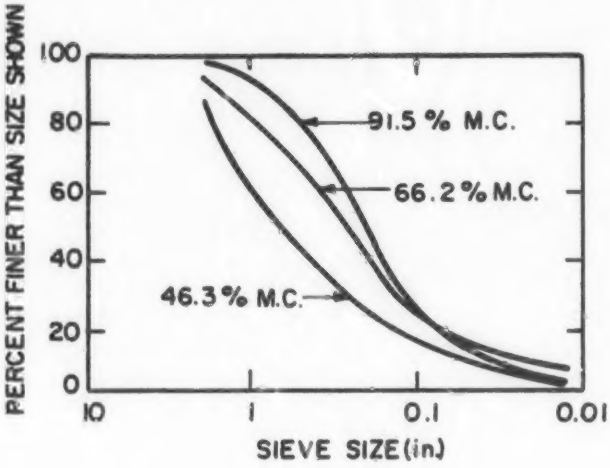

Figure 42 Effect of Moisture Content (MC) on Particle Size Distribution

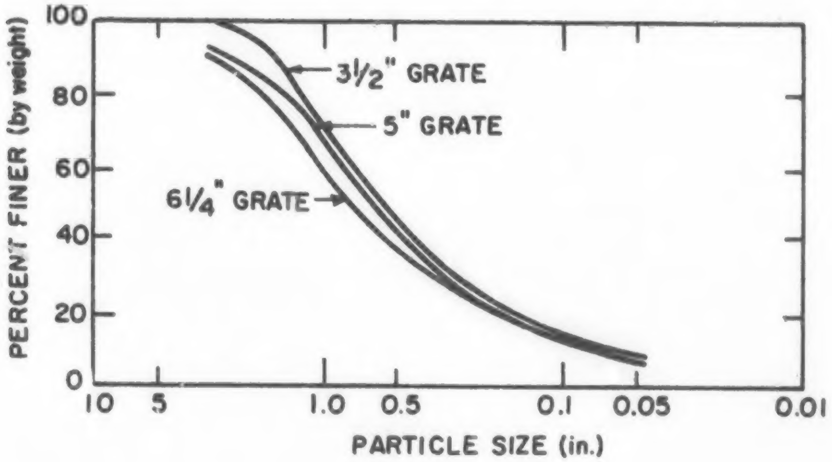

Figure 43 Effect of Grate Size on Particle Size Distribution at Madison

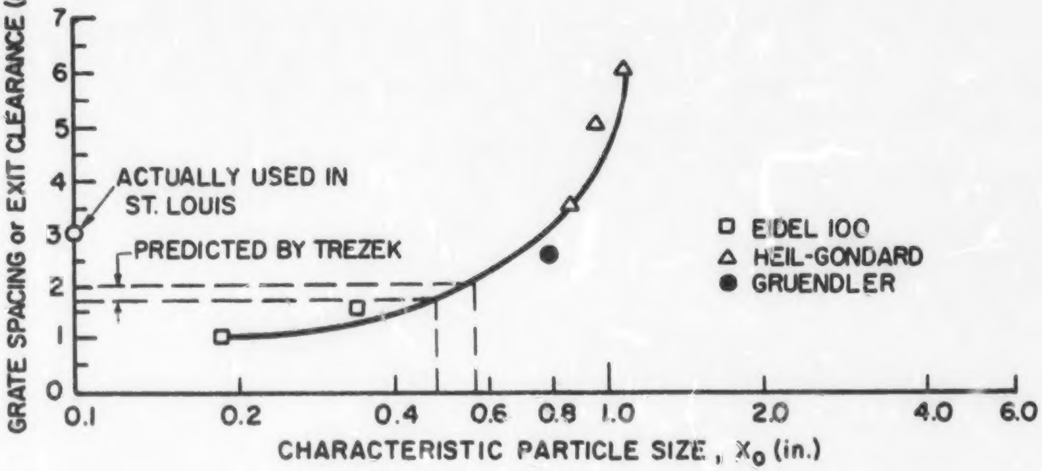

Figure 44 Characteristic Particle Size vs. Grate Spacing

clearance between the hammer tips and the housing is progressively enlarged, and worn edges do not shred as effectively. The wear effect on size distribution is described by the Madison data in terms of an exponential decay with time (Figure 46). Their relation for percent passing (μ) takes the form

$$y = b_o + b_1 \exp(-b_2 t) \qquad (2)$$

where t is the cumulative tons of refuse shredded since the installation of new hammers. Furthermore, the Madison group indicates that hammer wear is a more significant variable then moisture content in affecting the product size distribution.

FACTORS AFFECTING ENERGY CONSUMPTION

A range of n values from 0.7 to 1.3 resulted from the previously discussed size distribution analysis. In this range, it was found that the specific energy consumption was a function of the characteristic size x_o only (Figure 47) (18). The zero energy reference x_o equal to 6.0 in. was obtained from the raw refuse feed size distribution analysis. These results further indicate that the specific energy gradient is greater for small values of x_o. For the coarser values of x_o, the amount of energy needed to produce a given percent in x_o is less than that required for a similar amount of size reduction at the finer sizes. For example, 50% reduction in characteristic particle size from 6.0 to 3.0 in. would require about 2.2 Kwh/ton compared to 6.5 Kwh/ton

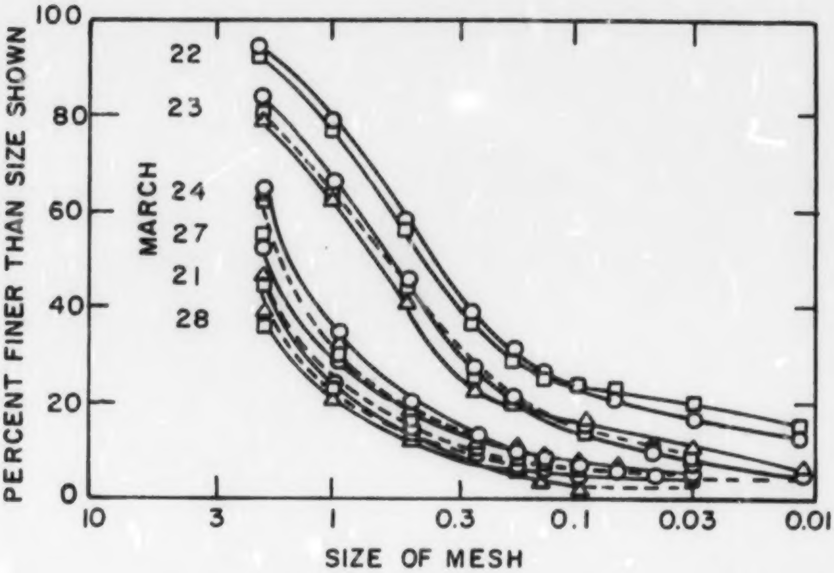

Figure 45 Effect of Hammer Wear on Particle Size Distribution - Tollemache Mill

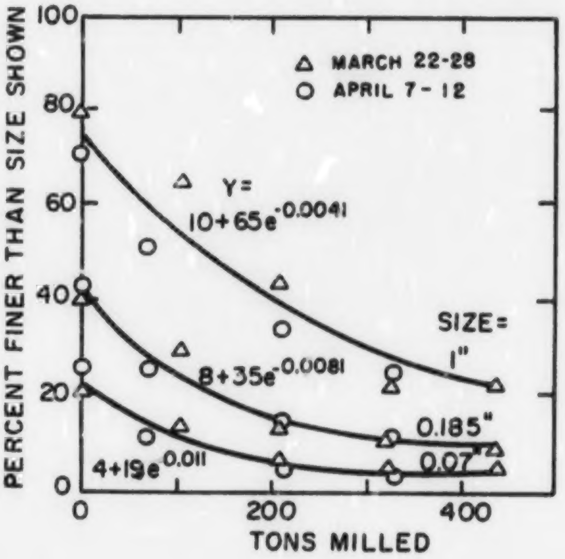

Figure 46 Changes in Particle Size Distribution as a Result of Cumulative Hammer Wear

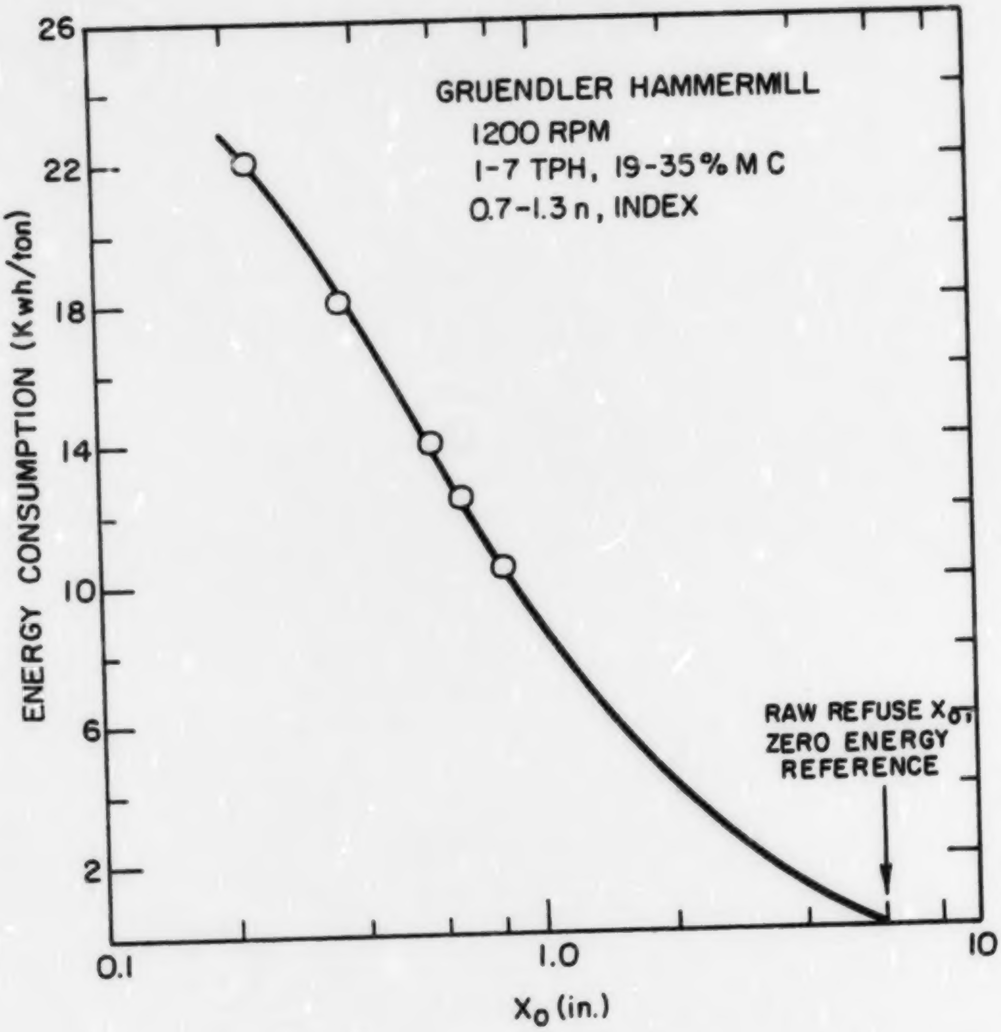

Figure 47 Specific Energy Consumption to Achieve a Given Characteristic Particle Size

for a similar percent reduction of x_o from 0.6 to 0.3 in.

The specific energy consumption is affected by the feedrate in the manner shown in Figure 48. As the feedrate increases beyond 2 tons/hr, the energy consumption increases significantly at higher grinding speeds. At a feedrate of 6 tons/hr, energy savings on the order of 48% can be realized by grinding at the lower speed of 790 rpm. The penalty is in the resulting coarser size distribution, which is evidenced by the fact that a 118% increase in specific energy was needed to obtain a size distribution at 790 rpm that is nearly identical to that at 1,200 rpm (Figure 49). In this case, both size distributions were obtained under nearly identical feedrate and moisture conditions. Specifically, for a dry feedrate of 6.4 Kwh/ton, whereas 27.2 Kwh/ton is required for grinding at 790 rpm to obtain the same size profile. Figure 49 also shows that a portion of the 555 rpm size distribution coincided with the 1,200 and 790 rpm distributions at the larger screen sizes. Thus, less material is contained in the finer size ranges, and slightly less energy was used (22.4 Kwh/ton) than at 790 rpm. The finer size distribution obtained at 790 rpm (Figure 49) at the same feedrate and moisture content required an increase in specific energy consumption from 10.7 to 27.2 Kwh/ton. Even though there was a significant increase in specific energy consumption, it seems somewhat anomalous that two different size distributions can be obtained under the same conditions of feedrate and moisture content. The physics of the comminution process determines the amount of energy required for size reduction. In this case, the raw refuse size distribution may have been different in each instance or the physical mechanisms of comminution may have been different, perhaps because of a difference in refuse composition.

The amount of moisture contained in refuse also has an effect on the comminution energy consumption. This effect is shown in Figure 50 for a range of moisture content conditions between 20% and 60% or feedrates from 1 to 7 tons/hr (dry weight) or from 1 to 13 tons/hr (wet weight). A minimum energy consumption occurs at moisture contents in the 35% to 50% range. These results are consistent with the tendency of lower grinding speeds to require less specific energy consumption and yield coarser size distributions. Furthermore, these results appear to agree with data obtained at Madison on the Tollemache mill. Here moisture contents of 24% and 36% gave specific energy consumptions of 10.9 Kwh/ton and 8.8 Kwh/ton, respectively. These results lie in our range of moisture content where specific energy consumption decreases with increasing moisture content.

Since the characteristic particle size (x_o) of commercial refuse is two to five times that of residential refuse, the specific energy consumption required to reduce commercial

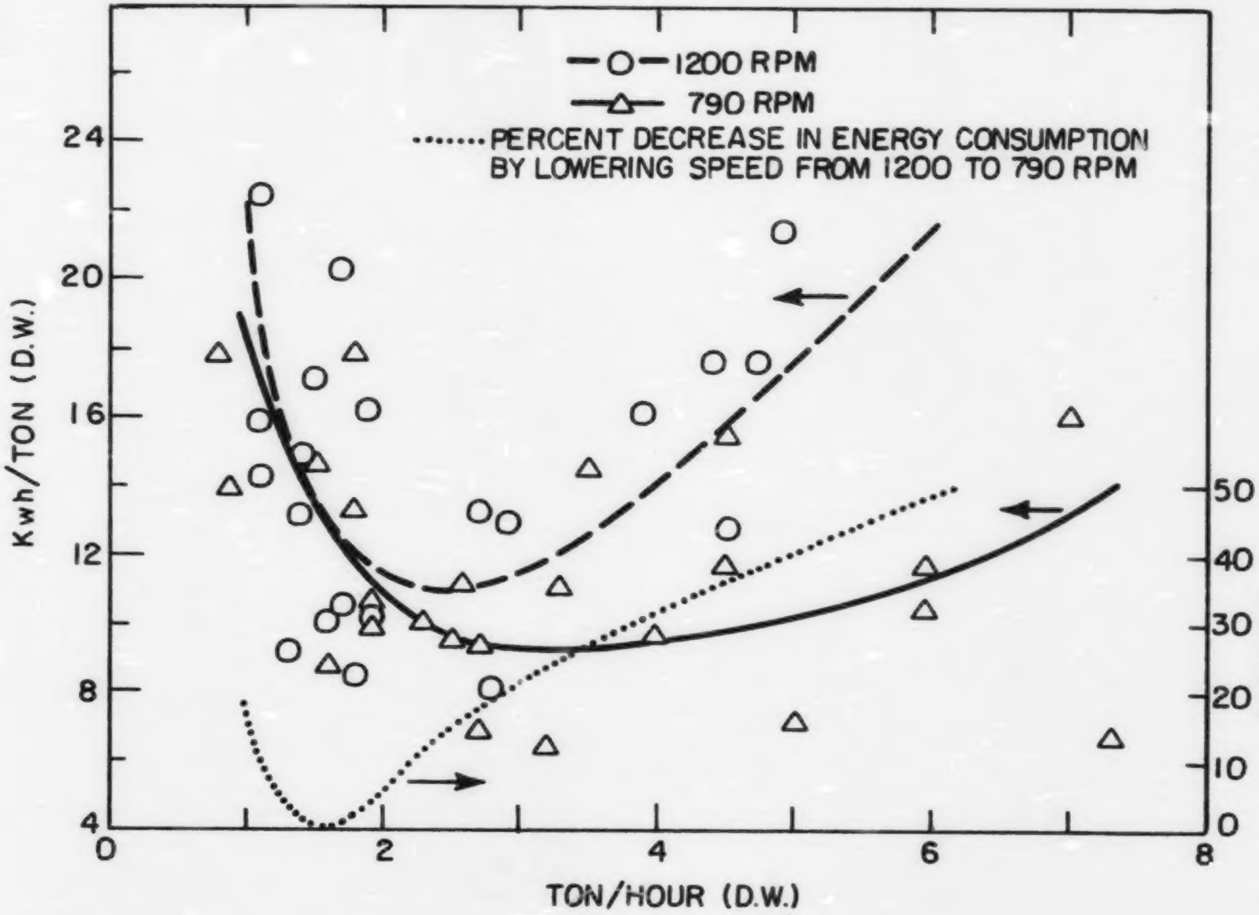

Figure 48 Specific Energy Consumption at Different Grinder rpm (Dry Weight Basis)

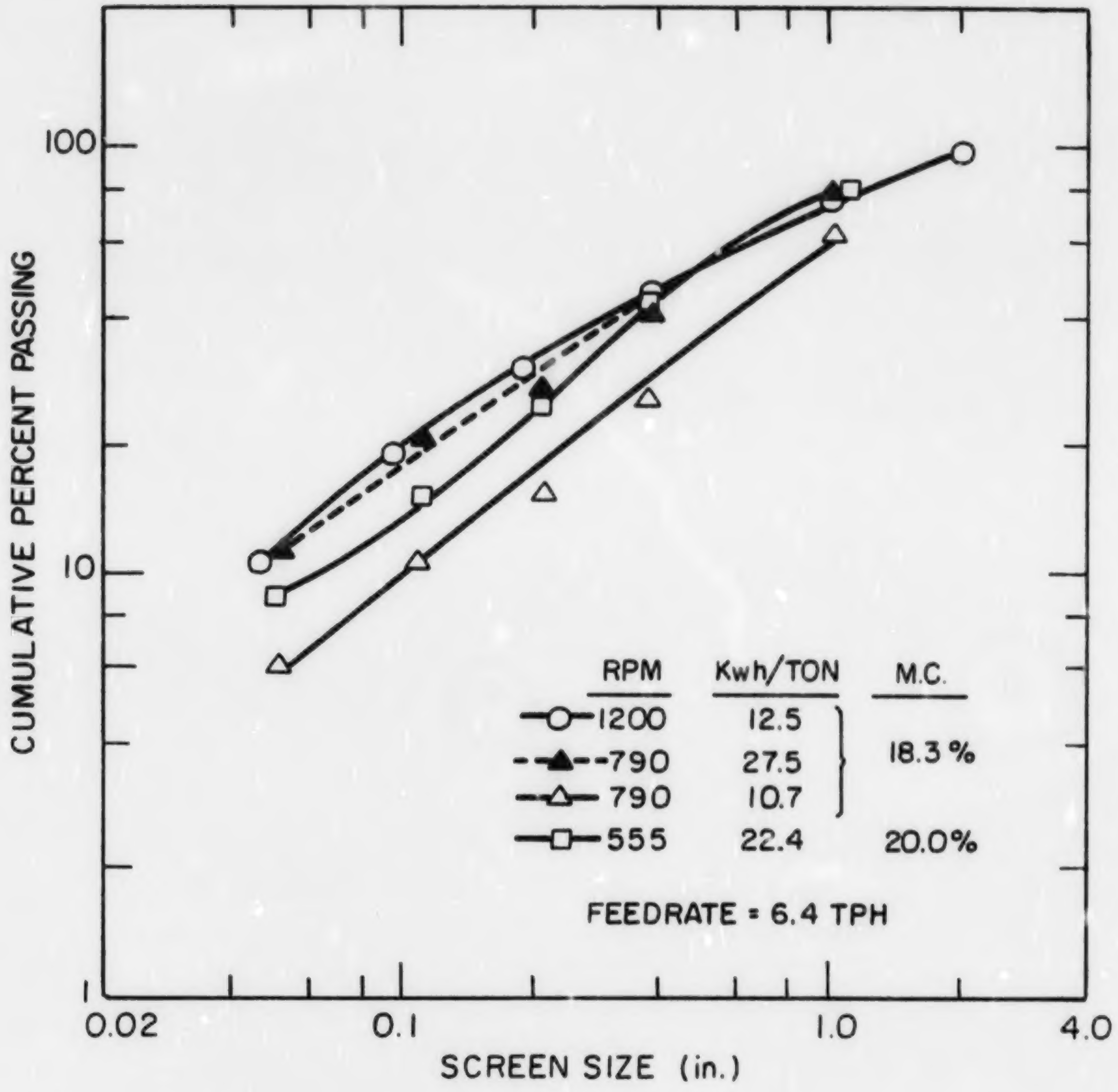

Figure 49 Influence of Grinder Rotor Speed on Energy Consumption vs. Size Distribution of Residential Refuse

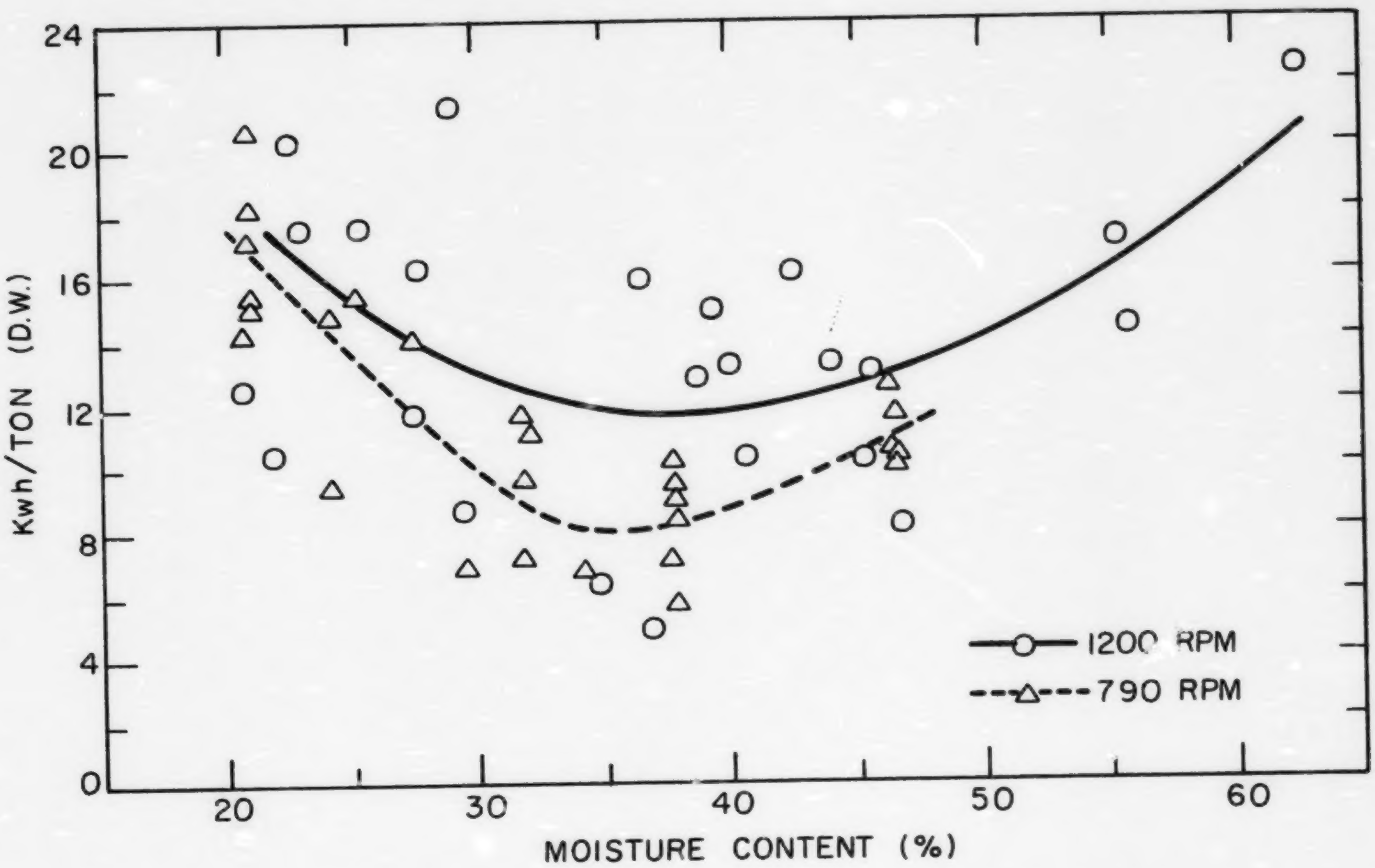

Figure 50 Effect of Moisture Content on Specific Energy Consumption for Grinder Rotor Speeds of 1,200 and 790 rpm

refuse, the specific energy consumption required to reduce commercial refuse to an equivalent residential size distribution must increase. For example, a comparison between grinding residential and commercial refuse to nearly the same size distribution yields energy consumption values of 13.5 Kwh/ton ($n = 1.0$, $x_o = 0.9$) and 19.0 Kwh/ton ($n = 0.96$, $x_o = 1.1$), respectively. This result is further illustrated in Figure 51.

The correct placement of hammers in certain machines can also have an effect on reducing the specific energy consumption. Investigators at Madison report that with the vertical Tollemache mill, the original 54-hammer configuration could be replaced with 34 optimally positioned hammers, resulting in increased production and decreased specific energy consumption.

COMPARISON OF SOME COMMERCIAL GRINDERS

The shredded refuse size distributions obtainable from several commercially available grinding machines are shown in Figure 52. The relative position of each size distribution is mainly a function of the grate spacing, or exit clearance dimension, of a particular grinder. Grinders that produce size distributions at the finer end of the spectrum consequently have smaller exit openings. Using the average size distributions obtained from different grinding machines for size reducing residential solid waste, a correlation between specific energy consumption and characteristic particle size (x_o) (Figure 53) was established. It is interesting to note that the data obtained at the St. Louis facility and analyzed by the Midwest Research Institute are in excellent agreement with prediction of specific energy consumption from characteristic particle size.

Observations of the performance of vertical and horizontal shredders at Madison indicate that for machines of comparable size, operating under comparable conditions, specific energy consumptions of 7.2 Kwh/ton and 12.5 Kwh/ton, respectively, were obtained. This result tends to suggest that horizontal shaft hammermills require more energy. However, the vertical Eidel machine shows the highest energy consumption (Figure 53) and correspondingly the smallest characteristic particle size. Consequently, comparison of energy consumption of various machine configurations should be in terms of comparable particle sizes.

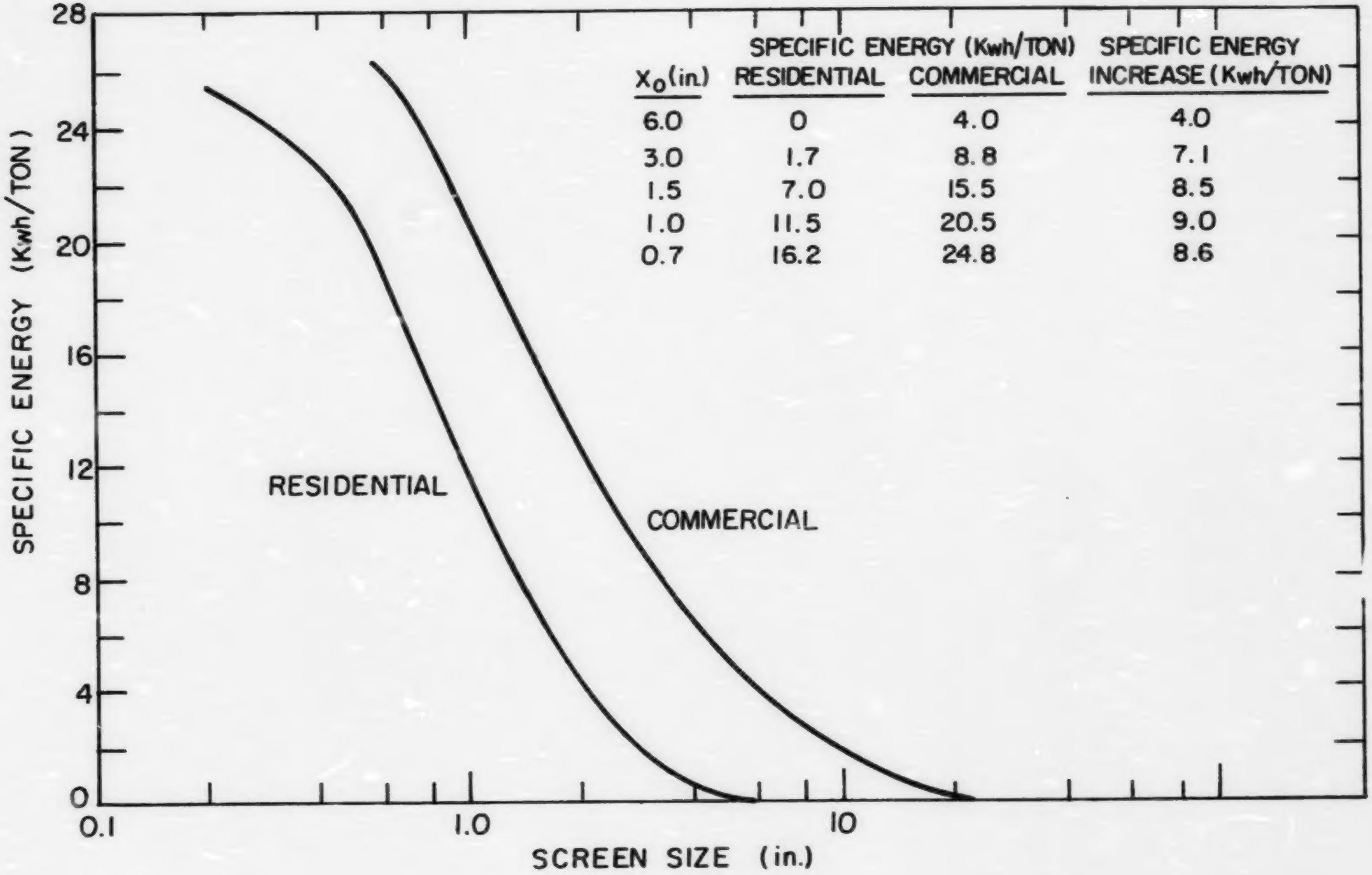

	SPECIFIC ENERGY (Kwh/TON)		SPECIFIC ENERGY
X_o (in.)	RESIDENTIAL	COMMERCIAL	INCREASE (Kwh/TON)
6.0	0	4.0	4.0
3.0	1.7	8.8	7.1
1.5	7.0	15.5	8.5
1.0	11.5	20.5	9.0
0.7	16.2	24.8	8.6

Figure 51 Comparison of Characteristic Particle Size (X_o) and Specific Energy for Commercial and Residential Solid Waste

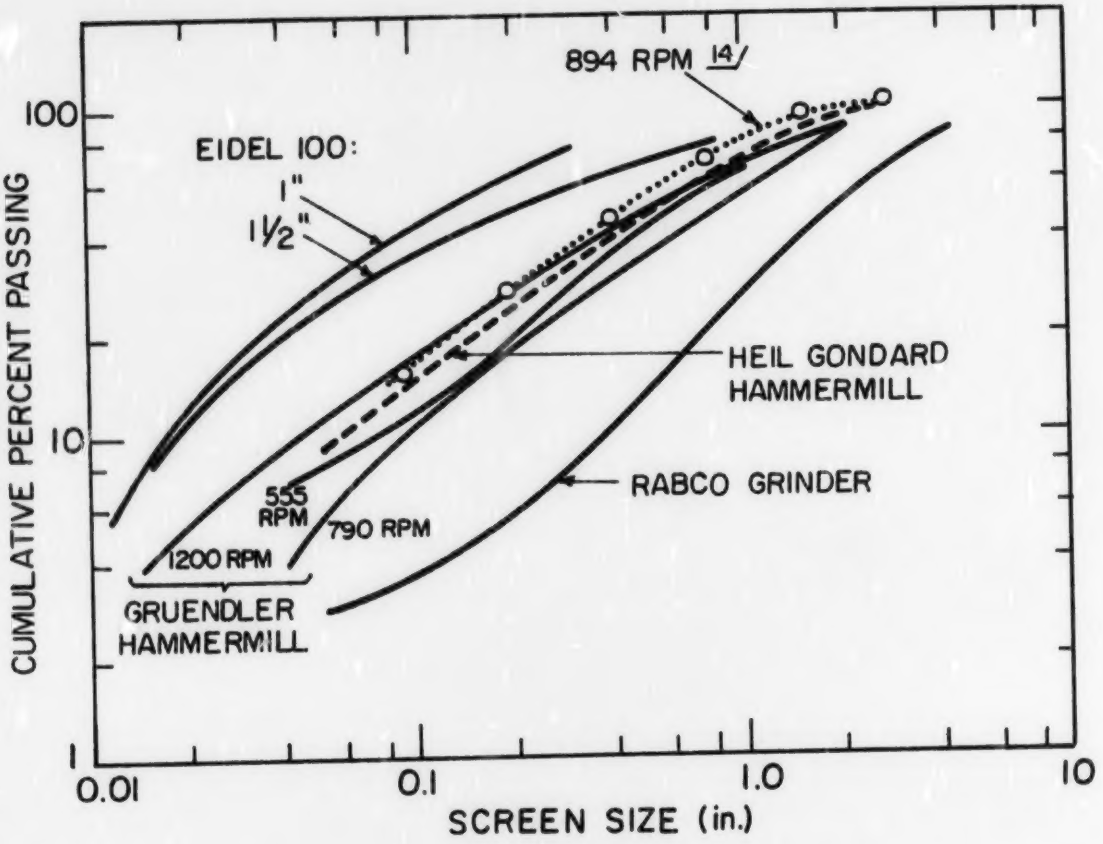

Figure 52 Size Distribution of Refuse from Various Shredders

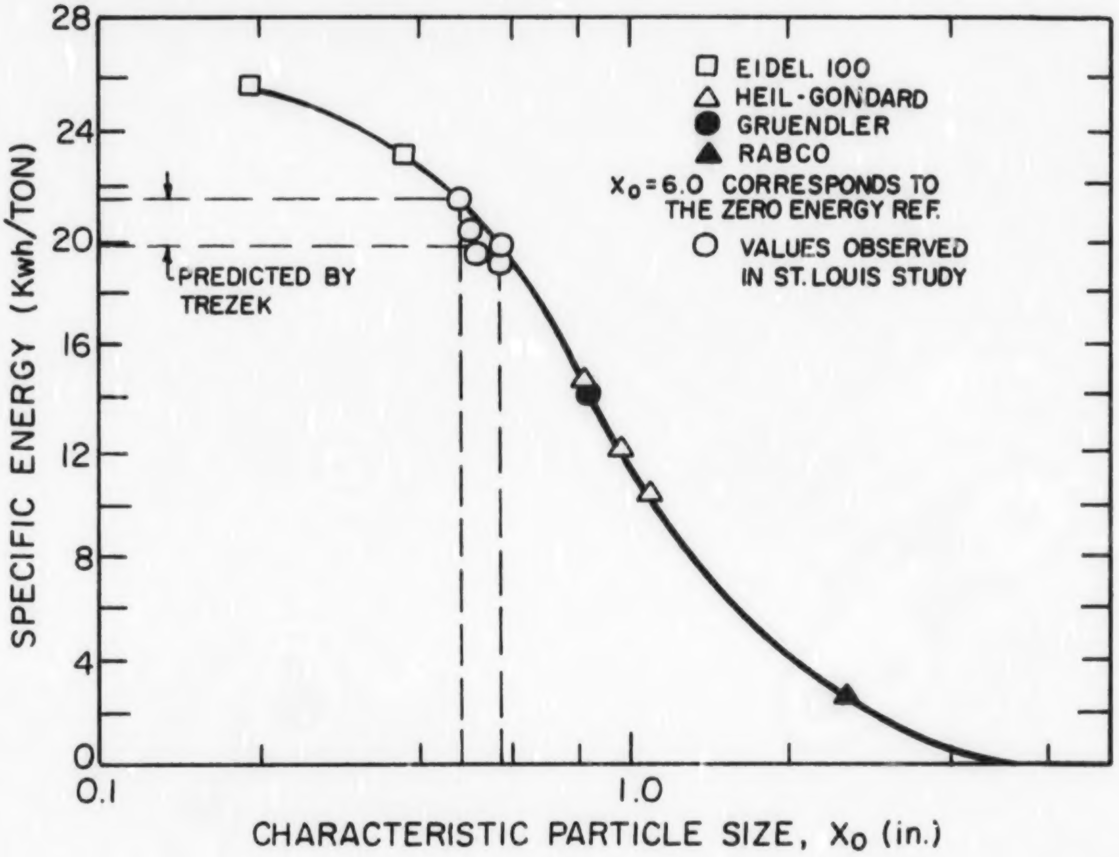

Figure 53 Characteristic Particle Size vs. Specific Energy Consumption

SECTION 4

WEAR, MAINTENANCE, AND SHREDDER SELECTION ASPECTS OF REFUSE COMMINUTION

Not only do comminution variables play a role in refuse size reduction, but they also give rise to a number of maintenance or operational considerations. These factors are usually reflected in the economics of the size reduction process or, depending on the accounting procedure, contribute to the cost of feeding material into the shredder. The following discussion first considers the question of hammer and grate bar wear and then other areas that have a bearing on maintenance considerations.

WEAR ASPECTS

Data related to hammer and grate bar wear were routinely monitored as part of the experimental protocol used in systematically studying the nature and behavior of the parameters involved in refuse comminution in our laboratory (19). In essence, the comminution parameter study involved the collection of a series of data sets where a particular data set consisted of runs at various feedrates for each of a specified series of moisture contents all at a constant grinder speed. Additional data sets were generated by changing the grinder speed and then repeating the feedrate-moisture content procedure. After the completion of a data set, the hammers and grates were removed and checked for wear.

At the beginning of the first data set experiment (1,200 rpm), 8 new, non-hard-faced hammers and 36 face-hardened hammers (Figure 54) were weighed, identified, profiled on paper, and placed in the grinder as depicted in Figure 55. All the new hammers were placed in the same row so that a representative wear pattern could be established for the new hammers. Opposing rows of hammers were carefully balanced to eliminate dynamic imbalance while the grinder was operating. Similarly, the 3-in. grate bars were weighed, identified, and placed in the grinder. Thus the grinder wear investigation included the determination of the parent hammer material and hardfacing material, the material loss of the face-hardened hammers, the non-hard-faced hammers, and the 3-in. grate bars.

The hammer material was an austenitic manganese steel containing 12.65 wt. % manganese. Such a steel (commonly called Hadfield's

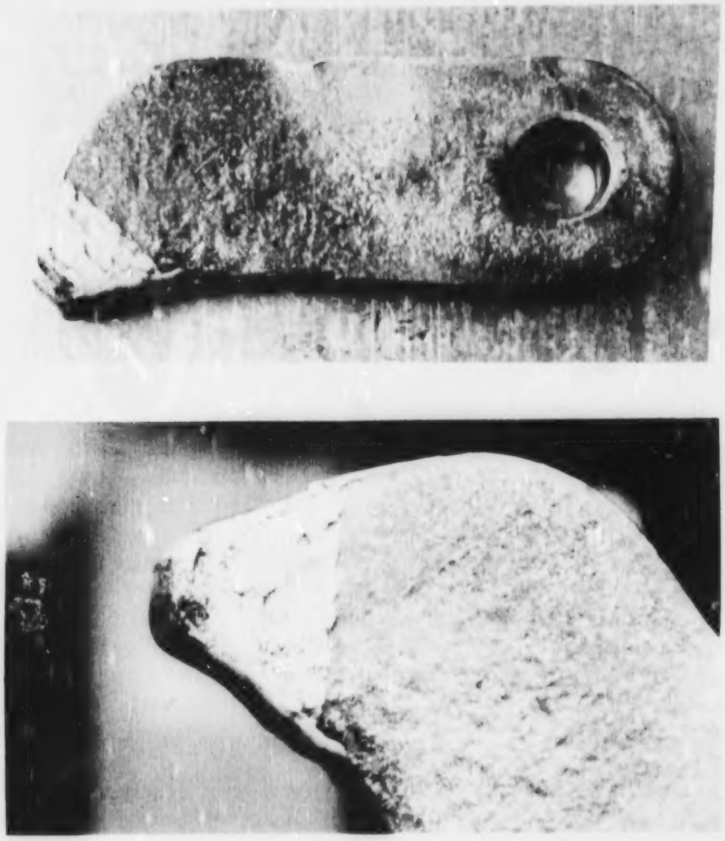

Figure 54 Manganese Steel Hammer with Hard Facing Weld Material Applied About the Crushing Face

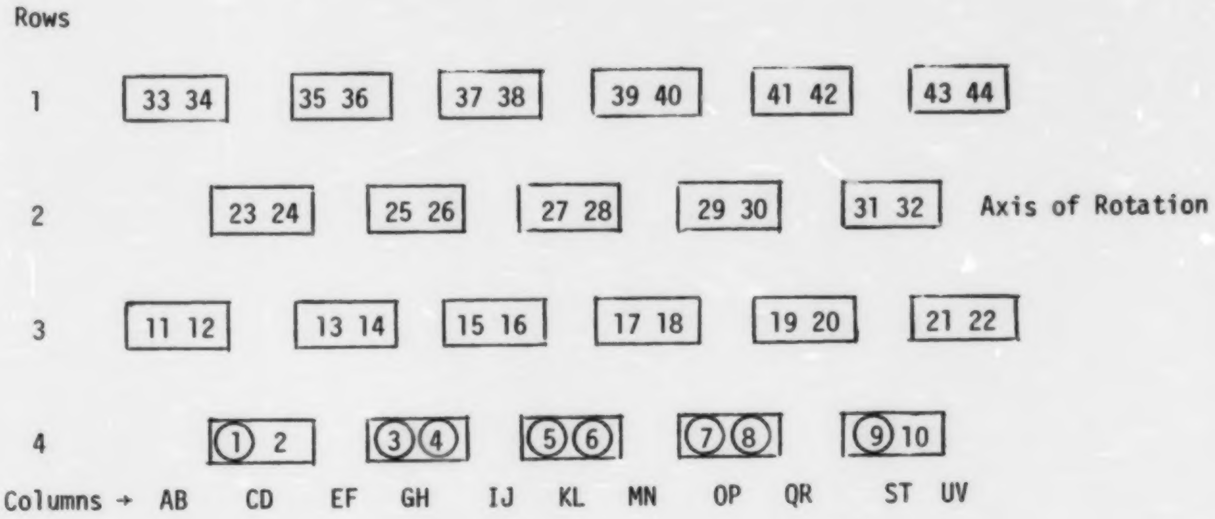
Rows
1
33 34
35 36
37 38
39 40
41 42
43 44
2
23 24
25 26
27 28
29 30
31 32
Axis of Rotation
3
11 12
13 14
15 16
17 18
19 20
21 22
4
① 2
③④
⑤⑥
⑦⑧
⑨ 10
Columns → AB CD EF GH IJ KL MN OP QR ST UV

Figure 55 Hammer Configuration

manganese steel) is extremely tough and is used in applications where heavy impact and abrasion are present. The Brinell hardness ranged from 179 to 209 over the surface of the hammers.

The face-hardening material applied to worn hammers was an austenitic manganese steel containing 10.5% manganese, 8.14% chromium, and trace amounts of nickel and molybdenum. This particular alloy belongs to the 2c subgroup of hard facing alloys and is used in applications where severe impact (greater than 1,000 ft-lb/in^2) and abrasion are encountered. The Brinell hardness of the hard facing welds varied from 321 to 385 over the surface of the weld deposit.

On the average, bare hammers weighed 9,464 g (20.85 lb), and the hard-faced hammers weighed 9,251 g (20.38 lb). Although there is no way of accurately determining the amount of hard facing that was present on the face-hardened hammers, an estimate of about 1 lb of weld material per hammer seems realistic.

MEASUREMENTS OF WEAR

During the first data set, the hammers and grate bars were exposed to the processing of 69 tons of municipal solid waste. A wide range of moisture (17.7% to 62.5%) and feedrates (1.75 to 8.10 tons/hr, wet weight basis) were presented to the wearing elements in the grinder. Likewise, the hammers and grates during the second data set were exposed to 50 tons of refuse ranging from 14.8% to 56.7% moisture and feedrates of 1.10 to 11.0 tons/hr.

According to the procedure previously mentioned, at the conclusion of the first data set, the grinder was disassembled, and the hammers and grate bars were removed. The individual hammers were weighed, photographed, and examined for metal failure and wear. The grate bars were also weighed and examined. The wear that the hammers and grate bars experienced during each data set is summarized in Tables 11 and 12.

TABLE 11. HAMMER WEAR

Item	Non-hard-faced hammers (lb)	Hard-faced hammers (lb)
1,200 rpm Operation:		
Max. wt. loss per hammer/ton	0.00290	0.00222
Min. wt. loss per hammer/ton	0.00159	0.00088
Avg. wt. loss per hammer/ton	0.00245	0.00155
790 rpm Operation:		
Max. wt. loss per hammer/ton	0.00158	0.00140
Min. wt. loss per hammer/ton	0.00128	0.00084
Avg. wt. loss per hammer/ton	0.00138	0.00106

TABLE 12. GRATE BAR WEAR

Item	Amount (lb)
1,200 rpm Operation:	
Total wt. of grates	1,427.0
Total wt. loss	3.6
Wt. loss/ton	0.053
790 rpm Operation:	
Total wt. of grates	1,423.4
Total wt. loss	1.7
Wt. loss/ton	0.034

The grate bars in the vicinity of the entering refuse stream were subjected to the greatest amount of wear. Less wear was apparent further away from the entering refuse stream. This trend was evident in the data collected from both experimental sets.

After completion of the first data set, there was evidence of abrasive wear on the bare hammers. A comparison of the worn non-hard-faced hammers against their original cast profiles (Figure 56) illustrates the general rounding of the edges of the hammers. The majority of the material loss, usually 1/2 to 9/16 in., occurred on the bottom edge of the hammer's crushing face, whereas the top edge sustained a material loss of about 1/8 to 3/16 in. (Figure 57). This pattern of wear, in which the bottom edge of the crushing face sustains the greatest amount of material loss, is consistent with the fact that the bottom edge of the hammer shreds and crushes the refuse against and through the grate bars. Some of the face-hardened hammers showed areas of severe impact. These impacts were marked by gouges, indentations, and suspicious flat surfaces on and about the crushing face of the hammers. The worn surfaces of the hard facings were indicative of abrasive wear, as was the case with the new hammers. A general rounding of edges and overall smoothness of the hard facing led to this conclusion. Nevertheless, areas of severe impacts were also present on some of the hard-faced hammers.

Upon termination of the 790 rpm data set, the hammers and grates were again subjected to physical examination. The bare hammers still exhibited the characteristic abrasive wear noticed in the first data set. As noticed after completion of the first data set, physical examination of the hammers showed few areas of severe impacts. Indications are that impact plays an insignificant destructive role compared to the abrasive forces at work during the comminution of refuse.

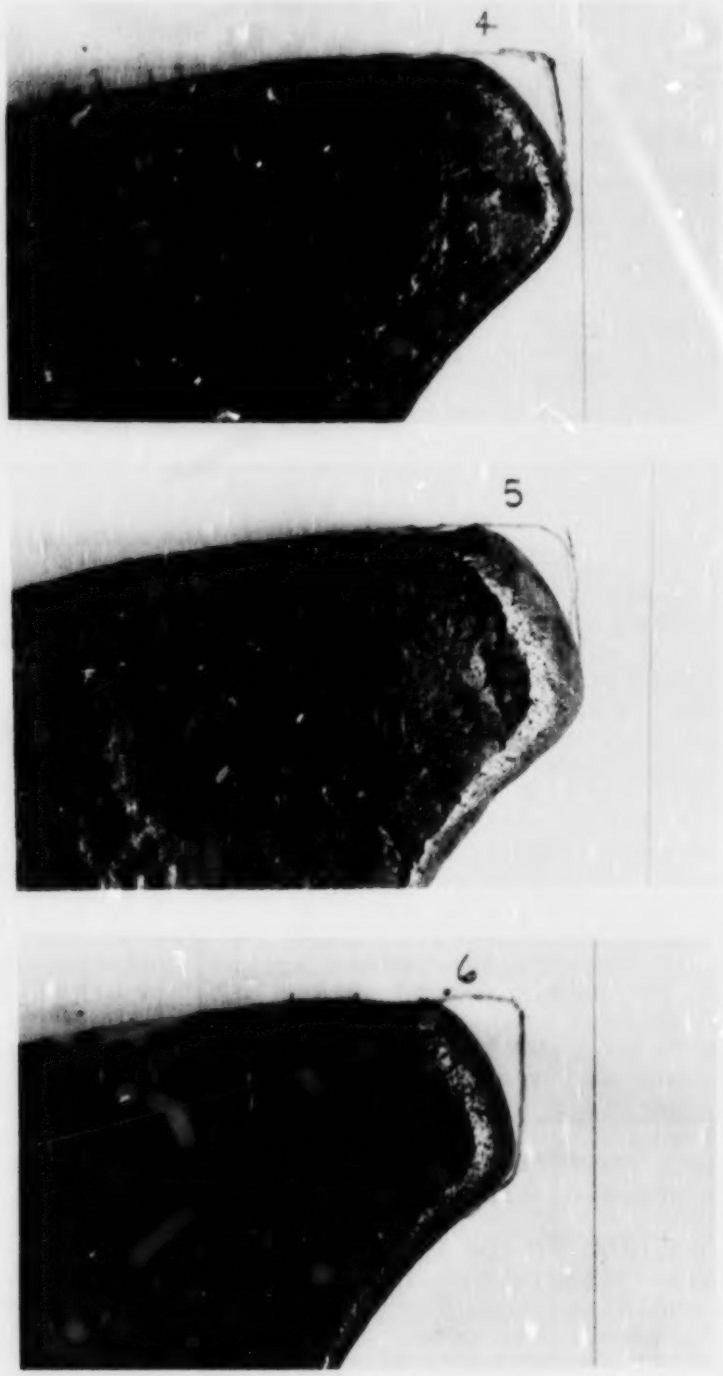

Figure 56 Non-Hard-Faced Hammers After Grinding 70 Tons of Refuse at 1,200 rpm

The wear pattern for the hammers used in each data set was established and exhibited an asymmetric profile about the grinder centerline. Both hard-faced and bare hammers on one side of the grinder experienced more wear than those on the other side. This pattern may be somewhat explained by the procedure used to load refuse on the input conveyor to the grinder. A front-end loader dropped refuse over the side hopper wall onto the conveyor belt. As a result of the restricted movement of the loader bucket, more refuse may have been dumped onto the near side of the conveyor, and thus the hammers on this side of the grinder may have sustained more wear (Figure 58).

This irregular wear of the hammers points out the importance of feeding the grinder uniformly across its width. Both machine rotor imbalance and premature hard facing or hammer replacement are possible penalties for a haphazard or poorly engineered grinder feeding system.

DISCUSSION OF WEAR PARAMETERS

The above experimental data provide an insight into the effect of shredding speed on the wearing properties of hard-faced and non-hard-faced hammers and the wearing durability of hard facing under different operating speeds. The important influence of speed on wear can be evaluated by referring to Table 11. For operation at 1,200 rpm, based on an average weight loss per hammer for the face-hardened and non-face-hardened hammers, the latter lost 57% more material under the same conditions and during the same time period. Compared to the average material loss of the hard-faced

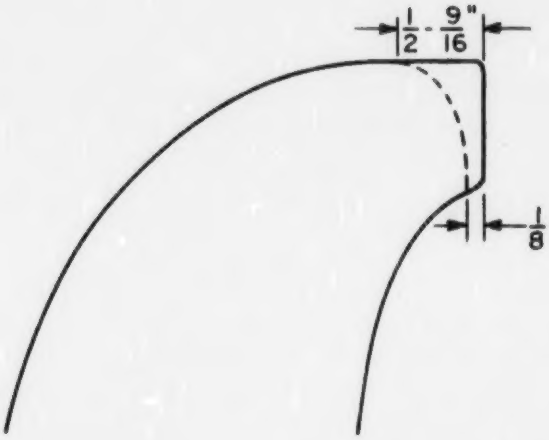

Figure 57 Summary of Worn Hammer Profiles

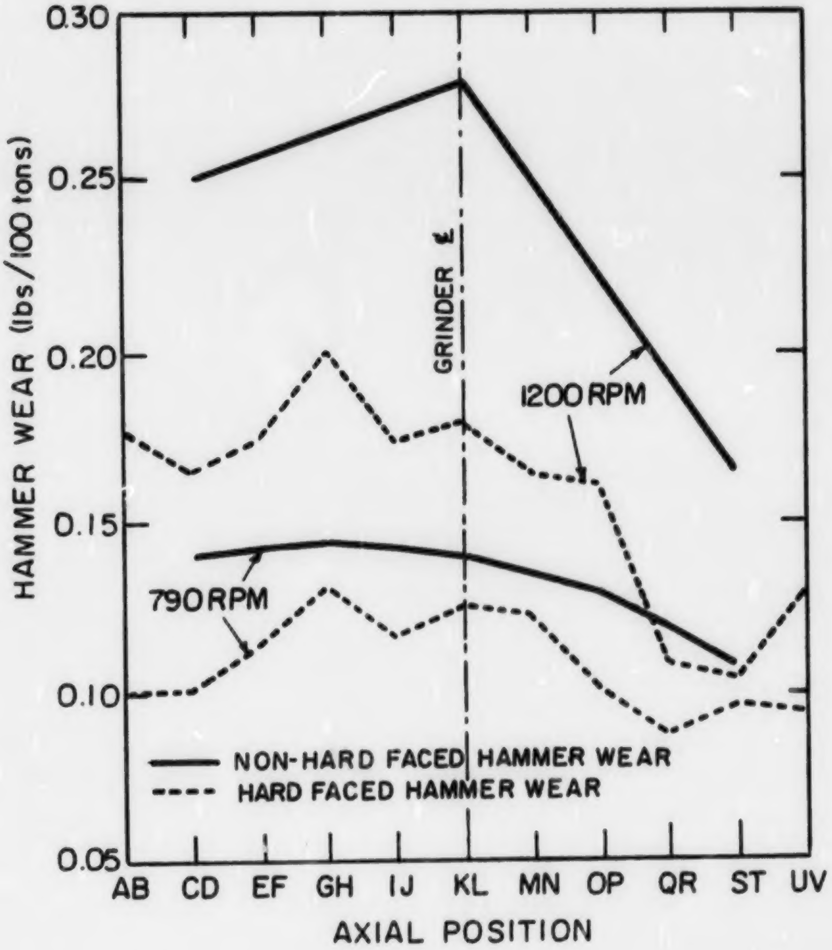

Figure 58 Effect of Grinder Speed on Hammer Wear

hammers, the range of increased wear for new hammers varied from 3% to 87%.

If the average weight loss per non-hard-faced hammer/ton of refuse is extrapolated to a full set of non-hard-faced hammers for this particular grinder, the estimated hammer weight loss per ton would be 0.107 lb/ton. Similarly, for a full set of face-hardened hammers, the weight loss per ton would be 0.068/ton. Hence the face-hardened hammers should exhibit about 37% less wear than hammers that are not face-hardened.

To estimate the actual grinder wear, both the hammer wear and the wear of the grate bars must be combined. The grate bar wear expressed in pounds of material lost per ton (0.053 lb/ton) can be expected to be about equal to the weight loss per ton for a full set of face-hardened hammers (0.068 lb/ton), or roughly half the weight loss per ton of a full set of non-face-hardened hammers (0.107 lb/ton). Therefore, the estimated wear for a grinder employing non-face-hardened hammers is 0.160 lb/ton; and for a grinder using face-hardened hammers, it is 0.120 lb/ton. Thus when the total wear of the hammers and grates is combined, face hardening of the hammers results in 25% less wear in the grinder.

Results at 790 rpm were similar to those at 1,200 rpm; the hard-faced hammers exhibited less material loss on the average (0.00106 lb/ton) than the non-hard-faced hammers (0.00138 lb/ton). Based on the average weight loss per hammer, the non-hard-faced hammers lost 30% more material than the hard-faced hammers under the same conditions and during the same time period. The range of increased wear for the non-hard-faced hammers when compared to the average material loss for the hard-faced hammers varied from a high of 49% to values that were actually lower than the average for the hard-faced hammers.

If the average weight loss per ton for non-hard-faced hammers is extrapolated to a full set of non-hard-faced hammers operating at 790 rpm, the estimated hammer weight loss per ton would be 0.061 lb. Similarly, for a full set of hard-faced hammers, the weight loss per ton would be 0.047 lb. Hence the hard-faced hammers would exhibit 23% less wear than hammers that are not hard-faced.

To estimate the total grinder wear, both the hammer wear and the grate bar wear for machine operation at 790 rpm must be combined. The grate bar wear produced at 790 rpm was 0.036 lb/ton. The grate wear can be expected to be about half the wear of the hard-faced hammers (0.061 lb/ton), or about 70% of the wear of the non-hard-faced hammers. The combined grate bar and hammer wear for the hammermill equipped with non-hard-faced hammers and operating at 790 rpm was estimated to be 0.095 lb/ton. On the other hand, total wear when hard facing is used is decreased to 0.081

lb/ton. The use of hard-faced hammers would represent a decrease of 11% in total grinder wear.

SIGNIFICANCE OF LOWER OPERATING SPEED

A definite reduction in hammer wear occurred while operating at the lower grinder speed of 790 rpm (Figure 58). The decrease in material loss was apparent in both non-hard-faced and hard-faced hammers. On the average, hammers with hard facing exhibited a decrease of 31% in material loss when the grinder speed was reduced from 1,200 rpm to 790 rpm (Table 13). At the same time, the bare hammers showed a 43% reduction in material loss. Grate wear also decreased by 36% as a result of operating at the lower speed.

At 1,200 rpm, the non-hard-faced hammers lost 57% more material than the hammers with hard facing, and at 790 rpm, the bare hammers lost 30% more material than their face-hardened counterparts. Thus there was a reduction in the performance of hard-faced hammers with respect to bare hammers of approximately 50% when the grinder speed was reduced. This finding indicates that at lower grinder speeds, expensive hard facing may be unnecessary, and that a less expensive material applied less frequently would appear to be a beneficial alternative.

Perhaps the most significant finding of this study involves the tempering of the wearing mechanisms on the non-hard-faced hammers through a reduction in operating speed. As Table 13 shows, the average hammer wear for bare manganese steel hammers at 790 rpm is 10% less than that for hard-faced hammers whirling at 1,200 rpm. This fact along with knowledge that the non-hard-faced hammers exhibited a decrease in wear of 43% point to the adoption of lower grinding speeds for the size reduction of refuse. Reduction of machine speed would appear to present a viable alternative to the costly and time-consuming maintenance required for hard facing grinder hammers.

At the reduced rpm, there was a slight shift in the size distribution towards a coarser product and a decrease in energy consumption that varied with feedrate. This is mentioned in passing to indicate that the reduction in speed from 1,200 rpm to 790 rpm had no significant effect on grinding efficiency or throughput capacity.

WEAR INFORMATION FROM VARIOUS SHREDDING FACILITIES

Though there is a general paucity of quantitative wear data, the operation of some shredding facilities over the past decade and the establishment of new facilities for energy and material recovery offer the potential for alleviating this situation. The

TABLE 13. AVERAGE WEAR FOR HAMMERS AND GRATE BARS AT DIFFERENT GRINDER OPERATING SPEEDS

Item	Average wear (lb/ton) 1,200 rpm	Average wear (lb/ton) 790 rpm	% Decrease in wear at lower speed
Full set of hard-faced hammers	0.068	0.047	31
Full set of non-hard-faced hammers	0.107	0.061	43
Grate bars	0.053	0.034	36

correlation of wear data is hampered by the fact that standard procedures for measuring and evaluating wear are not used in the industry. In some cases, wear is simply measured as the length of hammer recession or the number of inches of hammer tip lost after a certain number of tons of refuse have been processed. Some specific information regarding the amount of metal removal revealed the following facts: a) Correspondence with Mr. L.C. Herbert, Director, Municipal Machinery Ltd., Kent, England, manufacturers of the Gondard equipment, indicated that hammers tend to wear at a constant rate at any one plant. Furthermore, hammer wear can be expressed as 0.5 lb of hammer material/10 tons of refuse when the plant averages 1,500 tons/set of 48 hammers. Also of interest is his suggestion that hammer retipping may not necessarily be in the best economic interest. Principally, the custom of adding weld material or tipping was adopted as a means of keeping large rotors in balance once wear started to occur. Economics may be more favorable toward replacement rather than retipping. b) Some data from the Madison project indicated a hammer material loss of about 0.1 lb/ton of refuse. Other information from this site indicates a weight loss/100 tons on the order of 0.36%. The Madison investigators also question the idea of using hammer weight loss as the sole criteria for measuring hammer life. The validity of this criticism is somewhat substantiated by the fact that for some hammer configurations, a considerable wear or degradation of the cutting surface can take place with a relatively small loss in weight. In essence, even though hammers are heavy, a small weight loss may still result in a hammer that is considerably less effective. Hard facings have been reported to increase hammer life by a factor of nearly 5 for the Gondard mill. c) Some information on grinding parameters is also available in the joint EPA - New York City grinding study conducted on the Jeffrey Swing Hammer B3, 150 hp machine. Values of hammer wear reported as % weight loss/100 tons range from 0.3 to 1.0; a value of 0.8 corresponds to new hammers, and 0.3 to 0.4

appear to be more typical of used hammers. Investigators at this site also indicate that the hammer wear problem is sensitive to the nature and type of hard facing applied to hammer tips. Severe problems of rotor imbalance occurred as a result of rapid wear that was due to the loss of hard face material.

In summary, our wear measurements of 0.068 lb/ton and 0.107 lb/ton for hard-faced hammers and 0.047 lb/ton and 0.061 lb/ton for non-hard-faced hammers operating at 1,200 and 790 rpm, respectively, indicate that the range of 0.05 to 0.10 lb/ton (or in some cases slightly higher - 0.30 lb/ton) can be expected for hammermills shredding refuse.

HARD FACE COATINGS

Research into the area of hard facing has produced several avenues that could lead to improved life for grinder hammers. A base hammer material of an austenitic manganese steel appears to be the best choice among materials that could be considered for use in refuse grinding applications. Its toughness and abrasive resistance makes this steel a logical choice for the combined effects of abrasion resulting from glass, dirt, and paper, and of impact that is due to the presence of concrete, metal, etc. in refuse.

There are basically five groups of hard facing alloys. Each group has a given resistance to impact, abrasion, erosion, corrosion, and heat. Cost, ease of application, availability, compatibility with the base hammer material, abrasion, and impact-resistant properties of the weld material must all be considered when determining which hard facing alloy will give the most economical and best wearing service. As mentioned earlier, our hammers are coated with a typical Subgroup 2c alloy (basically impact resistant, but good abrasion resistance). Insofar as abrasion may be the predominant wearing process in the size reduction of solid waste because of the cumulative weight percentages of glass and paper (65% to 80%) in refuse, an abrasion-resistant alloy with good impact-resistance qualities may prove to be the best choice among alloys. Moving up to a Group 3 or 4 hard facing alloy would increase the abrasion resistance of the hammers, but it would also cost more. The cost of the hard facing material ranges from $0.50 to $9.00/lb over the span of the five hard facing groups. Group 3 or 4 alloys cost $5/lb; Group 5 alloys, the hardest and most wear-resistant of all hard facing materials, cost $9/lb.

Since physical examination of the worn hammers indicates that hammer wear is primarily abrasive and not representative of wear resulting from continual impact, hard facing alloys in Groups 3, 4, or 5 may substantially increase hammer life. However, experimentation would be necessary to determine if the increased life was worth the cost of these more exotic abrasion-resistant alloys. A Subgroup 2c alloy yielded 57% longer life at 1,200 rpm and 30% more life at 790 rpm; a Group 3, 4, or 5 alloy could conceivably result in a 100% to 150% longer life.

Various hard facing alloys are compatible with a manganese steel base material (Table 14). It should be pointed out that the application of the hard facing to a manganese steel requires care in welding. Manganese steel is unusually sensitive to reheating. Embrittling, transformations, or carbide precipitation resulting from heating can drastically reduce the characteristic toughness of the parent material. To prevent this undesirable effect, properly handled electric arc welding is necessary.

GRINDER MAINTENANCE

This discussion will focus on vertical and horizontal hammermills since these compose the majority of size reduction machines used in solid waste processing. Grinding maintenance can be broken down into two general areas: 1) rebuilding or replacing internal grinder parts (i.e., hammers, breaker bars, breaker plates, grates, wear plates, etc.); and 2) servicing the grinder drive system (i.e., grinder and motor bearings, couplings, etc.). The latter maintenance area requires a diligent servicing schedule with frequent inspections of the critical drive components, particularly the rotor bearings. For all components of the drive assembly, manufacturer's maintenance instructions should be conscientiously followed. Preventive maintenance significantly reduces the risk of premature failure of drive train components.

For example, a premature rotor bearing failure can take days or weeks to properly diagnose. After diagnosis, proper remedial action must be taken or the bearing may destructively fail. Unfortunately, most bearing failures are terminally diagnosed. That is, destructive failure occurs before any prior warning of imminent failure is noticed (e.g., increased operating temperature, unusual noise, etc.).

The replacement of a rotor bearing is usually a very time-consuming operation. Besides tearing down the grinder, examining the old bearing, and locating a replacement, the cause of the failure must be discovered. These operations usually shut down a shredding operation for 3 to 5 days. Obviously, the need for proper drive train component maintenance is very explicit.

Both rebuilding and replacement of the grinder's internal wear surfaces are accepted practice. Although each grinder and its mode of operation should be considered separately, experience has generally pointed toward some degree of hammer resurfacing (retipping) as being the preferred hammer wear maintenance technique.

TABLE 14. SUITABILITY OF HARD FACING COATINGS FOR VARIOUS BASE MATERIALS

Base material to be hard faced	Facing alloys					
	Iron-base				Tungsten carbide	
	To 20% alloy	Above 20%	Cobalt base	Nickel base	Inserts	Deposits
Carbon steels:						
0.10 to 0.35% C	Yes	Yes	Yes	Yes	Yes	Yes
0.35 to 1.0% C	Yes[a,b]	Yes[a,b]	Yes[a,b]	Yes[a,b]	Yes[a,b]	Yes[a,b]
Low-alloy structural and constructional steels; 0.30% max C	Yes	Yes	Yes	Yes	Yes	Yes
Gray, malleable and nodular irons	Yes[b,c]	Yes[b,c]	Yes[b,c]	Yes[b,c]	Yes[b,c]	Yes[b,c]
Low-hardenability martensitic stainless (410,403)	No	Yes[a,f]	Yes[a,f]	Yes[a,f]	Yes[a,f]	Yes[a,f]
High-hardenability martensitic stainless (420,440)	No	Yes[a,c,f]	Yes[a,f]	Yes[a,f]	Yes[a,f]	Yes[a,f]

TABLE 14 (Continued). SUITABILITY OF HARD FACING COATINGS FOR VARIOUS BASE MATERIALS

	Facing alloys					
	Iron-base				Tungsten carbide	
Base material to be hard faced	To 20% alloy	Above 20%	Cobalt base	Nickel base	Inserts	Deposits
Type 321 austenitic	No	Yes[c]	Yes[d]	Yes	Yes	Yes
Type 347 austenitic	No	Yes[c]	Yes	Yes	Yes	Yes
All other type 300 austenitic	No	Yes[c]	Yes	Yes	Yes	Yes
Monel	No	Yes[c]	Yes	Yes	Yes	Yes
Nickel	No	Yes[c]	Yes	Yes	Yes	Yes
13% Mn steels	Yes[e]	Yes[e]	Yes[e]	Yes[e]	No	Yes[e]

[a] Preheat.
[b] Gas welding preferred.
[c] For limited applications only.
[d] Use type 347 interlayer.
[e] Use nickel-base interlayer.
[f] Post-isothermal anneal.

The other components that are subjected to significant wear are the breaker bars, breaker plates, wear plates, and grates. Not all of these may be incorporated into the same grinder. These components generally require replacement or resurfacing with hard facing during the lifetime of the grinder. Replacement or resurfacing, as in the case of hammers, is usually process specific. That is, for a particular shredding operation, convenience and economy dictate which maintenance method (replacement or resurfacing) is most appropriate.

FACTORS AFFECTING GRINDER MAINTENANCE

Several factors relating to the grinder and drive system can have a significant impact on the performance of maintenance and maintenance costs, and these should be considered during the size reduction facility design phase and before grinder selection.

Since wear of the internal grinder components is inherent in the grinding process, consideration should be given to grinders that allow easy accessibility to the parts subjected to wear (e.g., hammers, grates, wear plates, etc.). Grinders that possess this accessibility feature will provide reduced maintenance costs for replacement or resurfacing as opposed to grinders that do not provide easy accessibility.

Hydraulic or pneumatic systems that open up or separate the grinder housing eliminate the need for overhead or portable cranes to disassemble the machine. Walkways and scaffolding built around the grinder allow workmen to move freely about and service the machine. In addition, sufficient headroom (above and below) and clearance around the other equipment should be incorporated into the design and layout of the grinder and its ancillary equipment. Last, the necessary clearance for part removal (e.g., hammer pins, grate bars, etc.) must be contemplated early in the design phase.

Since a rotor bearing replacement can be a time-consuming operation, a grinder that possesses easily accessible bearings is preferable over one that requires complete dismantling of the machine to free the bearings. In this regard, a horizontal mill may prove more convenient than a vertical mill. Removal of the bottom bearing(s) in a vertical hammermill usually requires disassembling the grinder and pulling out the rotor and hammers assembly.

MAINTENANCE COSTS

The prediction of hammermill maintenance costs is a very nebulous area. The costs are highly dependent on a number of factors. Some of the more important of these are:

1. Grinder model,

2. Composition and size distribution of the raw refuse,
3. Hammer tip speed,
4. Type of hardfacing,
5. Retipping schedule,
6. Part replacement schedule.

Because of the multiplicity of variables, two identical grinders operating under slightly different conditions (e.g., at different tip speeds or with different weld material as the hardface) can have significantly different maintenance costs. Most grinder manufacturers are very reluctant to forecast specific maintenance costs because of the unknown nature of the actual grinder operation and maintenance program.

Some manufacturers, however, have suggested a range in maintenance costs of $0.25 to $0.75/ton of refuse. Interestingly, the Madison hammermills, a Gondard mill, and a Tollemache mill had maintenance costs of $1.27/ton and $0.98, respectively. The Gainesville primary hammermill experienced maintenance costs of $0.76/ton. The Midwest Research Institute (17) estimated maintenance costs to be a function of hammermill capacity. Maintenance costs ranged from $0.30/ton for a throughput of 10 tons/hr to $0.70/ton for a throughput of 100 tons/hr.

GRINDER DESIGN AND SELECTION

The previously developed material in this report can be helpful in forming a firm background in MSW size reduction principles. In this section on grinder design and selection, the experimental results, variable interdependence, and other theoretical developments of the previous sections will be extended to actual grinding practice - namely design and selection considerations. Material presented here should provide the reader with the necessary information to 1) extend MSW grinding research data to "practical" use, 2) esimate the grinder power requirements for desired throughputs and product sizes, and 3) estimate the grate size required to furnish a desired size distribution.

Before further discussion, some other factors important in grinder selection should be considered, even though they do not involve feedrates, power requirements, and product size distributions. These factors concern the mill and the services that the manufacturer will deliver. Due consideration should be given to the manufacturer's knowledge and experience in the hammer retipping area. Since hammer resurfacing work contributes significantly to the total cost of grinder operation, the correct hardfacing material can generally reduce maintenance cost. Usually the manufacturer supplies the mill hammers already hardfaced. Consequently, a knowledgeable grinder manufacturer can save the grinder operator money by providing the hammers properly hardfaced. Proper hardfacing includes selection of a weld material that will provide good wearing characteristics and correct application of the weld material to the hammer base material. In addition, if in operation the hammer wear is unsatisfactory, the experienced manufacturer can recommend alternative weld materials that will provide better wear resistance and will be compatible with the hammer base material.

THE USE OF SPECIFIC ENERGY AND THE CHARACTERISTIC PARTICLE SIZE FOR DETERMINING GRINDER POWER REQUIREMENTS

Information developed in this report can be used to ascertain the net motor power required to achieve a given degree of size reduction. Determination of the net power requires specification of the product size distribution expressed as the characteristic particle size, x_o. Once the characteristic particle size has been chosen, the net horsepower can be calculated using the curve in Figure 59.

For example, consider a grinder that would be required to size reduce six tons of municipal refuse per hour to 90% passing 1.5 in. To use Figure 59, an x_o value must be estimated for the anticipated size distribution (i.e., 90% passing 1.5 in.). Estimating x_o requires some preliminary calculations. First, the value of $\ln(1/(1-y))$ must be calculated for use in conjunction with Figure 59:

$$\ln(1/(1-0.9)) = \ln(10) = 2.3 \qquad (3)$$

Second, a value of the n-index must be assumed for estimating purposes. An average value for municipal refuse shredding would be n = 1.0. The values for the $\ln(1/(1-y))$, 2.3, and the screen size, 1.5 in., specify a point on the graph in Figure 59.

An n-index of 1.0 implies a 45° slope through the point (1.5, 2.3). Intersection of this slope with the line $\ln(1/(1-y)) = 1.0$ provides the characteristic particle size, x_o, corresponding to a screen size of 1.5 in. In this case, the x_o value would be 0.65 in. Figure 59 indicates that a characteristic particle size (x_o) of 0.65 in. implies a specific energy consumption of 18 Kwh/ton.

The net power can be expressed as

$$KW_n = (E_o)(\text{tons/hr}) \qquad (4)$$

where KW_n = net power in kilowatts; E_o = specific energy, Kwh/ton; and tons/hr = tons of refuse per hour. In this instance, E_o = 18 Kwh/ton and tons/hr = 6.0. Therefore,

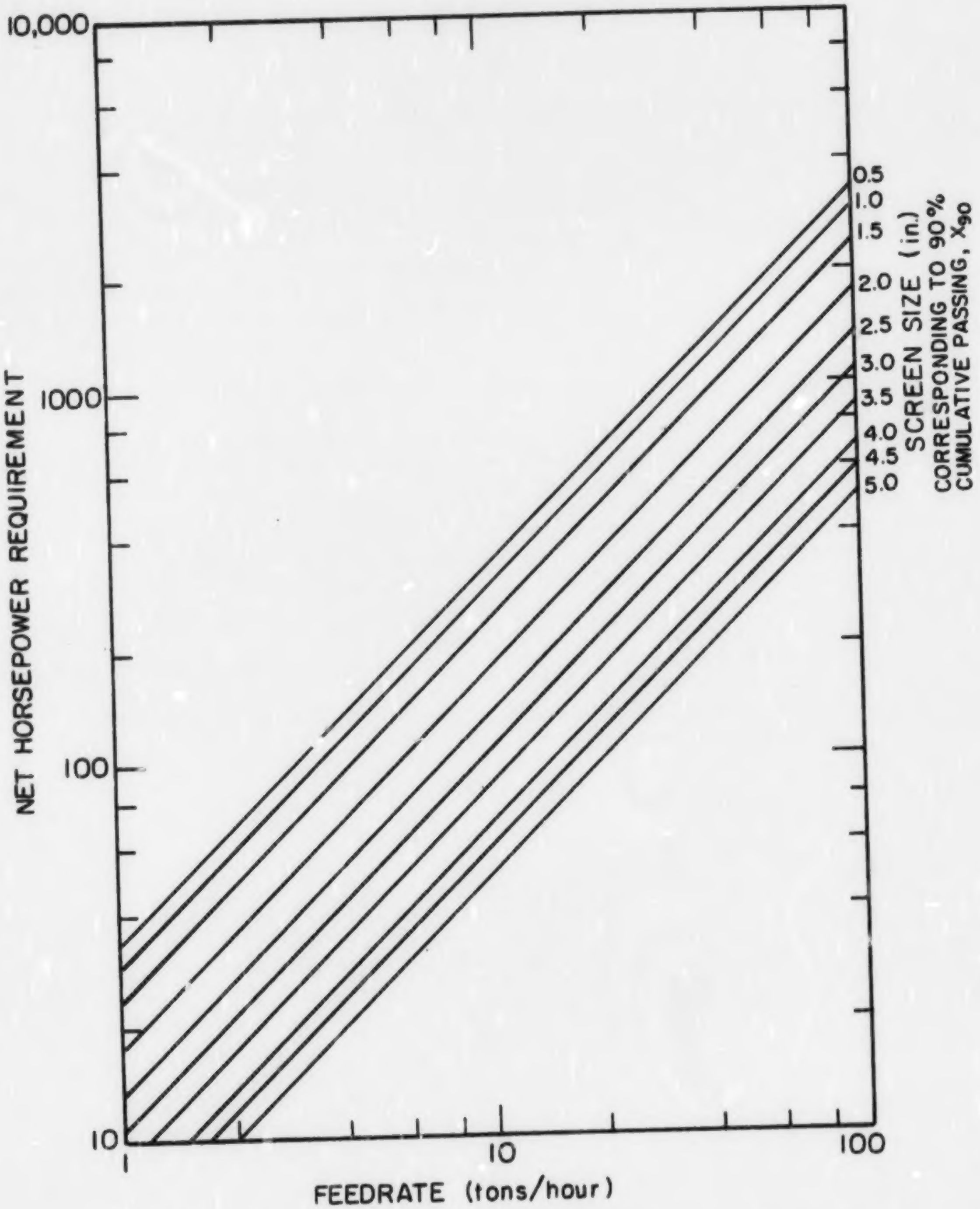

Figure 59 Horsepower Required for Size Reduction of MSW as a Function of Feedrate and Desired Product Size

$$KW_n = (18 \text{ Kwh/ton}) \text{ } (6 \text{ tons/hr}) \tag{5}$$

$$KW_n = 108 \text{ Kw} \tag{6}$$

For this example, the net power required for size reduction is 108 Kw.

To this net power consumption must be added the power required to overcome the bearing friction and the air resistance of the whirling hammers. For instance, our Gruendler mill (44 hammers, 36-in. tip-to-tip diameter) consumes approximately 30 Kw or 40 hp when operated at 1,200 rpm. Consequently, the actual motor horsepower is always larger than the net horsepower required solely for size reduction.

RELATIONSHIP OF GRINDER HORSEPOWER, FEEDRATE, AND PRODUCT SIZE

To introduce the jargon of the grinding industry, namely grinder horsepower and the 90% cumulative passing size (which henceforth will be abbreviated as x_{90}), the kilowatt power consumption and characteristic particle size (x_o), discussed previously, must be converted to the aforementioned industry-used terms. The kilowatt conversion is straightforward; that is, 1 hp equals 1.34 Kw. Likewise, 1 horsepower-hour/ton equals 1.34 Kwh/ton.

The conversion of x_o to x_{90} can be shown analytically to be solely a function of the n-index. In fact, the relationship of x_o, n, and the screen size corresponding to a given cumulative passing percent can be expressed as

$$x_o = \frac{x_i}{\{\ell n(1/(1-y_i))\}^{1/n}} \tag{7}$$

where x_o = characteristic particle size, x_i = screen size for a given cumulative passing percent (y_i), and n = the slope of the curve of the $\ell n(1/(1-y_i))$ versus the screen size x_i. Equation (5) reduces to

$$x_o = \frac{x_{90}}{2.3^{1/n}} \tag{8}$$

when the 90% cumulative passing size is used. If Equation 6 is solved for x_{90}, any x_o value can be converted to the equivalent x_{90} value,

$$x_{90} = (2.3^{1/n})\, x_o \qquad (9)$$

As mentioned previously, a value of $n = 1.0$ can be used for estimations of feedrates and power consumptions when dealing with MSW. Equation 7, therefore, reduces to

$$x_{90} = 2.3\, x_o \qquad (10)$$

Using these conversions ($h_p = 1.34$ Kw and $x_{90} = 2.3\, x_o$), a functional relationship among net horsepower, feedrate, and x_{90} has been established and is presented graphically in Figure 59. This figure may be used to estimate the net horsepower required to size reduce MSW at a given feedrate to a specific x_{90} size. As an example, to estimate the net horsepower required for a feedrate of 25 tons/hr and 90% passing 2.0 in., consult Figure 59 and follow these steps:

1. Locate the feedrate, 25 tons/hr, on the horizontal axis;
2. Find the intersection of the line corresponding to 25 tons/hr and the line $x_{90} = 2.0$ in.;
3. From the intersection point, proceed horizontally to the vertical axis (net horsepower requirement) and read 44 hp.

Figure 59 may be used to estimate horsepower requirements for 1 to 100 tons/hr and x_{90} values of 0.5 to 5.0.

ESTIMATION OF GRATE SPACING REQUIRED TO YIELD A DESIRED PRODUCT SIZE

As discussed earlier, there appears to be a relationship between grate spacing or exit clearance and the characteristic particle size (x_o) of the size reduced refuse (Figure 44). If an n-index of 1.0 is assumed to be representative for the size reduction of solid waste, then the information in Figure 59 can be reorganized to show the dependence of the 90% passing size (x_{90}) on the grate spacing (Figure 60).

To estimate the required grate spacing to provide a given degree of size reduction, Figure 60 may be used as a starting point. For example, if a product size of 90% passing 1.5 in. ($x_{90} = 1.5$ in.) is required, Figure 60 indicates a grate spacing of 2.5 in. should provide such a product.

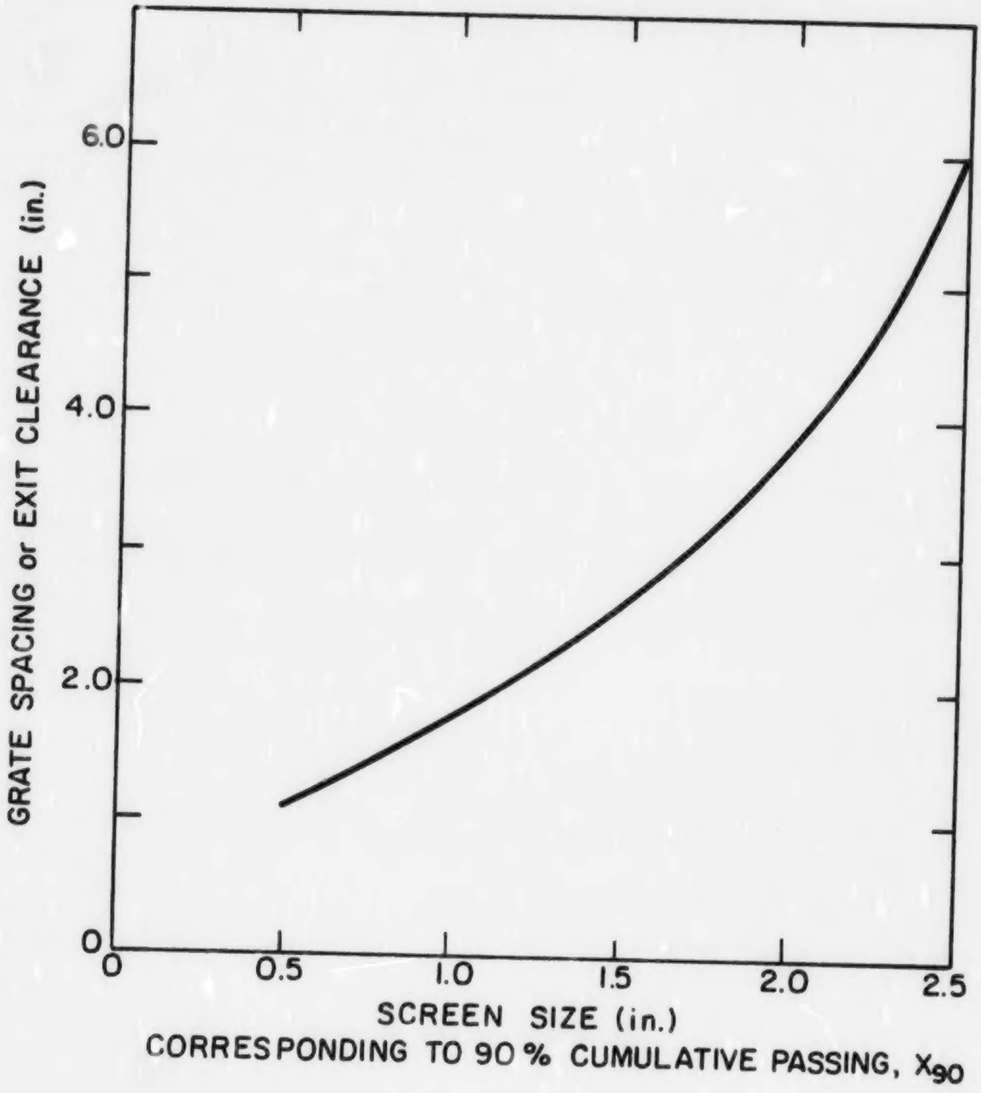

Figure 60 Grate Spacing Required to Produce a Desired Product Size

SECTION 5

ANALYTICAL ASPECTS OF COMMINUTION

The design of advanced refuse processing technology aimed at material and/or energy recovery can be advanced by a fundamental understanding of how to control waste stream comminution. Although refuse comminution is an emerging technology, it is becoming widely adapted in the industry. Analytical modeling of comminution processes for a heterogeneous mixture of brittle and nonbrittle materials, which is the nature of refuse, has heretofore not been the subject of extensive investigation. In fact, because of its complex nature, the predominant tendency has been to rely on empiricism rather than to pursue the fundamental approach. Advanced processing, often involving multiple comminution events that require control and manipulation of the subsequent product size distributions, along with process scaling cannot be optimally designed with only empirical means. A general comminution theory depends on a variety of factors. For example, the dominant mechanism of size reduction in any grinding machine influences the final product size distribution and is itself dependent on machine design and particle characteristics. The particle size distribution produced by a comminution device is the summation of the many single event distributions occurring as a result of the particular grinding action peculiar to the mill. The analytical approach developed for refuse comminution has its roots in the vast amount of experience and analysis already accumulated in the field of comminution of brittle materials. Consequently, a brief overview of the past brittle material work is germane.

Relating breakage energy of homogeneous brittle materials (rocks, coal, etc.) to the performance of size reduction machines has been the goal of much of the previous comminution research. Typically, grinding data were interpreted in terms of empirical energy-size relationships [Charles (20), Schuhmann (21)] or "laws of comminution" [Bond (22), Harris (23,24)] that were based on highly oversimplified descriptions of the fracture process.

A common failing of all the so-called laws is that they do not give information on the size throughput relations of a mill or on optimum operation conditions. A breakage process effects changes throughout all sizes of a complete size distribution, and a single parameter (such as surface area) cannot by itself describe changes of such complexity (25,26). Gaudin (27), Rosin and Rammler (28), Bennet (29), and Schuhmann (30) have advanced comminution theory by recognizing the frequently observed regularities of milled product size distributions and their relation to breakage mechanisms. Such experimental and theoretical studies are fundamentally of a statistical nature (31,32) and require the concepts of distribution and of averages. Various so-called laws, generally expressed in terms of a cumulative weight fraction smaller than any size x as a function of x raised to some numerical power, have been proposed as governing the size distributions of brittle material.

Formulations that account for repeated breakage, a normal occurrence in mills, have been advanced by Epstein (33), Bass (34), Broadbent and Callcott (35), and Brown (36). The basic concept involved is to characterize the operation by two parameters - the selection function and the distribution function. Basically, the selection function represents the fractional amount of any given size present in the mill that is selected for breakage in a differential increment of grinding; the distribution function represents the primary breakage distribution of a given size on breakage.

Bass (34) presented a mathematical theory for the milling process and was the first to derive the fundamental mass balance for batch grinding as an integrodifferential equation. Under certain restrictions he showed that the formal solution to the basic equation yields an expression equivalent to that of the previously semi-empirical Rosin-Rammler size distribution.

Using time-continuous population balance models, Austin and his co-workers [Gardner and Austin (37), Austin et al.(38)] and Fuerstenau and his co-workers [Herbst and Fuerstenau (39), Grandy et al. (40), Gumtz and Fuerstenau (41), Herbst and Mika (42)] have successfully simulated, on a laboratory scale, batch ball mill behavior for a range of operating conditions. An experimental study of breakage in a continuous grinding system was reported by Kelsall (43) in 1964 and led to a search for a workable mathematical representation for continuous grinding. By accounting for the residence time distribution of particles in the mill, Kelsall and Reid (44,45) and Kelsall, et al. (46,47,48) extended these models to simulate laboratory scale, continuous ball milling systems.

Other investigators [Broadbent and Callcott (35,49), Callcott and Lynch (50), Lynch and Rao (51), Lynch et al. (52), Meloy and Bergstrom (53), and Mori et al. (54)] have used discrete-time, steady state matrix models to develop mathematical descriptions of comminution devices. The main criticism of the latter approach is that the matrix models do not provide an adequate description of the dynamic behavior in a mill since time is not an explicit variable and material transport is (implicitly) assumed to occur by plug flow (55).

Other more recent comminution studies have been reported (56-70), including a review by Snow (71). Studies dealing with complex minerals, mixtures, and specially designed heterogeneous materials (72-74) have been reported.

Some details of the concepts discussed here will be given to elucidate the possible extensions from the field of size reduction of brittle materials to the comminution of nonbrittle heterogeneous materials.

INITIAL ENERGY COMMINUTION RELATIONS

The early energy size reduction laws attempted to determine an index for any given material that could be related to a standard range of size reduction and that could be used to compute the energy required to produce any other range of size reduction. This index c, depending physically on material properties and mill operating variables, is mathematically described by the following relation:

$$\frac{dE}{dx} = -\frac{c}{x^n} \qquad (11)$$

where E is the net energy required per unit weight in a given process of comminution, x is a factor related to size, and n is an exponent. Difficulties arise in expressing the size in a mathematical form, since in any actual process, the material being comminuted has a considerable range of size on entering and leaving the process; also, it is impossible to denote this size by a single index because of variations in the shapes of the particles.

The three most frequently quoted, so-called general laws of comminution, derived from Equation 11, are those attributed to Rittinger (75), Kick (76) and Bond (22). These are obtained as follows: When n = 2, integration of this basic equation gives Rittinger's law:

$$\Delta E = c_R\left(\frac{1}{x_2} - \frac{1}{x_1}\right) \qquad (12)$$

When n = 1, integration gives Kick's law:

$$\Delta E = c_K \log\left(\frac{x_1}{x_2}\right) \qquad (13)$$

Bond's third theory of comminution (22) is obtained by substituting n = 1.5 in Equation 11, integrating, and rearranging:

$$\Delta E = W_i \frac{R^{1/2}-1}{R^{1/2}} \left(\frac{100}{x_2}\right)^{1/2} \qquad (14)$$

where W_i is a work index and R is the size reduction ratio, x_1/x_2. Obviously, energy requirements for Bond's law lie between those predicted by the earlier two laws.

It is important to note that the three laws differ in their definitions of x_1 and x_2. Rittinger's (75) statement of his law claimed that the energy consumed in comminution is proportional to increase in surface area produced (surface theory). It follows from this that x_1 and x_2 must be defined as the particle sizes that have a surface area such that it is equal to the total surface area of a unit mass of feed or product divided by the total number of particles contained in that mass. Kick's (76) statement of his law - that analogous changes of configuration of geometrically similar bodies vary as the volumes of the bodies (volume theory) - implies that x_1 and x_2 are particle sizes that have their mass equal to the mean mass of the particles in the feed and product. Bond (22) defines his particle sizes as the apertures through which 80% by weight of the feed or product pass.

Before Bond's law appeared, it was known that Rittinger's law applied primarily in crushing relatively small particles, and Kick's law generally held for large particles. The evidence indicated that the value of n depended not only on the material crushed, but also on the kind of crusher used. Bond's equation made allowance for this variation in the work index, W_i, whose evaluation for any given material involved using arithmatic mean value energy per ton based on data accumulated from many kinds of crushers and grinding equipment of different efficiencies. As Bond (22) has indicated, these data are sometimes so widely scattered as to seem unsuitable for taking the arithmatic mean. Nevertheless, taking n as 1.5 proves more workable than either Kick's or Rittinger's laws in correlating many data from various types of crushing devices. Bond's law must be considered as an empirical rule of thumb that is principally useful as a means of codifying a mass of industrial experience so that interpolation and limited extrapolation can be made for known materials and equipment (25).

Using different approaches, Charles (20), Holmes (77), and Schuhmann (21) indirectly show that energy-size relations can have as a common base the simple relationship

$$\Delta E = Ck^{-m} \qquad (15)$$

where C is a machine constant, k is the size modulus (theoretical maximum size from size distribution curve), and m is a constant.

Recent work of Tanaka (78) relates the constant C of Equation 15 with collision, critical stress, and crack-tip propagation probabilities. Based on this work, Suzuki and Tanaka (79) find the relation between crushing efficiency and some operational variables and material constants.

The energy-size relationship does not provide a complete theoretical analysis of the comminution process; in some instances, this kind of approach has provided a basis for partial correlation of experimental data, but it is inadequate for meaningful process simulation (25,56,66,77).

SIZE DISTRIBUTION RELATIONS

Several empirical size-distribution equations have been proposed as a means of describing the physical nature of a comminuted product. Among them are the Gaudin-Schuhmann equation (27,30) and the Rosin-Rammler equation (28). The Gaudin-Schuhmann equation

$$Y(x) = \left(\frac{x}{k}\right)^{\alpha} \qquad (16)$$

relates the fraction of undersize $Y(x)$ to relative size x/k. In this relationship, $Y(x)$ is the cumulative fraction by weight finer than the stated size x, and k is a quantity called the size modulus (theoretical maximum size), which together with the slope parameter, α, characterizes the product. The slope parameter is usually close to unity (25,30,74,80).

The Rosin-Rammler equation relates the same relative fraction of undersize to the relative size modulus by an equation of different form

$$Y(x) = 1 - \exp\left[-\left(\frac{x}{x_o}\right)^{n}\right] \qquad (17)$$

where n is some numerical constant, and x_o is a characteristic particle size (63.2% cumulative passing).

Gaudin and Meloy (31) derived a theoretical size-distribution equation for single fracture in the form

$$Y(x) = 1 - \left(1 - \frac{x}{\bar{x}_o}\right)^{r} \qquad (18)$$

In this equation, $\bar{x}_o$ is a characteristic dimension of the feed particle before fracture, and r is the size ratio, which is a measure of the number of breaks in the particle. Bergstrom (81) modified the Gaudin-Meloy equation empirically by adding another parameter. He pointed out that the modified form

$$Y(x) = [1 - (1 - \frac{x}{x_0})^r]^q \qquad (19)$$

combines the fine and coarse size curve-fitting capacities of the Gaudin-Schuhmann and Gaudin-Meloy equations, respectively. Other size distribution equations (60,67,68) have been proposed with additional parameters, ostensibly for greater curve-fitting flexibility, as further generalizations of the above relations.

Because refuse is a heterogeneous material, it is unlikely that a single breakage law can describe all types of breakage. There are some difficulties in the applications of these various laws characterizing size distribution. One of the major deficiencies is that, although it seems natural to suppose that a breakage process operates according to some law, our experimental results indicate that the feed cannot be characterized by any of the previously derived size distribution relations. Thus when the process is supplied with some unusual distribution of feed, like refuse, it seems that the product need not obey any of the usual laws. The analysis of a breakage process by matrix method offers an excellent approach to overcome this difficulty, especially in the case of the simulation of a breakage process whereby the feed and discharge size distributions can be obtained.

MATRIX ANALYSIS OF THE BREAKAGE PROCESS

The principles of the matrix method of analysis of comminution processes leading to the simulation models developed for refuse are reviewed. In the matrix method, the size distribution given by the sieve analysis is replaced by a vector by considering the size range of the assembly of particles to be subdivided into n intervals, with maximum size x_1 and minimum size x_{n+1}. The ith size fraction is bounded by x_i above and x_{i+1} below and $x_i = rx_{i+1}$ ($i = 1,2,3,---, n-1$), with r (>1) being the geometric sieve ratio. Where it is necessary to specify the size of particles in a particular size fraction by a single number, the geometric mean is taken. When the size scale is logarithmic, this geometric progression of sizes appears as equally spaced points on the abscissa.

P_i designates the cumulative mass fraction of product material below x_i, and F_i is the cumulative mass fraction of feed material below size x_i where $i = 1,2,3, ---, n$. Then the feed and product size distributions can be described by $n \times 1$ column vectors $\bar{f}$ and $\bar{p}$ with elements f_i and p_i, where f_i and p_i are, respectively, mass fractions of feed and product materials that fall between x_i and x_{i+1}, thus:

$$\underline{f} = \begin{bmatrix} f_1 \\ f_2 \\ \cdot \\ \cdot \\ \cdot \\ f_n \end{bmatrix} \quad ; \quad \underline{p} = \begin{bmatrix} p_1 \\ p_2 \\ \cdot \\ \cdot \\ \cdot \\ p_n \end{bmatrix} \tag{20}$$

with

$$f_i = F_i - F_{i+1} \tag{21}$$

$$p_i = P_i - P_{i+1} \tag{22}$$

The percentage or fraction of material under the smallest size, the undersize, is described by

$$f_{n+1} = F_{n+1} = 1 - \underline{e}'\underline{f} \tag{23}$$

$$p_{n+1} = P_{n+1} = 1 - \underline{e}'\underline{p} \tag{24}$$

where $\underline{e}'$ is the transposition of the n x 1 column vector $\underline{e}$ with unity elements. The transformation of the feed to the product is thus expressed mathematically by a matrix algebra:

$$\underline{p} = \underline{\underline{X}}\,\underline{f} \tag{25}$$

where $\underline{\underline{X}}$ expresses the breakage process.

The sequence of rows and columns in the matirx, $\underline{\underline{X}}$, describing a transformation of a size distribution bears definite relations to particle size. Let i and j refer to the ith row and jth column of $\underline{\underline{X}}$, with elements X_{ij}. Then X_{ij} denotes the proportion of particles that were initially in size range j and afterwards in product size range i.

For size reduction, $\underline{\underline{X}}$ is lower triangular (35,55,57), and a knowledge of the n elements of $\underline{p}$ and the n elements of $\underline{f}$ does not suffice to enable a unique solution from the n equations of the $\frac{n(n+1)}{2}$ unknowns X_{ij} $(i \geq j)$. Several authors (37,38,55,81,82) have discussed the empirical evaluation of the matrix of an open-circuit grinding process. Their approach is essentially described by the following equation:

$$\underline{p}_j = \underline{\underline{X}}\ \underline{e}_j \quad (j = 1,2,3, \ldots, n) \tag{26}$$

where $\underline{\underline{X}}$ is unknown and $\underline{e}_j$ is the unity vector with all elements zero except the jth element (=1), the experimental determination of $\underline{p}_j$ gives the jth column of X. If particle interaction is absent, and if it is possible to use graded feeds ($\underline{e}_j$) down to the smallest size x_n, the experimental evaluation of $\underline{\underline{X}}$ should satisfactorily predict the output size distribution ($\underline{p}$) obtained on feeding ungraded material ($\underline{f}$) - that is, Equation 15.

Though the above approach does not disclose the mechanism determining the numerical values of the overall matrix, $\underline{\underline{X}}$, a mathematical model can be set up to describe the action in the mill, based on the concept of the probability of breakage according to Epstein (33). This concept has provided a convenient basis for the formulation of detailed comminution models (55). In these treatments, the process is represented by a series of discrete breakage events characterized by a probability of breakage for a given size particle (y) in any given event, which is called the selection function, S(y), and a resultant product size distribution from that breakage event, which is called the breakage function or redistribution function, B(x,y) (i.e., the proportion of the product whose size is less than x).

Instead of using continuous functions as done by Epstein, Broadbent and Callcott (49) cast the weight size distribution into finite intervals. Instead of using B(x,y), a parameter b_{ij} was defined as the fraction of material in size interval j that falls into size interval i after breakage. Thus the product of breakage of size 1 material is distributed - b_{21} into interval 2, b_{31} into interval 3, etc., and b_{n1} into the last interval of smallest particle size. The sum of the values of b_{i1} over all the values of i is one. Similarly, breakage of the second size interval yields products distributed - b_{32}, b_{42}, etc. The selection function was again defined as the fraction of any size interval selected for breakage, but it was expressed generally as a function of size, S_j.

According to Broadbent and Callcott, consider the mass fraction f_i of a size range i. If S_i is the appropriate value of the selection function, a proportional amount $(1 - S_i)$ of the size will remain unbroken in the grinding process and a fraction S_i will be broken. The way in which the material is broken is described by the breakage function B_{ij}. This is a size-discretized form of B(x,y) obtained by replacing x and y with the geometric mean sizes of the size intervals i and j, respectively* in the "general" breakage function (49)

$$B(x,y) = [1 - \exp(-x/y)]/[1 - \exp(-1)] \qquad (27)$$
$$0 \leq x \leq y$$

Particles in the size interval j on breakage will produce a fraction B_{ij} of particles of x_i and less. The fraction in the size range i denoted by b_{ij} will then be given by

$$\begin{aligned} b_{ij} &= B_{ij} - B_{i+1,j} \text{ , } (i > j) \\ &= 0 \text{ , } (i = j\text{, attrition is negligible}) \qquad (28) \\ &= 0 \text{ , } (i < j\text{, no agglomeration}) \end{aligned}$$

In all instances where the appropriate information has been obtained (37,38,44), breakage functions have been found to be normalizable in the sense of Epstein (33); that is,

$$B(x,y) = B(x/y) \qquad (29)$$

or, equivalently, in the case of a size discretized representation with a constant sieve ratio, $r(x_i = rx_{i+1})$

$$B_{ij} = B_{(i-j+1)1} \quad i=j, \ldots, n-1 \qquad (30)$$

The assumption of geometric similarity** for both the breakage function and the grade sizes implies that particles of every size break in the same way. Thus,

$$b_{ij} = b_{i+1,j+1} \qquad (31)$$

---

* The values of S_i and B_{ij}, determined experimentally and using discrete size intervals, are not the same numerically as S(x) and B(x,y), which are point values (38); in general, the values of S_i and B_{ij} change as the size interval used changes.

** The breakage functions used here are of the geometric similarity form.

Consequently, b_{ij} are the elements of a breakage matrix $\underline{\underline{B}}$. The matrix $\underline{\underline{B}}$ is similar to the breakage matrix $\underline{\underline{X}}$ except that $\underline{\underline{B}}$ is used in conjunction with a selection matrix $\underline{\underline{S}}$ to characterize the size reduction process. The selection matrix $\underline{\underline{S}}$ is a diagonal matrix with entries $S_1, S_2, \ldots, S_n$ along the diagonal and zeros elsewhere. Normally both matrices $\underline{\underline{B}}$ and $\underline{\underline{S}}$ are not known a priori, and so the b_{ij} and S_i must be estimated from experimental results. If some particles are selected for size reduction according to $\underline{\underline{B}}$, and if $\underline{\underline{S}}$ defines the proportions of each size grade of $\underline{f}$ that is selected, then $\underline{\underline{S}}\underline{f}$ are reduced according to $\underline{\underline{B}}$, and naturally $(\underline{\underline{I}}-\underline{\underline{S}})\underline{f}$ describes the distribution left unbroken, where $\underline{\underline{I}}$ is the identity matrix. If the broken and unbroken parts are combined, then the final product is

$$\underline{p} = \underline{\underline{B}}\underline{\underline{S}}\underline{f} + (\underline{\underline{I}}-\underline{\underline{S}})\underline{f}$$

that is,

$$p = \{\underline{\underline{B}}\underline{\underline{S}} + (\underline{\underline{I}}-\underline{\underline{S}})\}\underline{f} \qquad (32)$$

Thus Equation 25 is replaced by Equation 32, in which transformation of the feed to the product proceeds in accordance with the breakage matrix $\underline{\underline{B}}$ and selection matrix $\underline{\underline{S}}$; a single cycle of selection and breakage according to $\underline{\underline{B}}$ is said to have occurred.

BREAKAGE PROCESS MODELS

A matrix method similar to that employed by Callcott (82) for the comminution of coal in a swing hammermill was used to analyze the size reduction of refuse. Observations of refuse size reduction in the swing hammermill indicate that in general, the majority of material tends to pass through the mill without being subjected to repeated fracture. It is possible that mill operating conditions differing widely from those considered here will give rise to greater mill recirculation. Furthermore, unlike the process in a batch grinding system, the residence time of material in the hammermill is small. Estimates yield a residence time on the order of 1/80 records for a rotor speed of 1,200 rpm (28,29,32). In any event, similar to the procedure used by Broadbent and Callcott (49), the swing hammermill can be reasonably considered as a once-through grinder for the simulation of the refuse comminution process. Four simulation models summarized in the following subsections have been evaluated (83).

π-Breakage Process

The simplest breakage process is π-breakge in which the selection function $S(y) = \pi$ for all sizes y - i.e. a proportion π of the particles, independent of particle size, is broken according to the breakage function $B(x,y)$. In matrix terms, $\underline{\underline{S}} = \pi\underline{\underline{I}}$, and the equation describing the process is:

$$\underline{p} = \{\pi\underline{\underline{B}} + (1-\pi)\underline{\underline{I}}\}\underline{f} \qquad (33)$$

The parameter π then completely describes the process if $\underline{\underline{B}}$ is assumed to be known; it is a useful measure of the breakage effected by the process. The techniques for back-calculating the value of π from known feed and product distributions have been indicated by Broadbent and Callcott (36). They also pointed out that the simple simultaneous solution of elements of Equation 33 is not generally possible because of errors in measurement, and a least-squares technique was outlined.

π,κ-Breakage Process

This is similar to the π-breakage process except that the breakage matrix is replaced by $\underline{\underline{B}}^{\kappa}$, $\kappa \geq 1$ on the basis that some machines would cause more severe degradation on breakage than others, corresponding to repeated breakage of the particle products without their moving away from the grinding action and having to wait for reselection for breakage. We infer that a proportion π of the feed is selected for breakage, just as in π-breakage, but that the product of this breakage is rebroken. This is repeated until breakage has been effected κ times. The unbroken material passing through the grinding zone unaltered is, of course, $(1-\pi)$ of the feed. The process is characterized by two parameters, π and κ, and the matrix equation describing the process is:

$$\underline{p} = \{\pi\underline{\underline{B}}^{\kappa} + (1-\pi)\underline{\underline{I}}\}\ \underline{f} \qquad (34)$$

π,κ,ω-Breakage Process

This process involves the case where the probability of particle selection for breakage varies with some power ν of the particle size. Thus, the proportion of particles in the ith size range selected for breakage is

$$S_i = S_1(r)^{-\nu i} \qquad (35)$$

If $\omega = r^{-\nu}$ and the probability is π for the first size range, it is $\pi\omega$, $\pi\omega^2, \ldots,$ and $\pi\omega^{n-1}$ in the ranges that follow. If $\underline{\underline{\Omega}}$ is the matrix with 1, ω, $\omega^2, \ldots \omega^{n-1}$ along the main diagonal and zeros elsewhere, the selection matrix is $\pi\underline{\underline{\Omega}}$. The equation of the process is:

$$\underline{p} = (\pi\underline{\underline{B}}\underline{\underline{\Omega}} + \underline{\underline{I}} - \pi\underline{\underline{\Omega}})\underline{f} \qquad (36)$$

Repeated Breakage Cycles

When the feed and product size distributions do not cover the same sizes and the size ranges differ considerably, one may be able to assess the breakage process in terms of a series of cycles of mild breakage. The description may be written (50,82)

$$p = \{ \prod_{h=1}^{N} (\underline{\underline{B}}\underline{\underline{S}}_h + \underline{\underline{I}} - \underline{\underline{S}}_h) \} \underline{f} \qquad (37)$$

where h = 1,2,..., N refers to the hth cycle in which the probability of breakage is $\underline{\underline{S}}_h$. Given only p, f, and B, the evaluation of each $\underline{\underline{S}}_h$ and of N is not possible (50,81). We will adopt the following sequential model to simplify the analysis:

We assume that the probability of breakage $\underline{\underline{S}}_h$ is the same for all the cycles, hence Equation 37 becomes:

$$\underline{p} = (\underline{\underline{B}}\underline{\underline{S}} + \underline{\underline{I}}-\underline{\underline{S}})^N \underline{f} \qquad (38)$$

where $\underline{\underline{S}}$ is the selection matrix common to all the N cycles. If

$$D = (\underline{\underline{B}}\underline{\underline{S}} + \underline{\underline{I}}-\underline{\underline{S}}) \qquad (39)$$

then

$$\underline{p} = \underline{\underline{D}}^N \underline{f} \qquad (40)$$

The whole process in the mill is treated as a sequence of operations in which the product from the jth cycle becomes the feed for the (j+1)th cycle. To ensure that the undersize from any cycle of the process is correctly described, we make p and f (n+1)-column vectors, with the last elements, p_{n+1} and f_{n+1}, describing the undersize for the product and feed, respectively. We write $\underline{\underline{D}}$ as a (n+1) square matrix, with the (n+1)th row describing the proportions of the various size ranges that end up as undersize.

The number of cycles, N, is associated with the "stages of grinding" (55). Callcott (82) considered the hammermill to be made up of N obstructions or grinding zones (see Appendices). The product from the jth zone in passing through the (j+1)th zone is said to have undergone a single cycle of breakage. In the present model, the number of cycles, N, is not identified with the grinding zones, but it is introduced artificially as a means of repeatedly applying the single matrix $\underline{D}$ to the feed vector $\underline{f}$ in order to obtain $\underline{p}$ when the top sizes of the feed and product distributions differ considerably. If x_1 is the maximum size of the initial feed and x_m the maximum size of the final product (where $x_i = rx_{i+1}$, $i = 1,2,\ldots, m,\ldots,n-1$), then N is estimated from

$$N = (m - 1) \tag{41}$$

SIMULATION RESULTS

Because present comminution theories are not sufficiently developed, selection and breakage functions, particularly for a heterogeneous refuse material, cannot be obtained from first principles. Thus to use the previously described simulation models, these quantities were determined with an indirect estimation or semiempirical technique similar to that proposed by Broadbent and Callcott. Two forms of the breakage function were selected. The first, after a modified form of Broadbent-Callcott, was

$$B(x,x_0) = \{1 - \exp[-(\frac{x}{x_0})^n]\}/[1 - \exp(-1)] \tag{42}$$

where n is some positive index. Experimental results indicated that certain products of the size reduction conformed to the Rosin-Rammler distribution with an n index varying between 0.845 and unity. The second form of the breakage function was after the Gaudin-Meloy distribution equation:

$$B(x,\bar{x}_0) = B(x/\bar{x}_0) = 1 - (1 - x/\bar{x}_0)^r \tag{43}$$

This additional relation was necessary since, as will be shown, Equation 42 did not simulate primary grinding. The elements b_{ij} of the breakage matrices are calculated from Equations 28,30, and 31 using the various breakage functions in Equations 42 and 43. The values of these elements are tabulated in Table 15.

The selection functions were determined with the least-squares procedure for the π-breakage, π,κ-breakage and π,κ,ω-breakage processes for integer values of κ from 1 to 5 and $\omega = 1, 0.9, 0.8,\ldots,$ to 0.1 using the experimental feed and product size distributions. The "best" selection functions and the breakage matrices (i.e., those that yield least squared errors) are then used to calculate the product size distributions for the particular breakage model. For the repeated breakage cycles model, values of $\pi = 0.1, 0.2,\ldots,$ to 1 are chosen and used together with the breakage matrices to compute product size distributions. The

TABLE 15. BREAKAGE FUNCTION ELEMENTS OF THE FIRST COLUMN b_{i1}[a] ($b_{11} = 0$)

i	B-C n=1	B-C n=0.845	G-M r=10	G-M r=5
2	0.10027	0.08484	0.00000	0.00010
3	0.19037	0.16336	0.00012	0.01087
4	0.16588	0.14746	0.00417	0.05450
5	0.13599	0.12684	0.02513	0.10605
6	0.10676	0.10524	0.06516	0.13602
7	0.08129	0.08500	0.10573	0.14001
8	0.06057	0.06728	0.02944	0.12668
9	0.04444	0.05247	0.13261	0.10573
10	0.03226	0.04045	0.12088	0.08373
11	0.02323	0.03093	0.10189	0.06402
12	0.01664	0.02350	0.08142	0.04780
13	0.01188	0.01778	0.06271	0.03511
14	0.00845	0.01340	0.04708	0.02549
15	0.00600	0.01007	0.03472	0.01837
16	0.00426	0.00756	0.02529	0.01316
17	0.00302	0.00566	0.01826	0.00939
18	0.00214	0.00424	0.01310	0.00668

[a] Since the breakage matrix is a step matrix, i.e., $b_{ij} = b_{i+1,j+1}$, all the other elements of the breakage matrix $\underline{\underline{B}}$ can be calculated from the elements of the first column. A geometric sieve ratio of $\sqrt{2}$ is used in the computation of b_{ij}. That is, $x_1/x_2 = \sqrt{2}$.

particular selection function that gives the least-squared error is chosen as the parameter to represent the model. In all the above cases, computations were performed with a systematic variation of combinations of the selection breakage function so that the reported simulation results are those that yield the least-squared errors. The actual results of the simulation can be summarized according to the following.

π-Breakage Process

Figure 61 shows the comparison between the computed and experimental product size distributions for primary, secondary, and tertiary grindings using the π-breakage model for various selection and breakage functions. Here the breakage function based on Equation 43 with the index $r = 7$ predicts the primary product size distribution very well within experimental errors. Also, the breakage functions obtained from Equation 42 give better results for the secondary and tertiary grinding processes than the predictions from Equation 43.

π,κ-Breakage Process

Figure 62 shows the comparison between the computed and experimental product size distributions for primary grinding using this model. The results for $\kappa = 2$ and 3 using the modified Broadbent-Callcott equation represent the best among a host of other computed product size distributions, and since the above results do not in any way predict the actual experimental product size distribution, the π,κ-breakage process model is rejected as a representation of the refuse size reduction process in the hammermill. With $\kappa = 1$ (i.e., π-breakage process), Equation 32 does not come any closer in predicting the product size distribution. The computations based on the π,κ-breakage process model for the secondary and tertiary grinding conditions do not give any better results than those predicted with the simple π-breakage process model.

π,κ,ω-Breakage Process

This model is also rejected as a mathematical representation of the breakage process in the mill. The values of π for $\omega \leq 0.9$ are found to be greater than unity. Values of π greater than unity cannot be accepted because they violate the definition of π as a probability of a certain-sized particle being broken in passing through a process. If the values of π greater than unity were accepted, it would just mean that we were merely curve-fitting the computed results to the experimental data and the model would not be amenable to any physical interpretations.

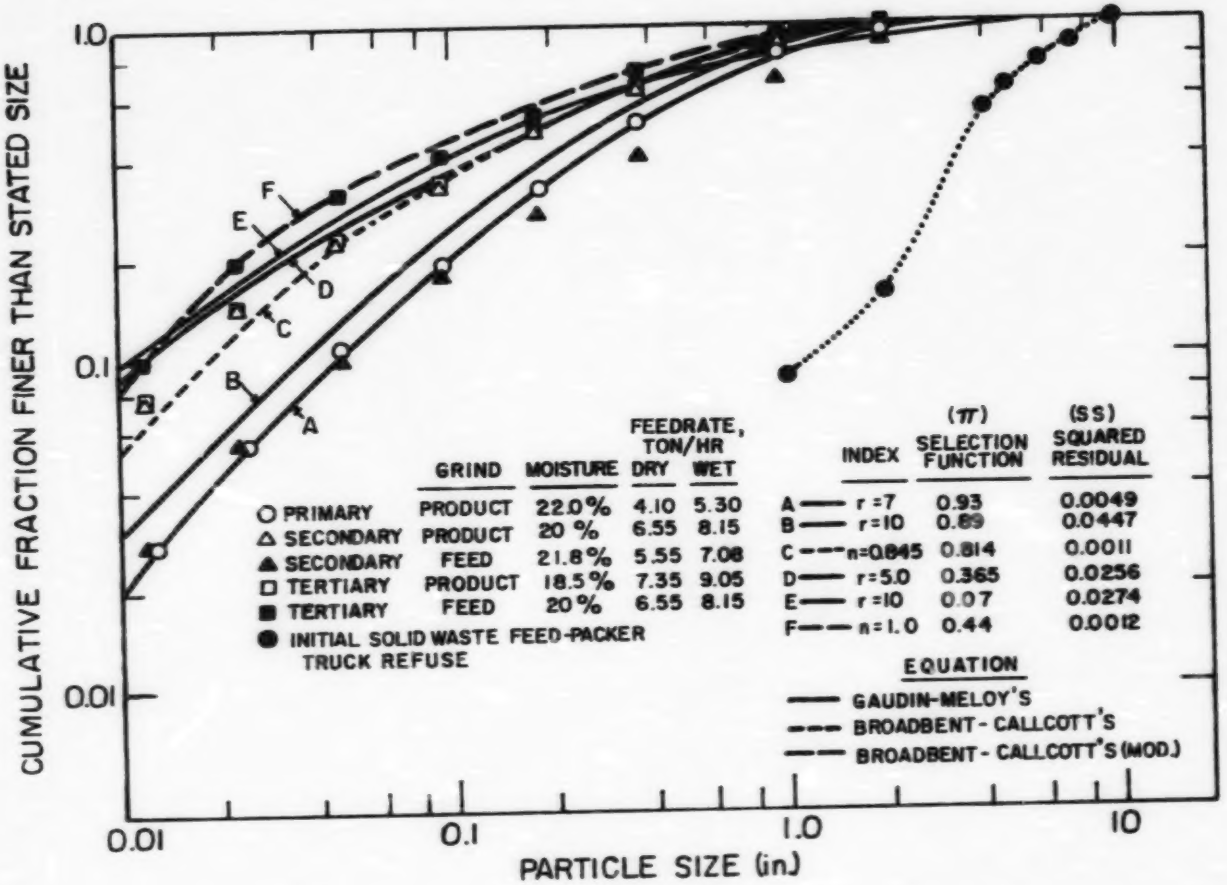

Figure 61 Comparison Between Computed and Experimental Product Size Distributions for Primary, Secondary, and Tertiary Grinding Using the π-Breakage Process Model

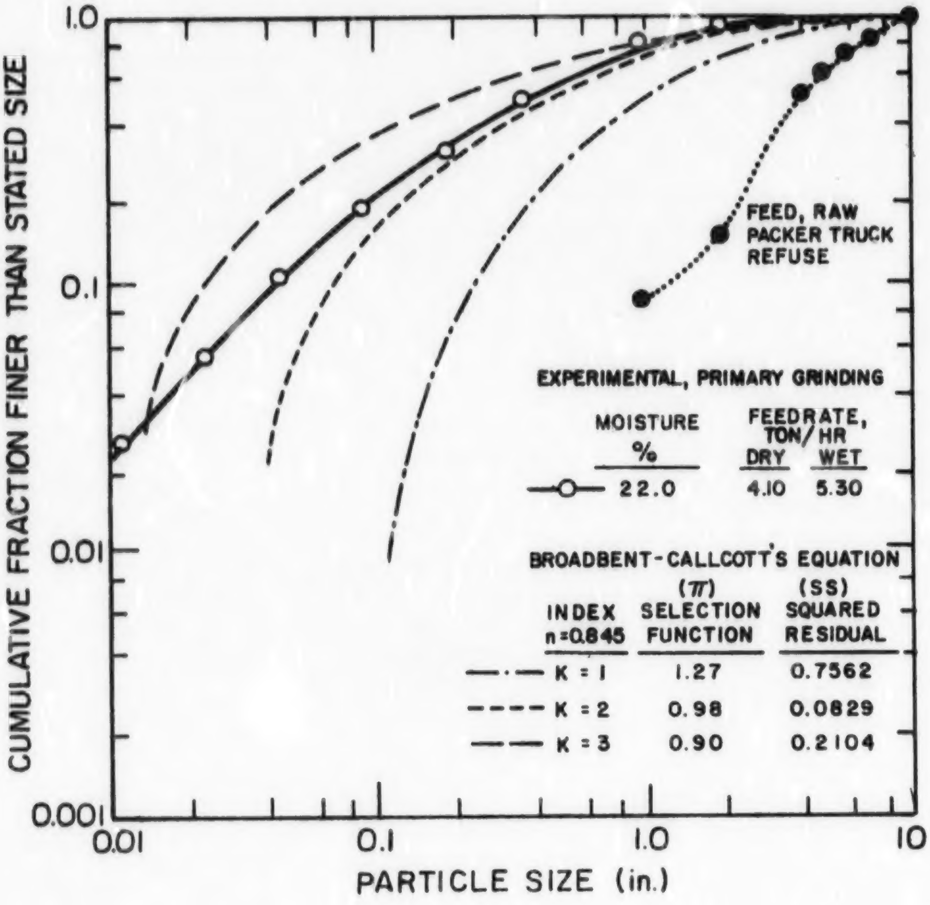

Figure 62 Comparison Between Computed and Experimental Product Size Distributions for Primary Grinding Using the π,κ-Breakage Process Model

The Repeated Breakage Cycle Model

Figure 63 shows the partial success of this model in computing product size distributions for primary, secondary, and tertiary grinding processes. Breakage functions based on Equation 20 yield good results for the primary grinding process for sizes down to 0.2 in. (5,080 μ), with about 32% passing stated size; below this size, the computed and experimental values diverge. There is a considerable improvement in the results of this model for the secondary and tertiary grinding process. The computed results are close to the experimental ones down to sizes as low as 0.02 in. (508 μ), with about 12% passing the stated size. In all the above cases, the breakage functions based on the modified Broadbent-Callcott equation or normalized Rosin-Rammler equation (Equation 42) give better results than those of the Gaudin-Meloy equation (Equation 43). The Gaudin-Meloy equation fails to predict well in the small size ranges.

In summation, a good model will include the most important features of the process, will be mathematically simple (if possible), will provide a minimum of assumptions, and will be fruitful for purposes of prediction and theoretical speculation. In the simulation of the various results in this paper, the two models, π,κ-breakage and π,κ,ω-breakage, are found to be untenable because they fail to predict the product size distributions within any reasonable accuracy. The π-breakage model is clearly superior to the repeated breakage cycle model; however, both give very good results for the products of primary, secondary, and tertiary grinding processes. The π-breakage model is clearly superior to the repeated breakage cycle model because it gives better results for all the three grinding conditions.

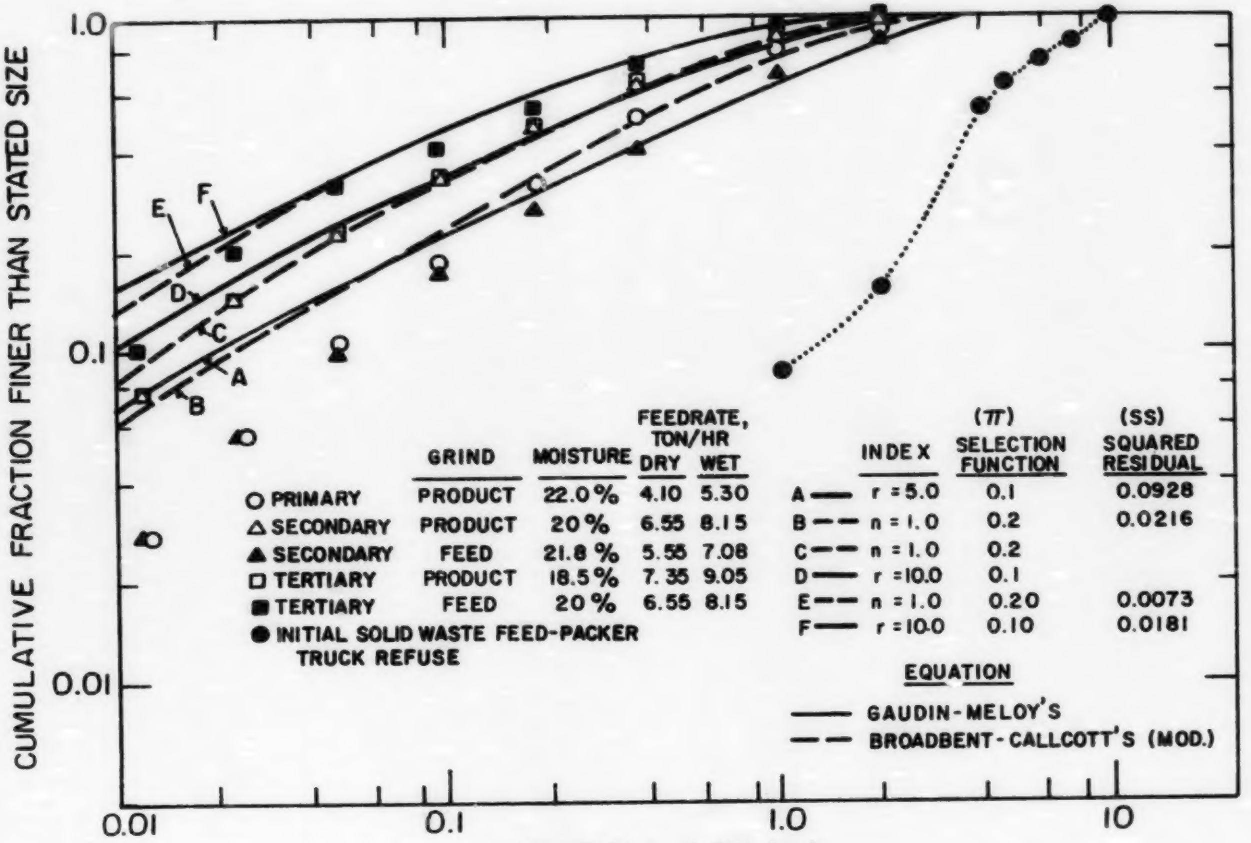

Figure 63 Comparison Between Computed and Experimental Product Size Distributions for Primary Grinding Using the Repeated Breakage Cycle Model

REFERENCES

1. Ham, R.K., "The Role of Shredded Refuse in Landfillings," Waste Age, Vol. 6, No. 12, December 1975, pp. 25-30.

2. Final Report on a Demonstration Project at Madison, Wisconsin, Vol. 1, 1966-1972, EPA Report, March 1973.

3. Resource Recovery from Municipal Solid Waste. National Center for Resource Recovery, Inc., Lexington Books, D.C. Heath & Co., Lexington, Mass., 1974, 182 pp.

4. Decision-Makers Guide in Solid Waste Management, U.S. Environmental Protection Agency, Second Ed. (SW-500), 1976.

5. Fan, Dah-Nien, "On the Air Classified Light Fraction of Shredded Municipal Solid Waste - Composition and Physical Characteristics," Resource Recovery and Conservation, Vol. 1, No. 2, 1975, pp. 141-150.

6. Trezek, G.J. and G. Savage, "MSW Component Size Distributions Obtained from the Cal Resource Recovery System," Resource Recovery and Conservation (In Press), 1976.

7. Trezek, G.J., D. Howard, and G. Savage, "Mechanical Properties of Some Refuse Components," Compost Science, Vol. 13, No. 6, Nov.-Dec. 1972, pp. 10-15.

8. Ruf, J.A., "Particle Size Spectrum and Compressibility of Raw and Shredded Municiple Solid Waste," Ph.D. Thesis, University of Florida, 1974.

9. The Feasibility of Baling Municipal Refuse. Prepared by Project Personnel of the Public Works Dept. of the City of San Diego, Calif. for the Solid Waste Program of the U.S. Public Health Service, April 1968, 123 pp.

10. High-Pressure Compaction and Baling of Solid Waste. Prepared by the American Public Works Assoc. for the Solid Waste Management Programs of the U.S. Environmental Protection Agency, EPA Publication No. SW-32d. Washington, D.C.: U.S. Government Printing Office, 1972, 163 pp.

11. Taggart, A.F., Handbook of Mineral Dressing, Wiley Handbook Series, John Wiley & Sons, Inc., 1945.

12. Trezek, G.J., "Size Reduction Equipment," *Compost Science*, Vol. 14, No. 5, Sept.-Oct., 1973, pp. 22-25.

13. Savage, G. and G.J. Trezek, "Size Reduction in Solid Waste Processing - Refuse Size Reduction Facility," Prepared for EPA Contract R801218, 1973.

14. "Solid Waste Shredding: Blueprint for Progress," *Waste Age*, Vol. 6, No. 8, July, 1975, pp. 10-15.

15. Winkler, P.F., and D.G. Wilson, "Size Characteristics of Municipal Solid Waste," *Compost Science*, Vol. 14, No. 5, Sept.-Oct. 1973, pp. 6-11.

16. Gawalpanchi, R.R., P.M. Berthouex, and R.K. Ham, "Particle Size Distribution of Milled Refuse," *Waste Age*, Vol. 4, No. 5, 1973, pp. 34-74.

17. Refuse Shredding, Midwest Research Institute Report, Prepared for EPA, 1975 (In press).

18. Trezek, G.J. and G. Savage, "Results of a Comprehensive Refuse Comminution Study," *Waste Age*, Vol. 9, No. 8, July 1975, pp. 49-55.

19. Savage, G. and G.J. Trezek, "On Grinder Wear In Refuse Comminution," *Compost Science*, Vol. 14, No. 5, Nov.-Oct. 1973, pp. 5-11.

20. Charles, R.J., "Energy-Size Reduction Relationships in Comminution," *Trans*. *AIME*, *208*, 1957 , pp. 80-88.

21. Schuhmann, R., "Energy Input and Size Distribution in Comminution," *Trans*. *AIME*, *217*, 1960 , pp. 22-25.

22. Bond, F.C., "The Third Theory of Comminution," *Trans*. *AIME*, *193*, 1952, pp. 484-494.

23. Harris, C.C., "On the Role of Energy in Comminution: A Review of Physical and Mathematical Principles," *Trans*. *I.M.M.*, *75*, 1966, pp. C37-C56.

24. Harris, C.C., "On the Limit of Comminution," *Trans*. *AIME*, *258*, 1967, pp. 17-30.

25. Austin, L.G., and R.R. Klimpel, "Theory of Grinding Operations," *I & EC Process, Design, and Development*, *56*, 1964, pp. 19-29.

26. Marshall, V.C., "Crushing and Grinding - Critique of Existing Laws," *Chem. and Process Eng*., April 1966.

27. Gaudin, A.M., "An Investigation of Crushing Phenomena," Trans. AIME, 73, 1926, p. 253.

28. Rosin, P. and E. Rammler, "Laws Governing the Fineness of Powdered Coal," Inst. of Fuel, 7, 1933, pp. 29-36.

29. Bennett, J.G., J. Inst. Fuel, 10, 1936, p. 22.

30. Schuhmann, R., "Principles of Comminution, 1.-Size Distribution and Surface Calculations," Tech. Publs. AIME, 1189, July 1940, p. 11.

31. Gaudin, A.M. and T.P. Meloy, "Model and a Comminution Distribution Equation for Single Fracture," Trans. AIME, 223, 1962, pp. 40-43.

32. Klimpel, R.R. and L.G. Austin, "The Statistical Theory of Primary Breakage Distributions for Brittle Materials," Trans. AIME, 232, 1965, pp. 88-94.

33. Epstein, B., "Logarithmico-Normal Distribution in Breakage of Solids," Ind. Eng. Chem., 40, 1948, pp. 2289-2291.

34. Bass, L., "Zur Theorie der Mahlvorgange," Zeits. Angew, Math. Phys., 5, 1954, pp. 283-292.

35. Broadbent, S.R. and T.G. Callcott, "A Matrix Analysis of Processes Involving Particle Assemblies," Phil. Trans. Roy. Soc., 249, 1956, p. 99, Series A.

36. Brown, R.L. J. Inst. Fuel, 14, 1941, p. 129.

37. Gardner, R.P. and L.G. Austin, "A Chemical Engineering Treatment of Batch Grinding, Part I: A Radioactive Tracer Technique for the Determination of Breakage Functions; Part II: The Prediction of Size-Weight Distributions from Selection and Breakage Data," Symp. Zerkleinern, 1st Eur. Symp. on Comm., Edit. H. Rumpf and D. Behrens, Verlag Chemie, Weinheim, 1962, pp. 217-248.

38. Austin, L.G., R.R. Klimpel, and A.M. Beattie, "Solutions of Equations of Grinding," Zerkleinern, 2nd European Symp. on Comminution, Edit. H. Rumpf and W. Pietsch, Amsterdam, 1966, Dechema-Monographien, 57, 1967, Part I, pp. 281-312.

39. Herbst, J.A. and D.W. Fuerstenau, "The Zero Order Production of Fine Sizes in Comminution and its Implications in Simulation," Trans. AIME, 241, 1968, pp. 538-549.

40. Grandy, G.A., G.D. Gumtz, J.A. Herbst, T.S. Mika, and D.W. Fuerstenau, "Computer Techniques in the Analysis of Laboratory Grinding Tests," *A Decade of Digital Computing in the Mineral Industry*, Edit. A. Weiss, AIME, New York, 1969, pp. 765-788.

41. Gumtz, G.D. and D.W. Fuerstenau, "Simulation of Locked Cycle Grinding," Paper presented at 98th Ann. AIME Meeting, Washington, D.C., February 1969.

42. Herbst, J.A. and T.S. Mika, "Mathematical Simulation of Tumbling Mill Grinding: An Improved Method," *Rudy*, No. 3/4, 1970, pp. 70-75.

43. Kelsall, D.F., "A Study of Breakage in a Small Continuous Open-Circuit Wet Ball Mill," Proceedings of VII International Mineral Processing Congress, New York, 1964, Edit. N. Arbiter, Gordon and Breach, New York, 1965, pp. 33-42.

44. Kelsall, D.F. and K.J. Reid, "The Derivation of a Mathematical Model for Breakage in a Small Continuous, Wet, Ball Mill," in *Application of Mathematical Models in Chemical Engineering Research, Design and Production*, AIChE-Inst. Chem. Eng. Symposium Series, No. 4, 1965, pp. 14-20.

45. Kelsall, D.F. and K.J. Reid, "Some Effects of a Change in Environment Size Distribution on the Grinding Behavior in a Continuous Wet Ball Mill," *Trans. Inst. Min. & Met.*, Section C, *78*, 1969, pp. C198-205.

46. Kelsall, D.F., K.J. Reid, and C.J. Restarick, "Continuous Grinding in a Small Wet Ball Mill. Part I: A Study of the Influence of Ball Diameter," *Powder Tech.*, *i*, 1968, pp. 291-300.

47. Kelsall, D.F., K.J. Reid, and C.J. Restarick, "Continuous Grinding in a Small Wet Ball Mill. Part II: A Study of the Influence of Hold-Up Weight," *Powder Tech.*, *2*, 1969, pp. 291-300.

48. Kelsall, D.F., P.S.B. Stewart, and K.J. Reid, "Confirmation of a Dynamic Model of Closed-Circuit Grinding with a Wet Ball Mill," *Trans. Inst. Min.& Met.*, *77*, 1968, Section C, pp. C120-127.

49. Broadbent, S.R. and T.G. Callcott, "Coal Breakage Processes," *J. Inst. Fuel*, *20*, 1956, pp. 524-539 and *30*, 1957, pp. 21-25.

50. Callcott, T.G. and A.J. Lynch, "An Analysis of Breakage Processes Within Rod Mills," *Proc. Austral. Inst. Min.& Met.*, *209*, 1964, pp. 109-131.

51. Lynch, A.J. and T.C. Rao, "Digital Computer Simulation of Comminution Systems," Proc. VIII Commonwealth Mining and Metallurgical Congress (Australia and New Zealand, 1965) - General, Edit. J.T. Woodcock, R.T. Madigan and R.G. Thomas, Eight Comm. Min. and Met. Congress, Melbourne, 1966, pp. 587-595.

52. Lynch, A.J., W.J. Whiten, and N. Draper, "Developing the Optimum Performance of a Multi-Stage Grinding Circuit," Trans. Inst. Min. & Met., Section C, 76, 1967, pp. C169-C181.

53. Meloy, T.P. and B.H. Bergstrom, "Matrix Simulation of Ball Mill Circuits Considering Impact and Attrition Grinding," Proc. of the VII Int. Min. Proc. Cong., New York, 1964, Edit. N. Arbiter, Gordon and Breach, New York, 1965, pp. 19-31.

54. Mori, Y., G. Jimbo, and M. Yamasaki, "Flow Characteristics of Continuous Ball and Vibration Mill Mixing Size Distribution, Dynamic Response of Flow Rate and Application," Zerkleinern, 2nd Eur. Symp. on Comm., Edit. H. Rumpf and W. Pietsch, Amsterdam, 1966, Dechema-Monographien, 57, 1967, Part II, pp. 605-632.

55. Austin, L.G., "A Review Introduction to the Mathematical Description of Grinding as a Rate Process," Powder Technol., 5, 1971/72, pp. 1-17.

56. Austin, L.G., P.T. Luckie, and R.R. Klimpel, "Solutions of the Batch Grinding Equation Leading to the Rosin-Rammler Distributions," Trans. AIME, 252, 1972, pp. 87-94.

57. Klimpel, R.R. and L.G. Austin, "Determination of Selection-for-Breakage Functions in the Batch Grinding Equation by Nonlinear Optimization," I.E.&C. Fundamental, 9, 1970, pp. 230-237.

58. Rampf, H., Fracture, Vol. 2, Edit. H. Liebowitz, Academic Press, New York, 1969.

59. Shoenert, K., "Role of Fracture Physics in Understanding Comminution Phenomena," Trans. AIME, 252, 1972, pp. 21-26.

60. Harris, C.C., "The Application of Size Distribution Equations to Multi-Event Comminution Processes, Trans. AIME, 241, 1968, pp. 343-358.

61. Harris, C.C., "Deficiencies in Two-Batch Grinding Hypotheses," *Powder Technol*., *3*, 1970, pp. 309-311.

62. Horst, W.E. and E.J. Freeh, "Mathematical Modeling of a Continuous Comminution Process," *Trans. AIME*, *252*, 1972, pp. 160-167.

63. Herbst, J.A., G.A. Grandy, and T.S. Mika, "On the Development and use of Lumped-Parameter Models for Continuous Open- and Closed-Circuit Grinding Systems," *Trans. AIME,* Section C, *80*. 1971, pp. C193-C198.

64. Luckie, P.T. and L.G. Austin, "A Review Introduction to the Solution of the Grinding Equations by Digital Computation," *Mineral Science and Engineering*, *4*, No. 2, April 1972, p. 24.

65. Herbst, J.A. and D.W. Fuerstenau, "Influence of Mill Speed and Ball Loading on Parameters of the Batch Grinding Equation," *Trans. AIME*, *252*, 1972, pp. 160-167.

66. Austin, L.G. and P.T. Luckie, "Grinding Equations and the Bond Work Index," *Trans. AIME*, *252*, 1972, pp. 259-266.

67. Harris, C.C., "A Method of Determining the Parameters of the 3-Parameter Size Distribution Equation," *Trans. AIME*, *244*, 1969, pp. 187-190.

68. Harris, C.C., "Relations for the xYt Comminution Surface," *Trans. Inst. Mining Met*., *79*, 1970, pp. C157-158.

69. Kelly, F.J. and R.F. Pilgrim, "Simulation of a Grinding Circuit and Encountered Problems," *Trans. AIME*, *252*, 1972, pp. 366-371.

70. Hogg, R. and D.W. Fuerstenau, "Power Relationships for Tambling Mills," *Trans. AIME*, *252*, 1972, pp. 418-423.

71. Snow, R.H., "Annual Review of Size Reduction," *Powder Technol*., *5*, 1971/72, pp. 351-364.

72. Fuerstenau, D.W. and P. Somasundaran, "Cinetique de la Fragmentation," in 6th Congres International de la Preparation des Minerals (Cannes), Edit. Saint-Etienne, 1963, pp. 39-48 (cf. also "Comminution Kinetics," in *Mineral Processing*, Edit. A. Roberts, Pergamon Press, Oxford, 1965, pp. 25-34.

73. Perov, V.A. and Y.A. Vasil'eva, "Kinetics of Grinding of a Two-Component Mixture in a Ball Mill," *Gornyi Zhurnal*, No. 1961, p. 69.

74. Kinasevich, S.R., "Application of the Schuhmann Single Event Hypothesis to Comminution," M.S. Thesis, Univ. of California, 1962.

75. Von Rittinger, R.P., "Lehrbuch der Aufbereitungskunde," Ernst und Korn, Berlin, 1857.

76. Kick, F., "Das Gesetz der Proportionalem Widerstand und seine Anwendung," Leipzig, 1885.

77. Holmes, J.A., "Contribution to the Study of Comminution - Modified Kick's Law," Trans. Inst. Chem. Engrs., 35, 1957, pp. 125-141.

78. Tanaka, T., "Comminution Laws," I & EC Process Design and Development, 5, No. 4, October 1966.

79. Suzuki, A. and T. Tanaka, "Crushing Efficiency in Relation to Some Operational Variables and Material Constants," I & EC Process Design and Development, 7, No. 2, April 1968.

80. Crabtree, D.D., S.R. Kinasevich, A.L. Mular, T.P. Meloy, and D.W. Fuerstenau, "Mechanisms of Size Reduction in Comminution Systems," Parts I and II, Trans. AIME, 229, 1964, pp. 201-210.

81. Bergstrom, B.H., "Empirical Modification of the Gaudin-Meloy Equation," Trans.AIME, 235, 1966, p. 45.

82. Callcott, T.G., "A Study of the Size Reduction Mechanisms of Swing Hammer Mills," J. Inst. Fuel, 33, 1960, pp. 529-539.

83. Obeng, D.M., "Comminution of a Heterogeneous Mixture of Brittle and Non-Brittle Materials," Ph.D. Dissertation, University of California, Berkeley, 1973.

84. Bennett, J.G., J. Inst. Fuel, 10, 1936, p. 22.

APPENDICES

APPENDIX A. MILL MATRIX CIRCUIT ANALYSIS

Callcott (82) assumes that a mill has N obstructions formed by breakage bars and grids (or screen). A symbolical representation is given by Figure A-1 in which

$\underline{m}_j$	represents the new feed vector to the jth stage
$\underline{\underline{C}}_j, \underline{\underline{D}}_j$	represent the classification and "mill" matrices for the jth stage
$\underline{q}_j$	represents the output vector of the jth stage or zone
$\underline{\underline{E}}_j$	represents the diagonal matrix of which the elements express the proportions of each size range of $\underline{q}_j$ that pass on to form $\underline{m}_{j+1}$
$\underline{g}_j$	represents the vector of material discharged between the jth and (j+1)th zone.

Mass flow rates are represented by M_j, Q_j, E_j.

The subscript j ranges over 1, 2, 3,---, N for all symbols, except that if some of the material characterized by N is returned to mix with the mill feed (m, M) j ranges from zero up to N + 1. Thus in N (equal or unequal, finite or infinite) steps, the mass of material with vector $\underline{m}$ is eliminated from the system.

The discharge of the jth ejection has a size distribution given by

$$\underline{q}_j = \underline{g}_j / \underline{e}' \underline{g}_j^{*} \qquad \text{(A1)}$$

and the size distribution of the entire output from $\underline{m}$ is

$$\underline{q} = \sum_{1}^{N} \underline{g}_j \qquad \text{(A2)}$$

$^{*}\underline{e}' = [1, 1, \text{---}\ 1]$

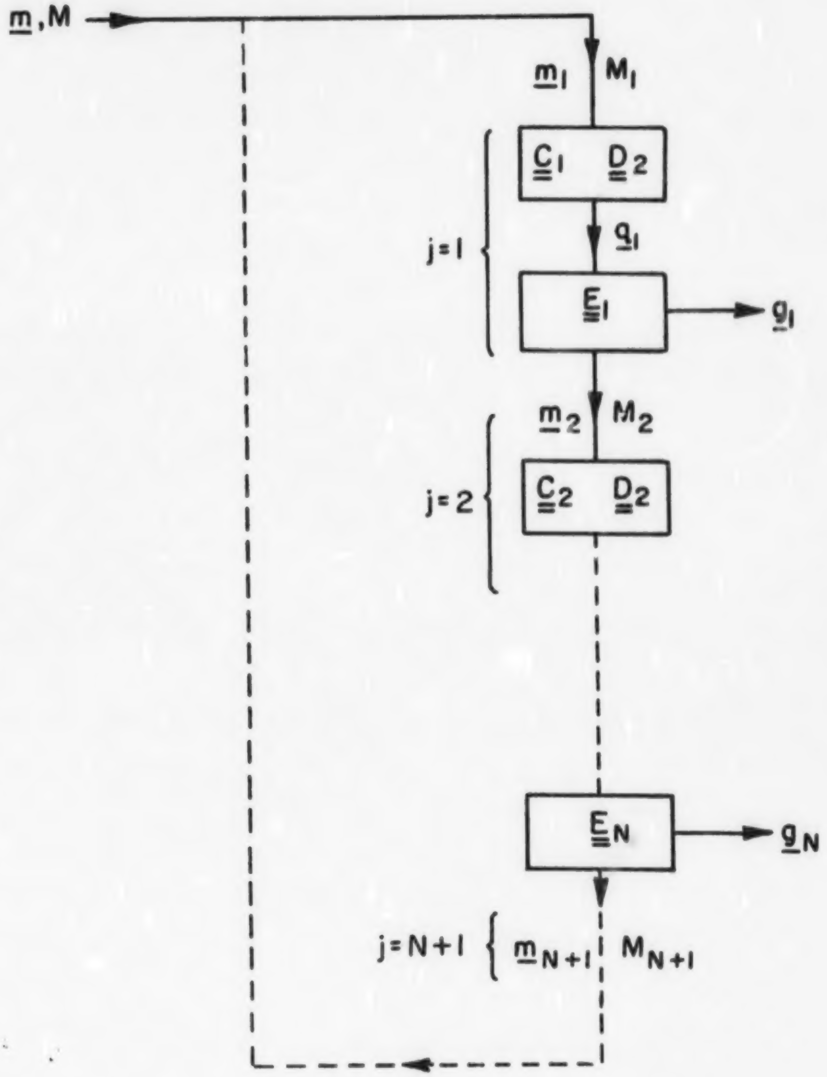
m, M
m1
M1
C1
D2
j=1
g1
E1
g1
m2
M2
j=2
C2
D2
EN
gN
j=N+1
mN+1
MN+1

Figure A-1 Hammermill Analysis

Two simple cases arise:

(i) No material is discharged until after the Nth obstruction, and none is returned to the starting point. That is,

$$\underline{\underline{E}}_j = \underline{\underline{I}} \ (j = 1, 2, 3, ---, N-1), \ \underline{\underline{E}}_N = \underline{\underline{0}}.$$

(ii) Some discharge occurs after each obstruction, and none returns to starting point. That is,

$$\underline{\underline{E}} \neq \underline{\underline{I}}, \ (j = 1, 2, 3, ---, N-1), \ \underline{\underline{E}}_N = \underline{\underline{0}}.$$

The general equation describing the transition from $\underline{m}$ to the mill discharge $\underline{q}$ for case (i) is

$$g_N = \underline{q} = \{ \overset{N}{\underset{j=1}{\pi}} \{\{\underline{\underline{I}}-\underline{\underline{C}}_j\} \underline{\underline{D}}_j \{\underline{\underline{I}}-\underline{\underline{C}}_j\underline{\underline{D}}_j\}^{-1}\}\}\underline{m} \tag{A3}$$

Now suppose that $\underline{\underline{C}}_j = \underline{\underline{C}}$, $\underline{\underline{D}}_j = \underline{\underline{D}}$ for all j; then

$$\underline{g}_N = \underline{q} = \{\{\underline{\underline{I}}-\underline{\underline{C}}\} \underline{\underline{D}} \{\underline{\underline{I}}-\underline{\underline{C}}\underline{\underline{D}}\}^{-1}\}^N \underline{m} \tag{A4}$$

For case (ii), the entire output from $\underline{m}$ is

$$q = \{ \sum_{j=1}^{N} \{\{\underline{\underline{I}} - \underline{\underline{E}}_j\}\underline{\underline{X}}_j \ \{ \sum_{k=1}^{j-1} \underline{\underline{E}}_k X_k\}\}\}\underline{m} \tag{A5}$$

The above equation is obtained by considering the local grinding circuits of the various grinding zones. Thus $\underline{\underline{C}}_j$ and $\underline{\underline{D}}_j$ become the local or internal classification and "mill" matrices, respectively. Using the results of the simple grinding closed-circuit analysis (84), we get the local discharge to be given by:

$$\underline{g}_j = (\underline{\underline{I}} - \underline{\underline{C}}_j) \underline{\underline{D}}_j \{\underline{\underline{I}} - \underline{\underline{C}}_j\underline{\underline{D}}_j\}^{-1}\underline{m}_j = \underline{\underline{X}}_j\underline{m}_j \tag{A6}$$

where

$$\underline{\underline{X}}_j = (\underline{\underline{I}} - \underline{\underline{C}}_j) \underline{\underline{D}}_j \{I - C_jD_j\}^{-1} \tag{A7}$$

By definition

$$\underline{m}_j = \underline{\underline{E}}_{j-1}.\underline{q}_{j-1} \tag{A8}$$

hence

$$\underline{g}_j = \underline{\underline{X}}_j\underline{\underline{E}}_{j-1}\underline{g}_{j-1} \tag{A9}$$

The output vector q_j of the jth grinding zone can be expressed in terms of outputs from preceding zones thus:

$$\underline{q}_j = \underline{\underline{X}}_j \cdot \prod_{k=1}^{j-1} \underline{\underline{E}}_k \underline{\underline{X}}_k \ \underline{m}_1 \tag{A10}$$

The material discharged between the jth and (j+1)th obstruction is given by

$$\underline{g}_j = (\underline{\underline{I}} - \underline{\underline{E}}_j)\ \underline{q}_j$$

$$= \{(I - E_j)\}X_j \mathop{}\limits_{k=1}^{j-1} E_k\ X_k\}\ \underline{m}_1 \tag{A11}$$

The entire output from the mill is obtained by summing up the individual discharges from the various grinding zones. Thus

$$\underline{q} = \{ \sum_{j=1}^{N} \{\{\underline{\underline{I}}-\underline{\underline{E}}_j\}\ \underline{\underline{X}}_j\ \{ \prod_{k=1}^{j-1} \underline{\underline{E}}_k\underline{\underline{X}}_k\}\}\}\underline{m} \tag{A12}$$

If we put $\underline{\underline{E}}_j = \underline{\underline{E}}, \underline{\underline{X}}_j = \underline{\underline{X}}$ for j=1, 2, ---, N, we get

$$q = \{ \sum_{j=1}^{N-1} \{\{\underline{\underline{I}}-\underline{\underline{E}}\}\ \underline{\underline{X}}\ \{\underline{\underline{E}}\ \underline{\underline{X}}\}^{j-1}\}\}\ \underline{m} + \underline{\underline{X}}\ \ \{\underline{\underline{E}}\ \underline{\underline{X}}\}^{N-1}\ \underline{m}$$

$$= \{\underline{\underline{I}}-\underline{\underline{E}}\}\ \underline{\underline{X}}\ \{\underline{\underline{I}}-\underline{\underline{E}}\ \underline{\underline{X}}\}^{-1}\{\underline{\underline{I}} - \{\underline{\underline{E}}\ \underline{\underline{X}}\}^{N}\}\underline{m} + \{\underline{\underline{E}}\ \underline{\underline{X}}\}^{N}\ \underline{m} \tag{A13}$$

and noting $0 \leq E_{ii} \leq 1$, $0 \leq X_{ij} \leq 1$, $X_{nn} = 1$, if $i \geq j$ and the eigen values of $\underline{\underline{E}}\ \underline{\underline{X}}$ are less than unity, $\{\underline{\underline{E}}\ \underline{\underline{X}}\}^N \to \underline{\underline{0}}$ as $N \to \infty$; even for relatively large N this will apply.

Hence

$$\underline{q} = \{\underline{\underline{I}}-\underline{\underline{E}}\}\ \underline{\underline{X}}\ \{\underline{\underline{I}}-\underline{\underline{E}}\ \underline{\underline{X}}\}^{-1}\ \underline{m} \qquad \text{(A14)}$$

and so is identical in form with the closed-circuit equation developed earlier.

Another special case of example (ii) arises when $\underline{\underline{E}}_j = \underline{\underline{I}}$ for $j = 1, 2, ---, r$; $\underline{\underline{E}}_j = \underline{\underline{E}}$ if $j = r$; $\underline{\underline{X}}_j = \underline{\underline{X}}$; namely

$$\underline{q} = \{\underline{\underline{I}}-\underline{\underline{E}}\}\underline{\underline{X}}^{r}\{\underline{\underline{I}}-\underline{\underline{E}}\ \underline{\underline{X}}\}^{-1}\ \underline{m} \qquad \text{(A15)}$$

This approach enables us to define any part of the grinding system using convenient if arbitrary decisions on the corresponding intervals j = ---, etc., and defining $\underline{\underline{E}}_j$, $\underline{\underline{X}}_j$ correspondingly.

Equation 34 in this report is obtained by considering the hammermill as a once-through grinder and neglecting any internal classification of the material. Thus if we put $\underline{\underline{C}} = \underline{\underline{0}}$ in Equation A4 we get

$$q = \underline{\underline{D}}^{N}\ \underline{m} \qquad \text{(A16)}$$

Similarly, if $\underline{\underline{E}} = \underline{\underline{I}}$, Equation A13 becomes

$$\underline{q} = \underline{\underline{X}}^{N}\ \underline{m} \qquad \text{(A17)}$$

Both $\underline{\underline{D}}$ and $\underline{\underline{X}}$ now represent the overall "mill" matrices that may be defined in terms of the breakage matrix $\underline{\underline{B}}$ and selection matrix $\underline{\underline{S}}$.

APPENDIX B. SOME SIZE DISTRIBUTION RELATIONS PREPARED BY D.M. OBENG (83)

Size Distribution Equations (for Brittle Materials)

Since the 1920's, repeated attempts have been undertaken by research workers to arrive at a mathematical description of the distribution of comminuted brittle materials. In the following paragraphs, a brief outline is given of some of the relations most frequently quoted in the literature.

Gaudin-Schuhmann Distribution Function--

Plotting on a log-log paper oversize particle weights retained by a successive series of $\sqrt{2}$ quotient Tyler screens, Gaudin observed frequency distribution to form a straight line in the finer particle ranges, leading to the discovery of the relationship

$$\Delta Y = cx^{\alpha} \tag{B1}$$

where ΔY represents the fractional weight of oversize particles between two successive Tyler screens.

Based on the findings of Gaudin, Schuhmann succeeded in deriving a cumulative distribution formula in the following manner:

Let the quotient of screen series be p; then, summing up over-size weights retained on the successive sieves according to Equation B1, we get

$$Y = c(\frac{x}{p}) + c(\frac{x}{p^2}) + c(\frac{x}{p^3}) + ---$$

$$= cx^{\alpha}(\frac{p^{-\alpha}}{1-p^{-\alpha}})$$

and thence conveniently combining the constants

$$Y = (\frac{x}{k})^{\alpha} \tag{B2}$$

where

$$k = \frac{1-p^{-\alpha}}{cp^{-\alpha}} \tag{B3}$$

By transforming Equation B2 into

$$\log Y = \alpha(\log x - \log k)$$

it may be represented on log-log paper as a straight line having inclination α. Parameter α is referred to by Schuhmann as the distribution modulus, and k, having a dimension of length, as a size modulus.

Substituting $x = k$ we get $Y = 1$; that is, k will be the largest particle size, and a sieve with an aperture of that size will let the complete charge pass.

Beyond $Y = 1$, the distribution formula will lose its validity, and at this point, a break will occur in the straight line contrary to the postulate that a distribution curve has to approach the 100% pass point asymptotically. In the coarse particle ranges, therefore, the line will decline downwards, implying that with unclassified ground products, Equation B2 will be valid up to a certain limit only, as suggested by Gaudin's original paper.

For the last 30 years or so, most of the vast experimental work conducted by American research workers has been based on the Schuhmann formula.

Rosin-Rammler Distribution Function--

The Rosin-Rammler empirical formula, the most widespread in European laboratory practice and research, can be written as follows:

$$Y\ (x) = 1 - e^{-bx^{n}} \qquad \text{(B4)}$$

It was later modified by Bennett (84) substituting $(1/x_o)^n$ for b and presenting an alternative to the original formula as

$$Y\ (x) = 1 - e^{-(\frac{x}{x_o})^{n}} \qquad \text{(B5)}$$

Experiments leading to the discovery of formula B4 by Rosin and Rammler were conducted with powdered coal. Testing the material in a tube mill, they reached the conclusion that output T (tons per hour) in relation to sieve-residual R is governed by the power law, irrespective of the size of screen aperture:

$$T = cR^{p} \qquad \text{(B6)}$$

For the same output T and different screen apertures they derive

$$T = cR_1^{p_1} = cR_2^{p_2} = k_1 \tag{B7}$$

and therefore

$$R = \left(\frac{k_1}{c}\right)^{\frac{1}{p(x)}} \tag{B8}$$

Variations of parameter p had to be determined as a function of screen aperture (particle size) x. Experimental results have shown that

$$p(x) = \frac{k_2}{x^n} \tag{B9}$$

and therefore

$$R = \left(\frac{k_1}{c}\right)^{\frac{x^n}{k_2}} \tag{B10}$$

and, finally, substituting e^{-b} for k,

$$R = 1-Y = e^{-bx^n} \tag{B11}$$

The above deduction is thus a combination of the two empirical observations that mill output and residual on the sieve are correlated by a parabola of pth order and that exponent p as a function of particle size can be plotted as a hyperbola of the (n+1)th order.

In the following, the Rosin-Rammler equation will be discussed under the modified form (B5) introduced by Bennett, and the significance of the constants in the formula will be investigated.

Substituting x for x_o we get $Y = (1 - 1/e) = 0.632$. Thus x_o has a dimension of length denoting 63.2% cumulative undersize - that is, the magnitude of a screen opening through which 63.2% of the particles pass.

By rearranging and applying double logarithms to the expression, we obtain

$$\ln\ln\left(\frac{1}{1-Y}\right) = n(\ln x - \ln x_o) \tag{B12}$$

As shown by this equation, the relation can be plotted as a straight line by a coordinate system made up from a log scale abscissa on one hand, and an ordinate with a double logarithmic scale of the reciprocal $(\frac{1}{1-Y})$ on the other. The slope of the straight line is n to be intercepted by particle size x_o on the horizontal line representing 63.2% undersize. Lower values of n are to be associated with a more scattered distribution, whereas higher values of n will imply an increasingly uniform particle structure. Size x_o may be referred to as the absolute size constant or characteristic particle size, and n as the uniformity coefficient of the particle pattern. In reality, n varies from 0.5 to 1.3 for brittle materials.

Gaudin-Meloy Size Distribution Function--

Gaudin and Meloy present a theoretical derivation of the distribution equation for single fracture that agrees with experimental results better than either the Gaudin-Schuhmann equation or the Rosin-Rammler equation. This equation is:

$$Y = \frac{M(x)}{M_o} = 1 - (1 - \frac{x}{x_o})^r \qquad \text{(B13)}$$

where M_o is the total weight of crushed sample, M(x) the weight of undersize contained, x the size considered, x_o the feed size, and r the size ratio (to be explained further below).

The above equation is used in this thesis as a breakage function $B(x, x_o)$ for the simulation of the process in the hammer-mill, and we find it instructive to give here its derivation as presented by Gaudin and Meloy in their paper.

It is assumed that the solid to be broken is isotropic, homogeneous, and that the fracture is a single event. The model of the fracture is as follows: Surfaces randomly oriented in position and direction pass through a crystal. The crystal fractures randomly along segments of these surfaces. All fragments have the same shape. The assumption that all fragments have the same shape puts constraints on how the surfaces cut the characteristic dimension of the feed crystal.

Consider a line segment x_o in length cut by r surfaces. The first goal is to determine the frequency distribution of z, the distance between any two adjacent cuts.

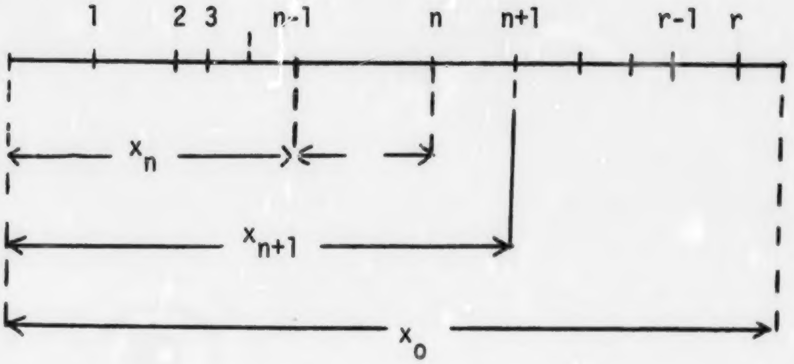

The probability of any cut being at a fixed point is $\frac{dx}{x_o}$. Specifically, for a cut being at x_n, it becomes $\frac{dx_n}{x_o}$. Similarly, the probability of another cut being at x_{n+1} is $\frac{dx_{n+1}}{x_o}$.

If the cut at distance x_n from 0 is the nth cut, then there are (n-1) cuts preceeding it. Therefore the probability of the cut x_n from the origin being the nth cut is $(\frac{x_n}{x_o})^{n-1}$, and likewise the probability of the cut x_{n+1} being the (n+1)th cut out of the r cuts is $(\frac{x_o-x_{n+1}}{x_o})^{r-n-1}$.

The probability $P_1(x_n, x_{n+1})$ of having all of these events happen simultaneously is the product of their individual probabilities,

$$P_1(x_n, x_{n+1}) = (\frac{x_n}{x_o})^{n-1} \cdot \frac{dx_n}{x_o} \cdot \frac{dx_{n+1}}{x_o} \cdot (\frac{x_o-x_{n+1}}{x_o})^{r-n-1} \qquad (B14)$$

Equation (B14) gives the probability that there will be (n-1) cuts between 0 and x_n, one cut at x_{n+1}, and (r-n-1) cuts between x_n and x_o. Since the r cuts were ordered after the event took place, a multinomial coefficient must be used to determine all possible ways r cuts can cut a line with only the nth and (n+1)th cuts having fixed positions. Since there are (n-1) cuts below x_n, and (r-n-1) above x_{n+1}, the multinomial coefficient γ is

$$\lambda = \frac{r!}{(n-1)!\,(r-n-1)!} \qquad (B15)$$

Thus, the probability $P_2(x_n, x_{n+1})$ of having r cuts at random on a line segment x_o in length, with the nth and (n+1)th cuts fixed is γP_1 or

$$P_2(x_n,x_{n+1}) = \frac{r!}{(n-1)!\,(r-n-1)!}\ \frac{(x_n{}^{n-1})(x_o-x_{n+1})^{r-n-1}}{x_o{}^r}\ dx_n\ dx_{n+1} \qquad (B16)$$

We are interested in the distribution of the distance Z between the nth and (n+1)th cuts. We have

$$x_{n+1} = z + x_n \qquad (B17)$$

Regarding x_n as fixed, while x_{n+1} varies we get

$$dx_{n+1} = dz$$

Substitute this value of dx_{n+1} and the value of γ into Equation B16 to obtain

$$P_3(z,x_n) = \gamma x_o{}^{-r} x_n{}^{n-1}\ (x_o - z - x_n)^{r-n-1} dz dx_n \qquad (B18)$$

Since Equation B18 is a joint distribution of two independent variables, it can be integrated with respect to x_n within the limits $0 \le x_n \le x_o - z$, thereby eliminating it. Hence

$$P_4(z) = \gamma x_o{}^{-r} \int_0^{x_o-z} x_n{}^{r-1}(x_o-z-x_n)^{r-n-1} dx_n \qquad (B19)$$

The form of the integral can be changed by defining a new variable y such that

$$x_n = (x_o - z)y \ ;\ \ dx_n = (x_o - z)dy \qquad (B20)$$

Substituting the above values into B19, we get

$$P_4(z) = \gamma x_o{}^{-r}\ (x_o-z)^{r-1} dz \int_0^1 y^{n-1}(1-y)^{r-n-1}\ dy \qquad (B21)$$

The integral in the preceding equation is the familiar β function

$$\int_0^1 y^{n-1}(1-y)^{r-n-1}\,dy = \beta(n,r-n) \tag{B22}$$

and can be expressed in terms of Γ functions:

$$\beta(n,\ r-n) = \frac{\Gamma(n)\Gamma(r-n)}{\Gamma(r)} \tag{B23}$$

Since both r and n are integers,

$$\frac{\Gamma(n)\Gamma(n-1)}{\Gamma(r)} = \frac{(n-1)!\ (r-n-1)!}{(r-1)!} \tag{B24}$$

Substituting the results of Equations B23 and B24 into Equation B21, we get

$$P_4(z) = \frac{r}{x_o{}^r}\,(x_o-z)^{r-1}\,dz \tag{B25}$$

From Equation B25, we can derive the size distribution equation. The relative volume of a fragment of size z to the original size x_o is $(\frac{z}{x_o})^3$. Hence the abundance, dN(z), of particles of size z is

$$dN(z) = (\frac{x_o}{z})^3\,\frac{r}{x_o{}^r}\,(x_o-z)^{r-1}\,dz \tag{B26}$$

The corresponding mass may be obtained by multiplying by the mass of each z particle, $\lambda\rho^3$, in which ρ stands for density, and λ for a shape factor. Hence

$$dM(z) = \lambda\rho x_o{}^{3-r}\,r(x_o-z)^{r-1}dz \tag{B27}$$

integrating between the limits of 0 and x

$$M(x) = \lambda\rho x_o{}^{3-r}\,r\int_0^x (x_o-z)^{r-1}dz \tag{B28}$$

gives the mass contained between zero and x. On completing the integration, inserting limits, and simplifying, we get

$$M(x) = \lambda \rho x_0^3 \left[1 - \left(1 - \frac{x}{x_0}\right)^r\right] \tag{B29}$$

Since the initial weight is $M_o = \lambda \rho x_o^3$, then

$$Y = \frac{M(x)}{M_0} = 1 - \left(1 - \frac{x}{x_0}\right)^r \tag{B30}$$

This equation is identical with Equation B13.